





SPECIAL ISSUE ARTICLE

Osteology and relationships of *Revueltosaurus callenderi* (Archosauria: Suchia) from the Upper Triassic (Norian) Chinle Formation of Petrified Forest National Park, Arizona, United States

William G. Parker¹  | Sterling J. Nesbitt²  | Randall B. Irmis^{3,4} | Jeffrey W. Martz⁵ | Adam D. Marsh¹  | Matthew A. Brown⁶  | Michelle R. Stocker²  | Sarah Werning⁷ 

¹Department of Resource Management and Science, Petrified Forest National Park, Petrified Forest, Arizona, USA

²Department of Geosciences, Virginia Tech, Blacksburg, Virginia, USA

³Natural History Museum of Utah, University of Utah, Salt Lake City, Utah, USA

⁴Department of Geology and Geophysics, University of Utah, Salt Lake City, Utah, USA

⁵Department of Natural Sciences, University of Houston-Downtown, Houston, Texas, USA

⁶Texas Vertebrate Paleontology Collections, The Jackson School of Geosciences, University of Texas at Austin, Austin, Texas, USA

⁷Department of Anatomy, Des Moines University, Des Moines, Iowa, USA

Correspondence

William G. Parker, Division of Resource Management, Petrified Forest National Park, P. O. Box 2217, Petrified Forest, AZ 86028, USA.

Email: william_parker@nps.gov

Abstract

Once known solely from dental material and thought to represent an early ornithischian dinosaur, the early-diverging pseudosuchian *Revueltosaurus callenderi* is described from a minimum of 12 skeletons from a monodominant bonebed in the upper part of the Chinle Formation of Arizona. This material includes nearly the entire skeleton and possesses a combination of plesiomorphic and derived character states that help clarify ingroup relationships within Pseudosuchia. A phylogenetic analysis recovers *R. callenderi* in a clade with Aetosauria and *Acaenasuchus geoffreyi* that is named Aetosauriformes. Key autapomorphies of *R. callenderi* include a skull that is longer than the femur, a complete carapace of dermal armor including paramedian and lateral rows, as well as ventral osteoderms, and a tail end sheathed in bone. Histology of the femur and associated osteoderms demonstrate that *R. callenderi* was slow growing and that the individuals from the bonebed were not young juveniles but had not ceased growing. A review of other material assigned to *Revueltosaurus* concludes that the genus cannot be adequately diagnosed based on the type materials of the three assigned species and that only *R. callenderi* can be confidently referred to *Revueltosaurus*.

KEYWORDS

Aetosauriformes, histology, *Krzyzanowkisaurus*, phylogeny, Pseudosuchia

1 | INTRODUCTION

Late Triassic non-marine vertebrate assemblages comprise a broad assortment of archosaurs that originate and go

extinct in the Triassic Period (e.g., non-dinosaurian avemetatarsalians, non-crocodylomorph pseudosuchians), crown-group archosaurs that originated in the Triassic but diversified later in the Mesozoic Era (e.g., crocodylomorphs,

This is an open access article under the terms of the [Creative Commons Attribution-NonCommercial-NoDerivs](https://creativecommons.org/licenses/by-nc-nd/4.0/) License, which permits use and distribution in any medium, provided the original work is properly cited, the use is non-commercial and no modifications or adaptations are made.

© 2021 The Authors. The Anatomical Record published by Wiley Periodicals LLC on behalf of American Association for Anatomy. This article has been contributed to by US Government employees and their work is in the public domain in the USA.

pterosaurs, and dinosaurs), and other abundant non-archosaurian archosauromorphs present only during the Triassic Period (e.g., tanystropheids, rhynchosaurs, allokotosaurians). The last two decades of research reveal that a number of these lineages endemic to the Triassic had unexpected morphological and ecological specializations (e.g., Dzik, 2003; Ezcurra, 2016; Ezcurra et al., 2020; Flynn et al., 2010; Foth et al., 2016; Irmis, Nesbitt, et al., 2007; Nesbitt, 2003; Nesbitt, 2005a; Nesbitt, 2007; Nesbitt & Butler, 2013; Nesbitt & Norell, 2006; Nesbitt et al., 2009, 2010, 2017; Nesbitt et al., 2014; Parker et al., 2005; Sengupta et al., 2017; Stocker et al., 2016; Sues, 2003). Many non-archosaur archosauromorphs and crown archosaurs possessed a suite of character states that were thought to be present exclusively in various groups of dinosaurs. For example, the poposaurid pseudosuchians *Shuvosaurus inexpectatus* and *Effigia okeeffeae* have an upright bipedal stance with theropod dinosaur-like skulls (Nesbitt, 2007; Nesbitt & Norell, 2006; Parker & Nesbitt, 2013), the dorsal portion of the cranium is expanded into a dome in both *Triopticus primus* and pachycephalosaurian dinosaurs (Stocker et al., 2016), and the non-archosaur archosauromorph *Azendohsaurus madagaskarensis*, the suchian archosaur *Revueltosaurus callenderi*, and the non-dinosaurian dinosauriform *Silesaurus opolensis* all have teeth that are nearly indistinguishable from those of early ornithischian dinosaurs (Dzik, 2003; Flynn et al., 2010; Irmis, Parker et al., 2007; Nesbitt et al., 2010, 2015).

Many of the “dinosaur-like” Triassic reptiles belong to the clade Pseudosuchia; these crocodile-line archosaurs are some of the most commonly recovered non-marine tetrapods from the Late Triassic Epoch across Pangea. Despite this excellent fossil record, the relationships of early-diverging suchians remain incompletely understood (e.g., Brusatte et al., 2010; Butler et al., 2014; Ezcurra et al., 2017; Gower & Wilkinson, 1996; Nesbitt, 2011; Nesbitt, Stocker, et al., 2018; von Baczko & Ezcurra, 2013). Renewed interest in those early-diverging pseudosuchians, along with new discoveries, has greatly improved our understanding of their diversity, disparity, and phylogenetic relationships (e.g., Butler et al., 2014; Butler et al., 2018; Desojo et al., 2013; Desojo et al., 2020; Ezcurra et al., 2017; Irmis et al., 2013; Marsh et al., 2020; Müller et al., 2020; Nesbitt et al., 2014; Nesbitt, Brusatte, et al., 2013; Nesbitt, Desojo, & Irmis, 2013; Nesbitt, Stocker, et al., 2018; von Baczko et al., 2020; von Baczko & Ezcurra, 2013). The discovery of early-diverging pseudosuchian taxa with a combination of plesiomorphic and apomorphic character states help clarify some of the in-group relationships within Pseudosuchia, but at the same time has also shown homoplasy in certain character states (e.g., Ezcurra et al., 2017; Marsh et al., 2020; Nesbitt, 2005a, 2005b; Nesbitt, 2011; Nesbitt et al., 2011; Nesbitt & Butler, 2013; Nesbitt & Norell, 2006; Parker et al., 2005).

One of these key early-branching pseudosuchians is *R. callenderi*, which was originally described as a putative ornithischian dinosaur based on isolated, but apomorphic, teeth from the Bull Canyon Formation (Dockum Group) of eastern New Mexico, United States (Hunt, 1989). Subsequent studies (e.g., Heckert, 2002; Hunt, 2001; Hunt & Lucas, 1994; Padian, 1990) identified additional dental specimens from other localities and continued to identify *R. callenderi* as an unambiguous dinosaur possessing ornithischian synapomorphies. Hunt (1994, 2001) also noted the presence of a partial skeleton of an armored pseudosuchian (NMMNH P-16932) from the type locality of *R. callenderi*, which he considered to be a distinct taxon, but never formally described. The discovery of associated skeletal material including cranial material with in situ teeth from a monodominant bonebed (sensu Eberth, Shannon, & Noland, 2007) in the Petrified Forest Member of the Chinle Formation at Petrified Forest National Park (PEFO), Arizona, United States, clearly demonstrated that *R. callenderi* was not a dinosaur, but rather an early-diverging pseudosuchian (Parker et al., 2005). Based on that new information, Hunt et al., (2005) referred NMMNH P-16932 to *R. callenderi*. Although the description of that material was brief, it is important for three reasons: (a) NMMNH P-16932 most certainly represents *R. callenderi* because the specimen includes a dentigerous maxilla with teeth preserving *R. callenderi* apomorphies; (b) it is from very near the type locality of *R. callenderi*, both geographically and stratigraphically (Hunt et al., 2005); and (c) NMMNH P-16932 is identical to the PEFO skeletal material assigned to *R. callenderi* by Parker et al. (2005). The genus *Revueltosaurus* included two other species, “*R.*” *hunti* Heckert, 2002, known from teeth and bones from the lower Chinle Formation of Arizona and Utah and lower Dockum Group of New Mexico, and “*R.*” *olseni* (Hunt & Lucas, 1994), known from teeth from the Pekin Formation of North Carolina, United States.

Neither Parker et al. (2005) nor Hunt et al. (2005) attempted a phylogenetic analysis of *R. callenderi* based on the new skeletal material. However, both groups noted several features of the hindlimb that were unambiguous synapomorphies of Pseudosuchia. Parker et al. (2005) hypothesized a possible sister-group relationship with aetosaurs, noting the morphological similarities of the squamosal and paramedian osteoderms. A similar position was proposed by Hunt et al. (2005) based on unspecified character states of the tarsus and the osteoderms. Brusatte et al. (2010) included *R. callenderi* in their analysis of early archosaur relationships, coding from the published figures and descriptions of Parker et al. (2005) and Hunt et al. (2005). That study recovered *R. callenderi* as the sister taxon to the early-diverging suchian clade Ornithosuchidae. Another broad-scale

analysis of archosaur relationships by Nesbitt et al. (2011) recovered *R. callenderi* in a well-supported position as the sister taxon to aetosaurs, a result supported by more recent studies (e.g., Butler et al., 2014; Marsh et al., 2020; Müller et al., 2020; Nesbitt & Butler, 2013; Nesbitt et al., 2014; Nesbitt et al., 2020; Nesbitt, Stocker, et al., 2018).

This contribution fully describes the osteology of *R. callenderi* based on a minimum of 12 individuals (based on femora count) from PEFO including three well-preserved associated partial skeletons collected between 2005 and 2015, provides osteohistological context, and discusses the taxon's importance for understanding early suchian evolution.

2 | GEOLOGICAL SETTING

2.1 | Stratigraphic position

This description of *R. callenderi* is predominantly based on material from several localities in the Chinle

Formation of Petrified Forest National Park (PEFO), Arizona, United States (Figure 1; see Systematic Paleontology). The Upper Triassic Chinle Formation in this area comprises predominantly fluvial and floodplain strata of alternating claystones, siltstones, sandstones, and conglomerates (Billingsley, 1985; Heckert & Lucas, 2002a; Martz & Parker, 2010; Woody, 2006). The Chinle Formation in the Petrified Forest National Park area preserves well-known fossil assemblages of plants (palynomorphs, leaves, wood), invertebrates, and vertebrates (e.g., Ash, 2005; Baranyi et al., 2018; Good, 1998; Irmis, 2005; Litwin, Traverse, & Ash, 1991; Parker, 2005b, 2006; Reichgelt et al., 2013). Most non-dentigerous and non-osteoderm specimens of *R. callenderi* from PEFO, including those described here, have been found immediately above Painted Desert Sandstone 3 (sensu Billingsley, 1985; Lithodendron Wash Bed sensu Heckert & Lucas, 2002a) in the middle part of the Petrified Forest Member (sensu Woody, 2006) of the upper part of the Chinle Formation (Heckert & Lucas, 2002a; Irmis, 2005; Padian, 1990; Parker, 2005b, 2006; Parker et al., 2005; Parker & Martz, 2011). Isolated teeth of *R. callenderi* have been

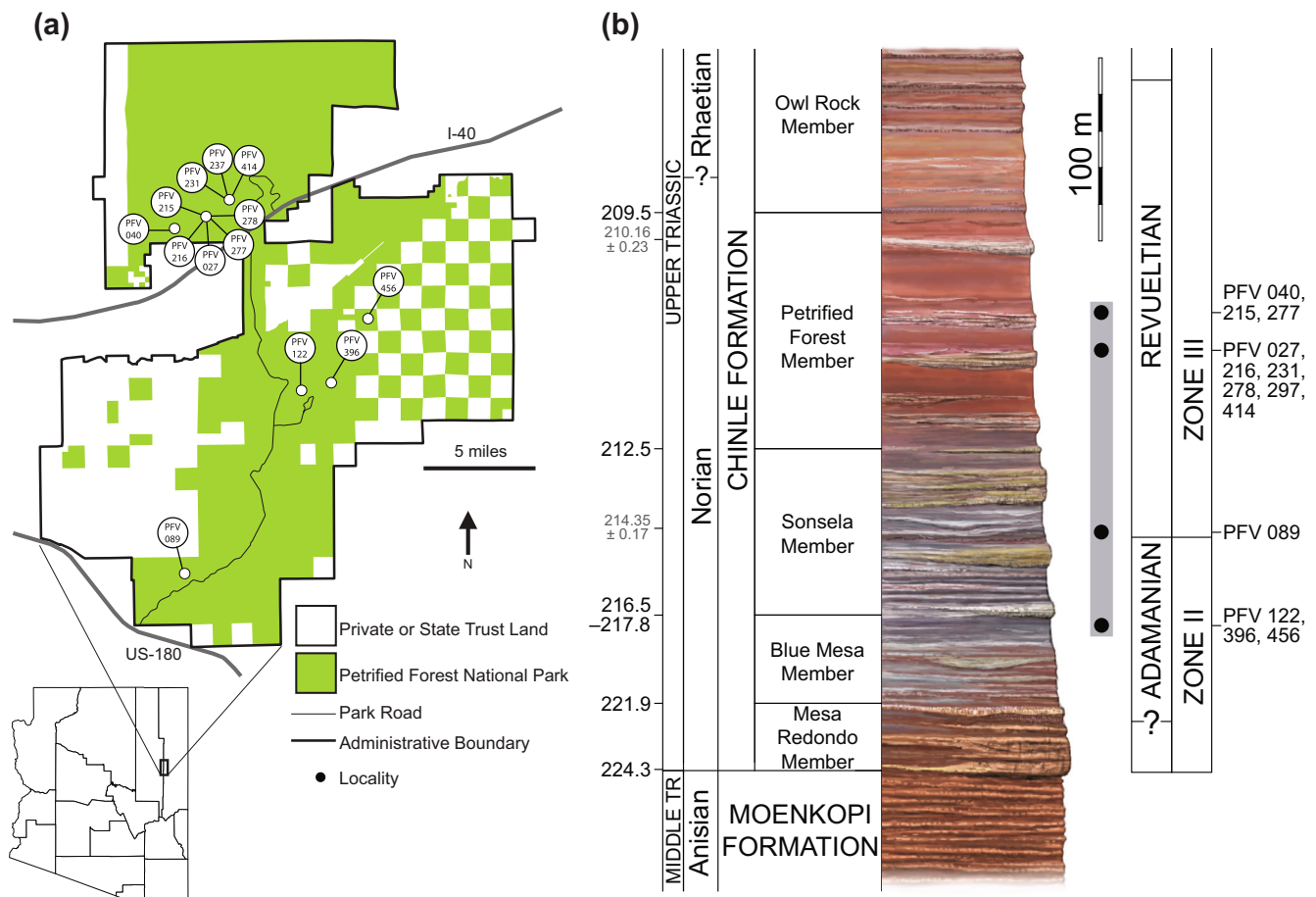


FIGURE 1 Localities at Petrified Forest National Park containing *Revueltosaurus callenderi* (a) and stratigraphic distribution of those localities in the Chinle Formation (b). Stratigraphic column modified from Marsh et al. (2020). Numbers on the left side of the column are numeric ages in millions of years (Ma); those at the boundaries between members are inferred from the age models of Rasmussen et al. (2020), the smaller numbers with uncertainties are key individual U-Pb zircon ages from the same study

recovered from microvertebrate assemblages from lower in the Chinle Formation at PEFO, extending the stratigraphic range of this taxon into the Sonsela Member and uppermost Blue Mesa Member (see Systematic Paleontology).

The three main localities that produced the specimens of *R. callenderi* described here (Data S1) are the *Revueltosaurus* Quarry (PFV 297), *Revueltosaurus* Quarry SW (PFV 414), and the Giving Site (PFV 231). These sites occur as paleosols in a stacked fluvial sequence in the middle of the Petrified Forest Member (Atchley et al., 2013; Loughney et al., 2011; Parker et al., 2005; Parker & Martz, 2011). PFV 297 and PFV 414 are separated spatially by 20 m and are in turn about 200 m to the southeast of PFV 231 (Figure 1a). Painted Desert Sandstone 3, which immediately underlies all three localities, is stratigraphically ~40–50 m above the base of the Petrified Forest Member (Figure 1b; Parker & Martz, 2011), and represents a sheet sandstone deposited by perennial flow in a high sinuosity river channel (Johns, 1988). PFV 297 and PFV 414 occur slightly higher in the sequence than PFV 231 (Parker & Martz, 2011).

Besides its eponymous taxon, the only other specimens from PFV 297 are fragmentary shuvosaurid bones (e.g., PEFO 34072) found ex-situ (Parker et al., 2005), and isolated large, serrated teeth. These include teeth identifiable to phytosaurs and a large mediolaterally compressed recurved tooth (crown length = 63.3 mm) with a resorbed root that might represent a large paracrocodylomorph (PEFO 41401). In contrast, PFV 231 preserves a more diverse assemblage including *R. callenderi* (e.g., PEFO 33791), the non-archosaur archosauriform *Vancleavea campi* (PEFO 33978), indeterminate small metoposaurid temnospondyls (e.g., PEFO 34081), shuvosaurids (e.g., PEFO 33953), rauisuchids (sensu Nesbitt, 2011; e.g., PEFO 33954), crocodylomorphs (e.g., PEFO 34090), mystriosuchine leptosuchomorph phytosaurs (PEFO 33980), the aetosaur *Typhorax coccinarum* (e.g., PEFO 33967), the early-diverging theropod dinosaur *Chindesaurus bryansmalli* (PEFO 33982), and a coelophysoid theropod (e.g., PEFO 33981; Parker et al., 2005; Parker & Irmis, 2005; Irmis, 2008; Parker & Barton, 2008; Parker & Martz, 2011; Marsh & Parker, 2020).

The Chinle Formation at PEFO is now well-dated by high-precision U–Pb zircon ages and magnetostratigraphy, indicating that the entire formation in this area is Norian–Rhaetian in age (Kent et al., 2018, 2019; Ramezani et al., 2011; Rasmussen et al., 2020). *R. callenderi* occurs in the uppermost Blue Mesa Member through middle Petrified Forest Member at PEFO, with a numerical age range of ~218.5–210 Ma (middle-late Norian; Rasmussen et al., 2020). There is some uncertainty in the age of the lower part of the Sonsela Member depending on the age model selected (Rasmussen et al., 2020) but this does not affect the age of the first or last occurrences of *R. callenderi* at PEFO.

2.2 | Taphonomy

Hundreds of elements of *R. callenderi* were collected from PFV 297, ranging from broken isolated bones to partially articulated skeletons. The accumulation of multiple individuals of predominantly one taxon classifies the locality as a monodominant bonebed (Eberth et al., 2007). The specimens were all recovered from a single horizon in a greenish-gray mudstone (“blue sites” of Loughney et al., 2011) that is adjacent to a channel facies of the Painted Desert Sandstone 3 (Parker et al., 2005), which probably represent levee deposits in the proximal portion of the floodplain (T. Demko, personal communication, March 18, 2004). Other vertebrate localities in the Petrified Forest Member occur within similar drab-colored beds that have been interpreted as representing poorly drained paleosols in abandoned channel fill that were at least seasonally water-saturated (Loughney et al., 2011; Therrien & Fastovsky, 2000). Monodominant assemblages commonly occur in wetland facies (e.g., overbank wetland/marginal pond) with low transport and reworking potential (Eberth et al., 2007), and this is consistent with the interpretation of the depositional environment of “blue sites” of Loughney et al. (2011). The presence of fossil equisetalean plants (e.g., PEFO 41412) in the quarry also supports this interpretation. In nearly all specimens from PFV 297 and PFV 414, the internal spaces of the bone have been permineralized by calcite spar, and in many cases, the bones are also overgrown by a thin calcite spar coating. Many elements have undergone slight plastic deformation and brittle deformation as evidenced by fracturing and displacement in specimens of long bones. Otherwise surface bone preservation is exquisite, preserving fine external details (e.g., muscle scars) in many specimens, especially in PEFO 34561.

The initial material from PFV 297 was discovered in early 2004 and collected mostly as surface “float” that eroded out of the fossiliferous horizon, with one in-situ articulated specimen with a partial skull (PEFO 33787). Counts of right ilia, right femora, and left frontals indicated the preservation of a minimum of five individuals (Parker et al., 2005). Subsequent excavation of in-situ specimens consisted of many isolated elements as well as four associated skeletons (PEFO 34269; PEFO 34561; PEFO 36875; PEFO 36876). PEFO 34561 represents as much as 90% of an individual and provides most of the description provided below. PEFO 36875 possesses a complete and mostly articulated skull as well as a partially articulated postcranial skeleton. An articulated skull (PEFO 38609) and another skeleton were collected in 2015 (PEFO 42442/UWBM 116869) from PFV 414; PEFO 42442/UWBM 116869 preserves the vertebral column and carapace of the trunk region in partial articulation, as well as a complete,

but flattened, skull. These skeletons occur as relatively isolated concentrations of bones from single individuals separated from each other in the same bedding plane by an average of 1–2 m. Together all of the material from PFV 297 and PFV 414 represents a minimum of 12 individuals based on femora counts. Mukherjee and Ray (2012) described a similar taphonomic setting for a rhynchosaur-dominated bonebed in the Upper Triassic Tiki Formation of India. As with the Indian assemblage, it is probable at PFV 297 and PFV 414, with the fine-grained sediments and in-situ equisitaleans, that soft-tissue decomposition at shallow water depth and subsequent weathering processes disarticulated the individuals of *R. callenderi*. These skeletons were later subjected to partial dispersal by low energy fluvial agents and eventually burial in floodplain deposits (Mukherjee & Ray, 2012). The rarity of small elements such as gastralia and chevrons in otherwise nearly complete specimens, as well as the presence of isolated skull, girdle, and limb bones of the same taxon, supports this latter dispersal event (Mukherjee & Ray, 2012). No specimens display any signs of scavenging behavior.

The cause of death of these individuals is unknown; however, monodominant bonebeds are commonly formed by single catastrophic events where mixing of taxa, often the result of long-term attritional accumulation, does not occur (Eberth & Brinkman, 1997). Curiously, the individuals at PFV 297 and PFV 414 are close to the same size (Data S2) and presumably were at similar ontogenetic stages (but see Griffin et al., 2020 for a discussion on size and ontogenetic status); however, PFV 231 contains individuals of various sizes including specimens much larger than those at the other two sites; for example, the frontal of PEFO 41453 is ~40% anteroposteriorly longer than that of PEFO 34561. Documented cases of monodominant accumulations of juvenile dicynodonts and dinosaurs suggest that the identical sizes of the specimens in the quarries may represent siblings or individuals from a single seasonal hatch (Brinkman et al., 2007).

3 | METHODS

3.1 | Collection and preparation

Specimens collected as “float” and small individual elements were labeled and bagged in polyethylene sandwich bags, and closely associated or articulated elements were consolidated with Vinac B-15 polyvinyl acetate (Air Products and Chemicals, Inc.) dissolved in acetone, pedestaled, and jacketed with plaster bandages. Excavation was done with small hand tools (e.g., picks, awls, and brushes). Because of the close association of many elements water was used as a tool for trenching. Water was applied with

droppers to the mudrock matrix areas between elements and scraped to create a small trench, these were slowly enlarged using the same method, which allowed for precise trenching between the elements to create small plaster jackets for removal. Small bones in the way of the desired trench were removed separately.

Jackets were opened in the laboratory at PEFO and all specimens were mechanically rough prepared without magnification using a carbide needle in a pin-vise. Water, acetone, or a mixture of 50% acetone/water was used with an acid brush to soften the mudstone matrix. Fine preparation took place under a Wild M7 stereomicroscope using a carbide needle, a Microjack #4 (PaleoTools, Inc.), and an ARO Marxall aircscribe modified with an HW-10 (HW, Co.) microtip adaptor. Chemical preparation with acetic acid (15%) was attempted to further define specimens where individual elements were fused together through a diagenetic coating of calcite spar (e.g., PEFO 34269). These efforts generally were unsuccessful, and chemical preparation was discontinued. During preparation, matrix and bone were consolidated thoroughly with Vinac B-15 dissolved in acetone, and joins were made in the specimens collected in 2004–2006 with Paleobond PB-40 and PB-100 cyanoacrylates (Uncommon Conglomerates, Inc) and with Paraloid B-72 (Rohm and Haas Co.) for the specimens collected in 2012 and 2015. Missing fragments in some elements were reconstructed with Paleosculp two-part epoxy putty (Uncommon Conglomerates, Inc) where it was necessary for stability of the element. Manipulation of bones in three dimensions was key in the identification of isolated cranial elements and understanding of the overall skull morphology. Some elements were molded using Plastalina sulfur-free modeling clay to temporarily embed in two-part molds. Small or more delicate specimens were molded with Platsil 71-10 addition-cure silicone rubber (Polytek, Inc.), and more robust elements were molded with Platsil 71-20 and Tinsil 70-25. Isolated cranial elements were molded and subsequently cast in plaster. The plaster casts fit together nearly perfectly and allowed for the creation of a 3-D reconstruction of the skull used for the description and reconstructions. Later, individual skull and postcranial elements were laser scanned using a NextEngine HD scanner, digitally articulated using ScanStudio, Rapidworks, Meshmixer and Meshlab, and 3D printed on a Formlabs 1+ printer. These can be accessed on Morphobank project P620.

3.2 | Phylogenetic methods

We tested the phylogenetic position of *R. callenderi* in the most comprehensive global early-diverging archosaur

study to date (Nesbitt, 2011) including modifications by Butler et al. (2014), Nesbitt et al. (2017); Nesbitt, Stocker, et al. (2018), and Marsh et al. (2020). This dataset has the broadest sampling of pseudosuchians thus far, but does not have the more complete sampling of taxa and characters associated with ornithosuchids (Müller et al., 2020), erpetosuchids (Lacerda et al., 2018) present in the Ezcurra et al. (2020) dataset, or the larger sampling of paracrocodylomorphs in Desojo et al. (2020) or Nesbitt et al. (2020); these data will be included elsewhere. Characters 1–412 are from Nesbitt et al. (2011) with some modifications noted below, Character 413 is from Butler et al. (2014), Characters 414–419 are from Nesbitt et al. (2017), 420–434 are from Parker (2016a) modified by Marsh et al. (2020), and 435–444 are from Marsh et al. (2020). We modified the latest version of the dataset (Marsh et al., 2020) with the following character changes: characters 101 and 114 were revised based on Nesbitt, Stocker, et al. (2018); Character 428 from Marsh et al. (2020) (Lateral osteoderms: absent [0]; present [1]) was deleted because it is a repeat of character 406 from Nesbitt et al. (2011). Additionally, we modified the dataset of Marsh et al. (2020) with the following taxon changes: *Parringtonia gracilis* (from Marsh et al., 2020) was replaced with “*Parringtonia gracilis* combined” from Nesbitt, Stocker, et al. (2018), and Characters 414–445 were coded based on NMT RB426, NMT RB28 and NHMUK PV R8646; “*Teleocrater rhadinus* combined” from Nesbitt et al. (2017) replaced “*Teleocrater* holotype”; character scores for *R. callenderi*, *Longosuchus meadi*, and *Stagonolepis robertsoni* were incorporated from Nesbitt, Stocker, et al. (2018) that were not present in Marsh et al. (2020); character 406 was rescored from the repeated and eliminated character 428. Character 406 now is coded as 0 for *Chanaresuchus bonapartei*, *Tropidosuchus romeri*, *Smilosuchus gregorii*, *Dibothrosuchus elaphros*; it is coded as 1 for *Euscolosuchus olseni* and *Acaenasuchus geoffreyi*. A full character list and Nexus matrix can be found in Data S3.

The matrix was constructed in Mesquite v3.10 (Maddison & Maddison, 2019) and consists of a total of 444 characters for 91 taxa. The rhynchosaur *Mesosuchus browni* was used as the outgroup to root the most parsimonious trees (MPTs). The dataset was analyzed in PAUP*4.0b10 (Swofford, 2002) using a heuristic search subjected to 1,000 random addition replicates with tree bisection and reconnection branch swapping. Characters 32, 52, 121, 137, 139, 156, 168, 188, 223, 247, 258, 269, 271, 291, 297, 314, 328, 356, 371, 399, 413, 430, and 432 (see Nesbitt et al., 2020 for ordering modifications of the original Nesbitt, 2011 dataset) were ordered. Zero-length branches were collapsed if they lacked support under any of the most parsimonious reconstructions. The same

topology and the same number of MPTs was recovered when all of the characters are run unordered, although a different tree length was found. Bootstrap support was calculated from 1,000 replicates using a heuristic search strategy with random taxon addition sequence and TBR branch swapping.

3.3 | Histology preparation, sampling, imaging, and terminology

To better understand the ontogenetic status of the PEFO *R. callenderi* sample, we made thin-sections of a left femur (PEFO 33843) and paramedian osteoderm (PEFO 33940a) from PFV 297 to study their osteohistology. Because similar osteoderms had previously been assigned to juvenile aetosaurs (Heckert & Lucas, 2002b), we also sampled a paramedian osteoderm (UCMP 175058) of *Krzyzanowskisaurus hunti*.

Prior to histological sampling, all elements were measured, sketched, and photographed. The elements were then molded using GT-5092 condensation cure silicone rubber base catalyzed with CA-5275 Fast Catalyst silicone curing agent (GT Products, Inc.) with no mold-release. After whole-element molding, the mid-diaphysis of the femur was removed along pre-existing breaks. This region preserves a greater ontogenetic span of the cortex than other areas of the bone and is subject to less remodeling (Stein & Sander, 2009) relative to other regions within the diaphysis. The removed portion of the femur was then molded using Silputty platinum-cured room temperature vulcanizing silicone (Silpak, Inc.). All three whole elements and the mid-diaphyseal femoral segment were then cast using TC-891 A/B rigid polyurethane casting resin pigmented neutral gray with a mix of black (6836) and white (6834) liquid pigments (BJB Enterprises, Inc.). Whole-element casts of the femur have been deposited in the collections at PEFO and the UCMP.

We produced histological thin-sections of fossil specimens using standard fossil histological techniques (e.g., Chinsamy & Raath, 1992; Stein & Sander, 2009; Wilson, 1994), with the following chemical and equipment modifications. The removed mid-diaphyseal portion of the femur and both entire osteoderms (because of their small size) were embedded in Silmar-41 clear polyester casting resin (Interplastic Corporation) catalyzed with methyl ethyl ketone peroxide (Norac, Inc.) at 1% by mass and allowed to cure for 72 h before sectioning. We then cut several sections (1–1.5-mm thick) from the embedded bones using a diamond-tipped wafering blade on a low-speed Isomet lapidary saw (Buehler, Inc.). The femur was sampled transversely through the removed mid-diaphyseal portion, and both osteoderms were sampled longitudinally

along an anterior–posterior axis. PEFO 33940a was sectioned through the dorsal eminence; this part of the osteoderm was not preserved in UCMP 175058, so we sectioned it more medially, where a full cross-section was preserved. We wet-ground the mounting-side of these sections manually using 600/P1200-grit CarbiMet abrasive papers and an EcoMet 3 grinder/polisher (Buehler, Inc.). We mounted the resulting samples to glass slides using water clear 2-ton epoxy (Devcon) and allowed them to cure for at least 24 h. We then wet-ground the slides using CarbiMet abrasive papers of increasing grit size (120/P120, 180/P180, 320/P400, 400/P800, 600/P1200) and an EcoMet 3 grinder/polisher (Buehler, Inc.) at 80–110RPM to optical clarity (~30–50 μm). Opaque areas of the slide were further hand-ground using 600/P1200 CarbiMet papers. We then polished the slides using 5.0 μm aluminum oxide abrasive powder (Buehler, Inc.) and a MicroCloth synthetic polishing cloth (Buehler, Inc.). Copies of slides have been repositied in the collections at PEFO and the UCMP.

We examined slides using an Optiphot-2 Pol light transmission microscope (Nikon) under regular transmitted light and a single plane-polarizing filter, under a full wave tint plate (i.e., in elliptically polarized light; $\lambda = 530 \text{ nm}$), and under crossed plane-polarizing filters. The tint plate and polarizing filters were used to enhance birefringence. Histological descriptions were made from direct observations of slides under the microscope by SW.

Digital photomicrographs of the femur were taken both with and without the above filters using a D300 DSLR camera (Nikon) through an Optiphot-2 Pol light transmission microscope (Nikon) at multiple magnifications (5x, 10x, 25x, and 100x total magnification). All digital photomicrographs were taken as 8-bit jpgs (quality = fine, compression = optimal quality, image size = large/4288x2848 pxl). Our interface program (e.g., for focusing, white balance) was Camera Control Pro 2 (Nikon) running on a Windows 7 (64-bit) computer (HP). We took overlapping digital photographs (overlap 50% by eye in both the X and Y directions) across the entire section at 5x total magnification and radial “transects” of the section (from the endosteal to periosteal surface) at 10x and 25x total magnification, as well as representative images at 100x total magnification. Slides were kept wet with water during photography to increase transparency and image clarity. Images taken at 100x were then adjusted using Photoshop CS5 Extended (Adobe) for brightness and contrast (evenly applied across the entire image) and to add scale bars.

We then assembled photomontages of full cross-sections and the radial “transects” using Autopano Giga 2.0 64Bit (Kolor), with the following settings: Detection settings: detection quality = high, layout = free. Optimization settings: strong (for partial cross-section and radial “transects”)

and gigapixel (for full cross-section), optimizer stages: local approach, strong algorithm, first optimization, clean up control points or links, keep only control points below the error RMS = 2.0, final optimization, advanced distortion. Panorama settings: preferred projection = automatic, preferred extend = clamp to panorama content, initial type of anchor = mono transfer function. Render settings: size = 100%, algorithms: interpolating = bicubic, blending = smartblend, format = jpg, depth = 8 bits, layers = none, DPI = 72. Measurements were made using the analytical features of Photoshop CS5 Extended. Further processing of montaged images (e.g., to adjusting brightness or contrast, or to add text and scale bars) was completed using Photoshop CS5 Extended.

All measurements of the femur were made using the Analysis tools in Photoshop CS5 Extended. We traced LAGs and the periosteal surface using Pen Tool and measured the resulting stroked paths to obtain circumference, total area, circularity, major axis width, and minor axis height. Other measurements (e.g., medullary cavity width and height, osteocyte length) were measured using Ruler Tool. Osteoderm histological slides were imaged in plane and cross-polarized light using a Zeiss Axio Imager.M2m petrographic microscope with accompanying Zen 2 v2.0.0.0 software at the University of Utah.

Digital copies of all images have been repositied at PEFO. Additionally, high-resolution histological images are digitally repositied online for scholarly use at MorphoBank project P620 (<http://MorphoBank.org>).

Our histological descriptions are based on our direct observations of slides under the microscope. We use the histological terminology of Francillon-Vieillot et al. (1990), but with the following clarifications regarding how our diagnoses of certain histological characters were made: Collagen fiber orientation (lamellar, parallel-fibered, woven) was diagnosed using a full tint wave plate (“crossed Nicols”) and/or crossed plane polarizing filters, and confirmed with osteocyte orientation. We determined osteocyte orientation by focusing through the plane of the section under the microscope in order to observe the orientation the long axes of the cells. Lines of arrested growth (LAGs) were diagnosed using two criteria: a break in bone deposition visible at multiple magnifications (determined by focusing through the hypothesized LAG) that continues around all or nearly the entire circumference of the section. Locally, LAGs may grade into annuli (bands of parallel-fibered bone) for short segments, but if these segments extend at least one-third of the circumference, we term it an annulus and not a true LAG.

Two or more lines running parallel to each other in extremely close succession are diagnosed as double, triple, or several LAGs. The individual lines in these LAG “packets” share very subtle changes in morphology that

are not shared by the previous or subsequent LAG, which are separated by more typical (larger) annual zones of deposition. Double and triple LAGs have been reported in other extinct and extant vertebrates (e.g., Botha & Chinsamy, 2004; Castanet, 2006; Guarino & Erismis, 2008; Sanchez et al., 2010), including other archosaurs (e.g., Chinsamy et al., 1998; Chinsamy & Elzanowski, 2001). When measuring LAG circumference for a LAG packet, we measured either the innermost LAG of the packet or the most complete LAG (i.e., the LAG that least graded into an annulus locally).

In addition to the terminology of Francillon-Vieillot et al., 1990, we use the term “vascular orientation” to describe how the long axes of vascular canals are oriented within the element (e.g., longitudinal, radial, circumferential, reticular), and the term “vascular arrangement” to refer to the positions of the canals themselves relative to each other (e.g., longitudinal canals arranged radially). Similarly, the term “osteocyte orientation” refers to how the long axes of osteocytes are oriented relative to the long axis of the bone, and “osteocyte arrangement” refers to the positions of osteocytes relative to each other and/or to vascular canals.

3.4 | Institutional abbreviations

AMNH, American Museum of Natural History, New York, New York, United States; NHMUK PV, The Natural History Museum, Palaeontology Vertebrates, London, United Kingdom; IVPP, Institute of Vertebrate Paleontology and Paleoanthropology, Beijing, China; MCZ, Museum of Comparative Zoology, Harvard University, Cambridge, Massachusetts, United States; MNA, Museum of Northern Arizona, Flagstaff, Arizona, United States; MSM, Arizona Museum of Natural History, Mesa, Arizona, United States; PEFO, Petrified Forest National Park, Arizona, United States; NCSM, North Carolina Museum of Natural Sciences, Raleigh, North Carolina, United States; NM, National Museum, Bloemfontein, South Africa; NMMNH, New Mexico Museum of Natural History and Science, Albuquerque, New Mexico, United States; NSM, Nova Scotia Museum, Halifax, Nova Scotia; PFV, Petrified Forest Vertebrate Locality, Petrified Forest National Park, Arizona, United States; PVL, Fundación Miguel Lillo, San Miguel de Tucumán, Tucumán, Argentina; SMNS, Staatliches Museum für Naturkunde, Stuttgart, Germany; SNSB-BSPG, Staatlich Naturwissenschaftliche Sammlungen Bayerns, Bayerische Staatssammlung für Paläontologie und Geologie, Munich, Germany; TMM, Texas Vertebrate Paleontology Collections, The University of Texas at Austin, Austin, Texas, United States; TTU, Museum of Texas Tech

University, Lubbock, Texas, United States; UCMP, University of California Museum of Paleontology, Berkeley, California, United States; UMMP, University of Michigan Museum of Paleontology, Ann Arbor, Michigan, United States; YPM, Yale Peabody, New Haven, Connecticut, United States; ZPAL, Institute of Paleobiology of the Polish Academy of Science, Warsaw, Poland.

4 | SYSTEMATIC PALEONTOLOGY

Archosauria Cope, 1869, sensu Gauthier & Padian, 1985
 Pseudosuchia Zittel, 1887–1890, sensu Gauthier & Padian, 1985

Suchia Krebs, 1974, sensu Sereno, 1991

Aetosauriformes Hay, 1930 clade nov

4.1 | Definition

The most inclusive clade containing *R. callenderi* Hunt, 1989, *A. geoffreyi* Long & Murry, 1995, *Aetosaurus ferratus* Fraas, 1877, and *Desmotosuchus spurensis* Case, 1922 but not *Rutiodon carolinensis* Emmons, 1856, *Ornithosuchus woodwardi* Newton, 1894, *Postosuchus kirkpatricki* Chatterjee, 1985, *Crocodylus niloticus* Laurenti, 1768, *Poposaurus gracilis* Mehl, 1915, *Erpetosuchus granti* Newton, 1894, or *Passer domesticus* Linnaeus, 1758 (Butler et al., 2014; Marsh et al., 2020; Nesbitt, 2011).

4.2 | Diagnosis

Aetosauriformes (Figure 2) differs from all other archosaur clades in possessing the following unique combination of character states (Nesbitt, 2011; Butler et al., 2014; Marsh et al., 2020; this study): convex distal edge of distal maxillary teeth (shared with some loricatans including crocodylomorphs); rounded and thick facet on the medial side of the posterior process of the squamosal for the paroccipital process (shared with *Turfanosuchus dabanensis*); diapophysis and parapophysis on middle trunk vertebrae expanded on stalks (shared with ornithischian dinosaurs, ornithosuchids, *E. okeeffeae*, and crocodyliforms); radius is shorter than 80% of the length of the humerus (shared with Dinosauria, *Protosuchus richardsoni*, and *Alligator mississippiensis*); and presacral paramedian osteoderms are mediolaterally wider than anteroposteriorly long (shared with *Riojasuchus tenuisiceps*, protosuchid crocodyliforms, phytosaurs, and the archosauriform *V. campi*); lateral osteoderms present throughout most of the carapace (shared with erpetosuchids, *A. geoffreyi* and aetosaurians).

4.3 | *Revueltosaurus* (Hunt, 1989)

Revised diagnosis

We conclude that the diagnosis of the genus is not sustainable and restricted to the genus as originally diagnosed by Hunt (1989) and amended by Heckert et al., (2012) (see reasoning below). Therefore, we only provide a revised diagnosis for *R. callenderi* based on the holotype and referred material.

4.4 | *Revueltosaurus callenderi* (Hunt, 1989)

Revised diagnosis

R. callenderi possesses the following unique combination of character states (autapomorphies marked with an asterisk)

(Butler et al., 2014; Marsh et al., 2020; Nesbitt, 2011): maxillary teeth well inset from the lateral margin of the skull (= buccal emargination) (shared with ornithischian dinosaurs); random patterning on dorsal surface of rectangular paramedian osteoderms (as opposed to radial patterning; shared with *T. coccinarum*); skull length exceeds that of the femur (shared with phytosaurs, proterochampsids, and pterosaurs) where the femur is ~61% the length of the skull; descending process of the nasal fits into a concave socket on the premaxilla (shared with *T. dabanensis*); small external nares (maximum dimension ~1/3 the length of the orbit anteroposterior length)*; posterior process of jugal fits into a V-shaped slot in the quadratojugal*; strongly verticalized parabasisphenoid (basitubera are dorsal to the pterygoid processes) (shared with some loricatans); median pharyngeal recess of the parabasisphenoid divided by a strong vertical ridge*; external surface of the squamosal laterally

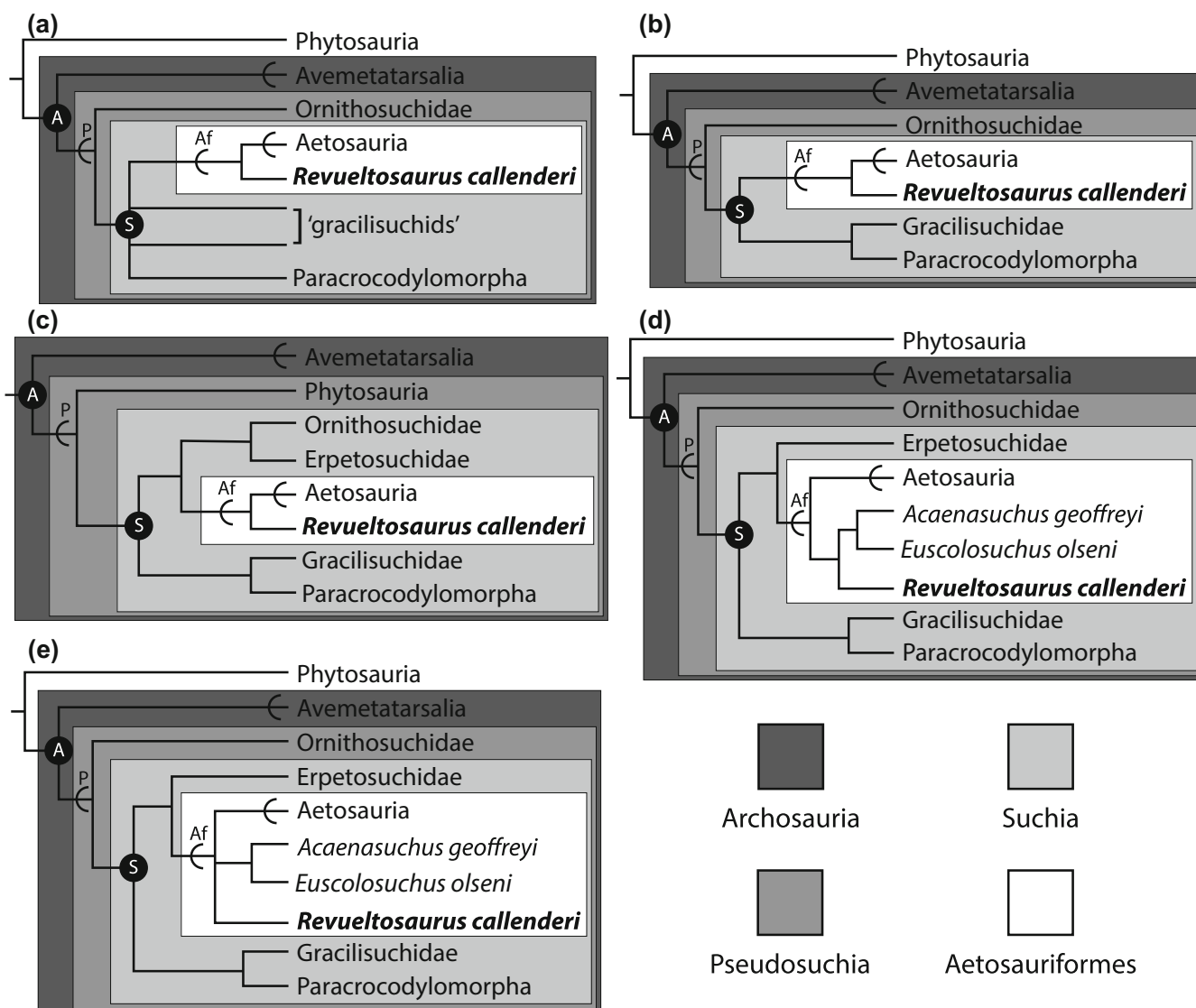


FIGURE 2 Hypothesized evolutionary relationships of *Revueltosaurus callenderi* hypothesized by Nesbitt (2011, a), Butler et al. (2014, b), Ezcurra et al. (2017 supplement, c), Marsh et al. (2020, d), and the revised analysis in this study (e). A, Archosauria; Af, Aetosauriformes; P, Pseudosuchia; S, Suchia

displaced with respect to the quadrate (shared with aetosaurs, *Gracilisuchus stipanicorum*, and *Tarjadia ruthae*); posterior caudal osteoderms fused into a solid tube*; dorsal eminence of the paramedian osteoderms offset laterally from the osteoderm center; lateral osteoderms that are markedly oblong (as opposed to equant or nearly equant) (shared with erpetosuchids); articulating set of ventral osteoderms (shared with aetosaurs, for example, *S. robertsoni*).

4.5 | Holotype

NMMNH P-4957, nearly complete premaxillary tooth.

4.6 | Referred specimens

This osteological description is based primarily on: PEFO 33787, PEFO 33788, partial skull; PEFO 33789, right scapulocoracoid; PEFO 33819, two sacral centra; PEFO 33845, left posterior portion of the iliac blade; PEFO 33847, fused gastralia; PEFO 33848, dorsal rib; PEFO 33861, cervical vertebra; PEFO 33870, incomplete manus; PEFO 33874, left and right frontals; PEFO 33875, sacral centrum; PEFO 33876, partial right ilium; PEFO 33892, right ilium; PEFO 33894, left ilium; PEFO 34056, partial right ilium; PEFO 34269, partial skeleton and skull; PEFO 34273, left tibia; PEFO 34274, left maxilla and lacrimal; and PEFO 34561, nearly complete skull and associated skeleton; PEFO 34570, partial braincase; PEFO 34833, articulated cervical vertebrae; PEFO 36875, nearly complete skull and associated specimen; PEFO 36876, partial skeleton; PEFO 42442/UWBM 116869, mostly complete skeleton; PEFO 38609, complete skull; PEFO 33791, right ilium; and PEFO 33991, right ilium. Additional key specimens include NMMNH P-16932, partial skeleton (Hunt et al., 2005), and other NMMNH specimens listed in Heckert (2002). The single element specimens listed above match elements found in the partial associated skeletons and thus are unambiguously assignable to *Reveultosaurus callenderi*. A full list of specimens referred to *R. callenderi* is provided in Data S1 and linear measurements of relevant specimens are provided in Data S2. Select 3D models from PEFO 34561 are provided in Data S4.

4.7 | Type locality and age

Reuelto Creek (NMMNH L-001), Bull Canyon Formation, Dockum Group, Quay County, New Mexico, United States. Upper Triassic (mid-Norian, Marsh & Parker, 2020); Revuelitian holochronozone (Martz & Parker, 2017).

4.8 | Referred localities and age

The geographic and stratigraphic relationships of all referred localities at PEFO are shown in Figure 1: The Coprolite Layer (PFV 396), and Thunderstorm Ridge (PFV 456), upper part of the Blue Mesa Member, Chinle Formation; The Bowman Site (PFV 089), upper part of the Jim Camp Wash beds, Sonsela Member, Chinle Formation; Lacey Point SW1 (PFV 027), RAP Hill (PFV 216), The Giving Site (PFV 231), Jeremiah's Perch (PFV 278), The *Reveultosaurus* Quarry (PFV 297), and The *Reveultosaurus* Quarry SW (PFV 414) just above Painted Desert Sandstone 3, Petrified Forest Member, Chinle Formation; Dinosaur Hill (PFV 040), Zuni Well Mound (PFV 215), and RAP Hill N (PFV 277), just above Painted Desert Sandstone 4, Petrified Forest Member, Chinle Formation (Martz et al., 2012; Parker & Martz, 2011). Specific locality data are kept in the museum archives at PEFO.

The uppermost part of the Blue Mesa Member containing *Reveultosaurus* fossils is dated to between 218.5 and 216.5 Ma depending on the preferred age model (Kent et al., 2019; Rasmussen et al., 2020), whereas the single Sonsela locality in the Jim Camp Wash beds dates to 215–214 Ma (Rasmussen et al., 2020). The PEFO localities in the Petrified Forest Member are from the middle third of the member, and date to between 212 and 210 Ma in age (Kent et al., 2018, 2019; Ramezani et al., 2011; Rasmussen et al., 2020). All of the PEFO localities are Upper Triassic (Norian) in age and occur in the Adamanian and Revuelitian holochronozones (Martz & Parker, 2017).

5 | OSTEOLOGICAL DESCRIPTION

5.1 | Skull reconstruction

The exquisite three-dimensionally preserved skull elements of PEFO 34561 allow for an accurate reconstruction of the skull of *R. callenderi*. As mentioned above, plaster casts were made of all of the individual elements, and these casts easily fit together to form the current reconstruction (Figures 3a, b). This reconstruction is further supported by a slightly crushed, articulated skull (PEFO 38609; Figures 3c, d). The current reconstruction differs from the initial one presented by Parker et al. (2005) in the following ways: (a) the skull is dorsoventrally deeper, anteroposteriorly shorter, and broader mediolaterally; (b) the prefrontal, postorbital, and lacrimal were originally misidentified based only on isolated and/or crushed elements; and (c) the morphology of the anterior portion of the premaxillae, including the external nares, can now be accurately reconstructed. Moreover, PEFO 34561 preserves much of the mandible,

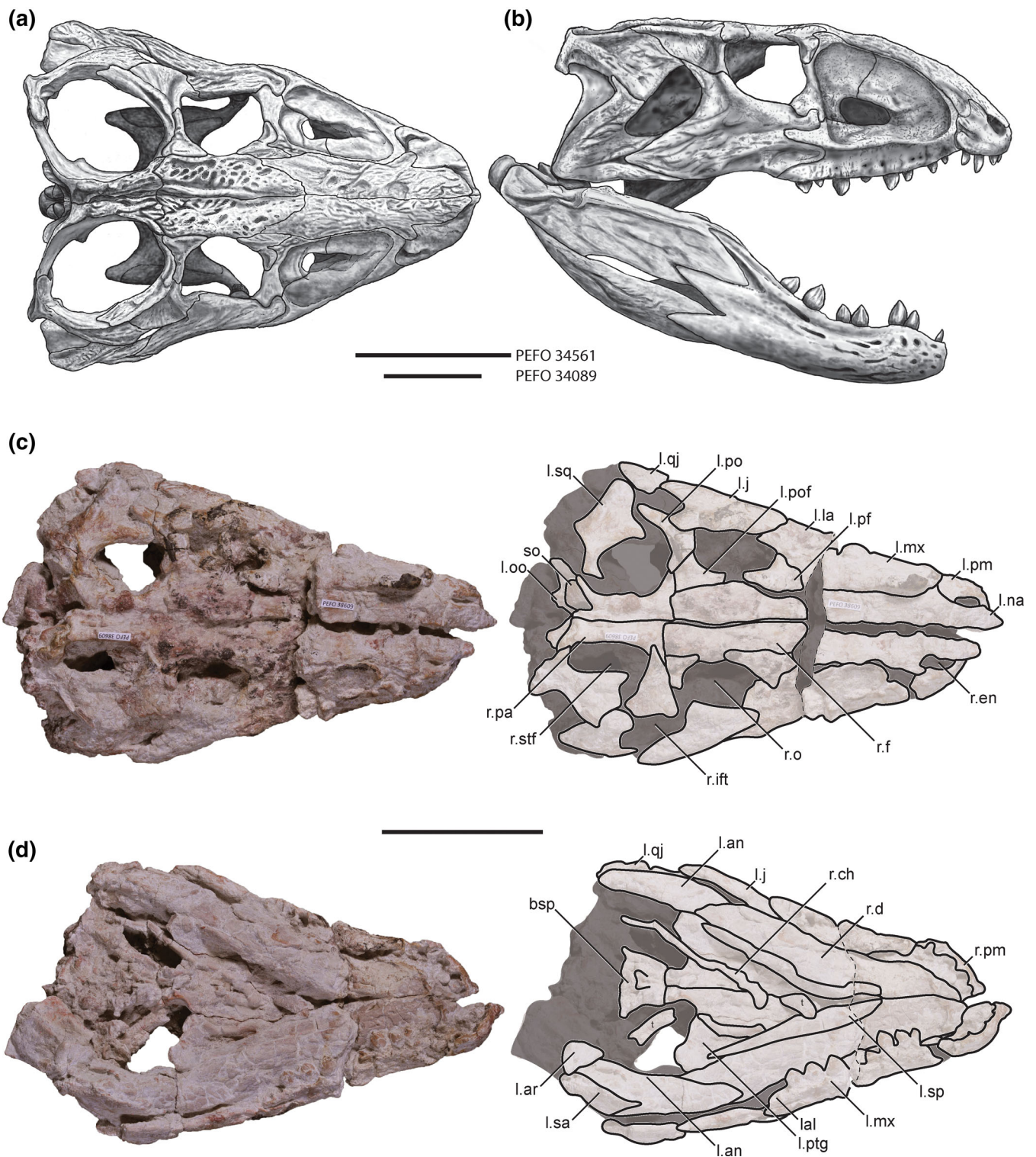


FIGURE 3 Reconstruction of the skull and mandible of *Revueltosaurus callenderi* (a, b) based off of PEFO 34561 and PEFO 34089 and articulated skull and mandibles referred to *R. callenderi* (c, d, PEFO 38609) in dorsal (a, c), ventral (d), and lateral view (b). an, angular; ar, articular; bsp, basisphenoid; ch, ceratohyal; d, dentary; en, external naris; f, frontal; ift, infratemporal fenestra; j, jugal; l., left; la, lacrimal; lal, last alveolus; mx, maxilla; na, nasal; o, orbit; oo, otoccipital; pa, parietal; pf, prefrontal; pm, premaxilla; po, postorbital; pof, postfrontal; qj, quadratojugal; r., right; sa, surangular; so, supraoccipital; sp, splenial; sq, squamosal; stf, supratemporal fenestra; t, tooth. Dashed lines indicate a fault, which obscures the antorbital fenestra. Scale bars equal 5 cm

palate, and occiput, which were previously only known from distorted elements.

One particular feature of note is the relative size of the skull compared to the individual postcranial elements. The anteroposterior length of the reconstructed skull of PEFO 34561 is 153 mm, compared to 94 mm for the femur length of the same individual. Triassic pseudosuchians (potentially excluding phytosaurs) generally have a skull length of less than two-thirds of the femur length (Nesbitt, 2011, p. 135). Having a skull length greater than the femur length is a distinguishing feature of *R. callenderi* among non-crocodyliform Pseudosuchia, shared potentially with gracilisuchids, erpetosuchids, and ornithosuchids (Butler et al., 2014; Ezcurra et al., 2017; von Baczko et al., 2020). Aetosaurians have a skull length less than the femur length (Desojo et al., 2013), and this feature presently cannot be ascertained for *A. geoffreyi* (Marsh et al., 2020).

5.2 | Skull

Isolated and associated skull elements and skulls are common at PFV 297. The best-preserved skull is from PEFO 34561, which provides the basis for this description, whereas other specimens that supplement the description are noted. Nearly complete, mostly articulated skulls are known from PEFO 36875 and PEFO 38609, which confirm the accuracy of the skull reconstruction from PEFO 34561.

5.2.1 | Premaxilla

The premaxillae are well-preserved in PEFO 34561, and the left side is preserved in articulation with the nasal (Figures 4a, b). The overall morphology of the premaxilla of *R. callenderi* is unique in comparison to other archosauriforms with its greatly reduced external naris (maximum dimension $\sim 1/3$ the length of the orbit anteroposterior length). The premaxilla holds five teeth in deep alveoli. Tooth size increases mesially where the more mesial teeth are nearly double the basal circumference of the distalmost premaxillary tooth. However, the mesialmost tooth does not follow this trend, and, instead, is similar in size to the distalmost premaxillary tooth. The tooth roots are exposed more dorsally on the lingual side relative to the labial side.

A small posteriorly projecting process on the anteromedial side of the premaxilla articulates with the palatal process of the maxilla. The medial surface of this premaxillary process meets an identical process on the opposite premaxilla. In articulation, the left and right

premaxillae meet anteroventral to the external naris at an anteroposteriorly short, triangular symphysis and together form a broad, gently rounded “snout” in dorsal view. The external surface of the premaxilla is smooth. There is a concavity between the main body of the premaxilla and the anterodorsal process that connects with the external nares.

The anterodorsal process of the premaxilla is short, thin, and arcs dorsally to contact the anterior portion of the nasal (Figure 4a). In lateral view, the posterodorsal process is triangular and slightly recurved posteriorly at its tip. This entire process inserts into a triangular slot of the nasal between the anterior portion of the nasal and the ventral process (= descending process) of the nasal. The gracilisuchids *T. dabanensis*, *G. stipanicorum*, and possibly *Yonghesuchus sangbiensis* share this condition (Butler et al., 2014; Nesbitt, 2011; Wu & Russell, 2001), but in gracilisuchids the process is straight and anteroposteriorly narrow, whereas in *R. callenderi* it is broad and slightly recurved at its tip. The anterior side of the posterodorsal process and part of the medial surface preserves a rugose surface that is similar to that present on the nasal. A fossa is located on the posterior side of the posterodorsal process in which the rounded ventral process of the nasal fits and creates an immobile articulation.

The premaxilla forms the anterior, posterior, and ventral margins of the external naris. The ventral process of the nasal and the posterodorsal process of the premaxilla meet and exclude the maxilla from participating in the external naris (Figure 4a). Exclusion of the maxilla from the margin of the external naris is plesiomorphic among early-diverging archosaurs (Nesbitt, 2011); however, in the loricatan *Batrachotomus kupferzellensis*, aetosaurs such as *S. robertsoni*, and the ornithosuchid *O. woodwardi*, the maxilla forms a portion of the narial margin (Gower, 1999; Schoch, 2007; Walker, 1961, 1964). Some aetosaurs (e.g., *Aetosauroides scagliai*; PVL 2052, PVL 2059) possess the plesiomorphic condition (Desojo & Ezcurra, 2011), as do *G. stipanicorum* (Butler et al., 2014) and *T. ruthae* (Ezcurra et al., 2017).

The posterior portion of the body of the premaxilla articulates broadly with the anteroventral portion of the maxilla, and there is no gap at the ventral margin between the two elements. The lateral surface of the premaxilla is marked by a prominent groove that originates along the premaxillary/maxillary border ventral to the articulation with the nasal and ends just dorsal to the third premaxillary tooth position (Figure 4a). It is uncertain if this groove is homologous to the small foramina formed by the junction between the premaxilla and the maxilla as in *P. kirkpatricki*, *S. inexpectatus*, *B. kupferzellensis*, and *Herrerasaurus ischigualastensis* (Nesbitt, 2011).

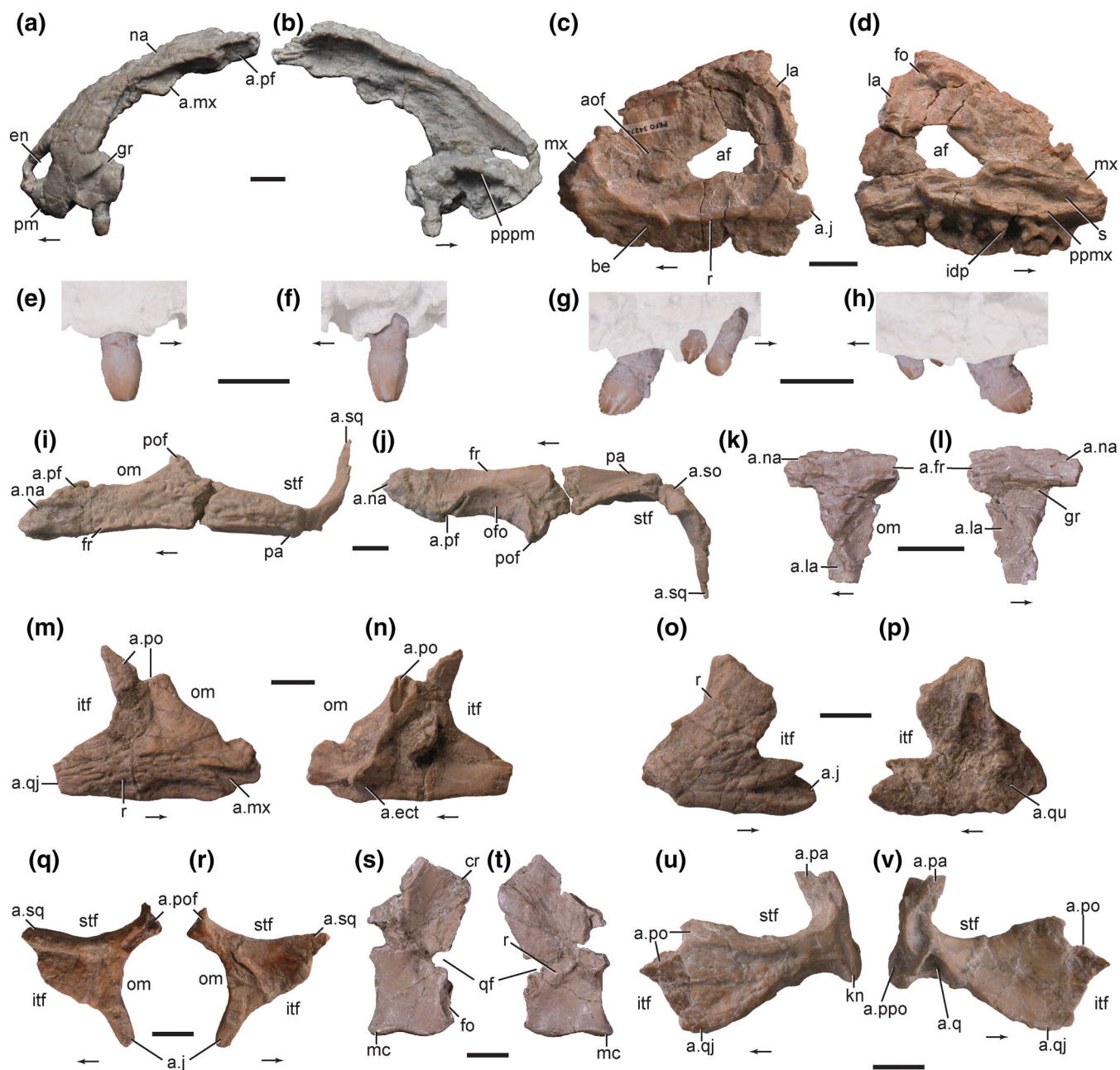


FIGURE 4 Skull elements of specimens referred to *Revueltasaurus callenderi*. Left nasal and premaxilla (a, b, PEFO 34561), left maxilla and lacrimal (c, d, PEFO 34274), right premaxilla and tooth (e, f, PEFO 34561), right maxilla and teeth (g, h, PEFO 34561), right frontal postfrontal, and parietal (i, j, PEFO 34561), left prefrontal (k, l), right jugal (m, n, PEFO 34561), right quadratojugal (o, p, PEFO 34561), right postorbital (q, r, PEFO 34561), right quadrate (s, t, PEFO 34561), and left squamosal (u, v, PEFO 34561) in lateral (a, c, e, g, i, k, m, q, u), medial (b, d, f, h, j, l, n, r, v), dorsal (i), ventral (j), posterior (s), and anterior view (t). a., articulates with; af, antorbital fenestra; aof, antorbital fossa; be, buccal emargination; cr, crest; ect, ectopterygoid; en, external naris; fo, fossa; gr, groove; idp, interdental plates; itf, infratemporal fenestra; j, jugal; kn, knob; la, lacrimal; mc, medial condyle; mx, maxilla; na, nasal; ofo, orbital fossa; om, orbital margin; pa, parietal; pf, prefrontal; pm, premaxilla; po, postorbital; pof, postfrontal; ppmx, palatal process of maxilla; ppo, paroccipital process of the otoccipital; pppm, palatal process of the premaxilla; q, quadrate; qf, quadrate foramen; qj, quadratojugal; r, ridge; sq, squamosal; s, sulcus; stf, supratemporal fenestra. Scale bars equal 1 cm, arrows point in anterior direction

5.2.2 | Nasal

The elongated nasal (at least eight times anteroposteriorly longer than mediolaterally wide) is covered with faint

longitudinally oriented grooves and pits. The ventral margin of this element (~4–5 mm thick at the midline of PEFO 34561) articulates with the lacrimal posteriorly and with the ascending process of the maxilla anteriorly (Figure 4a).

The lateral edge of the nasal lacks the distinct lateral ridge present in gracilisuchids (Butler et al., 2014). Furthermore, the lateral and dorsal surfaces of the nasal of *R. callenderi* grade into each other rather than an abrupt change of slope between the nasal ridge and flat dorsal surface as in gracilisuchids (Butler et al., 2014). The anterior portion of the nasal is bifurcated; the medial process extends further anteriorly and tapers strongly medially to contact the thin anterodorsal process of the premaxilla and forms the dorsal margin of the external naris, whereas the medial process is a subrounded descending ventral process that fits into a socket in the premaxilla. This bifurcation forms a deep triangular slot that receives the posterior ascending process of the premaxilla. In some specimens (e.g., PEFO 34561), the suture between the premaxilla and nasal is nearly closed. This bifurcation of the anterior portion of the nasal for reception of the ascending process of the premaxilla is shared by *R. callenderi* and gracilisuchids in relation to other pseudosuchians, but is also similar to the condition found in erythrosuchids such as *Erythrosuchus africanus* (NM QS1473; Gower, 2003: fig. 7b). The posterior articulation with the frontal tapers posterolaterally; thus, both nasals form a “V” in dorsal view.

5.2.3 | Maxilla

The best-preserved maxilla, PEFO 34274, is from the left side and was found isolated but articulated with the corresponding lacrimal (Figure 4c, d). This maxilla preserves nine alveoli. The alveoli increase in circumference distally, whereas alveolus three, four, and five are subequal and are the largest in the maxillary row. Distally, alveoli 6–9 decrease in circumference. The largest alveoli correspond with the greatest mediolateral thickness of the maxilla. The maxillary tooth roots are more exposed lingually, similarly to the premaxillary teeth, and interdental plates separate the alveoli.

The largely concave anterodorsal (= ascending) process is mediolaterally slender relative to the body of the maxilla. A large antorbital fossa occupies much of its lateral surface, similar to gracilisuchids, aetosaurs, and erpetosuchids (Butler et al., 2014; Nesbitt, 2011; Nesbitt, Stocker, et al., 2018). The anterior rim of the antorbital fossa is separated from the anterior margin of the maxilla by a distinct, sharp ridge. The posteriormost portion of the anterodorsal process is dorsoventrally expanded and meets the anterior portion of the lacrimal dorsal to the antorbital fenestra, excluding the nasal from participation in the fenestra margin. The dorsal margin of the anterodorsal process has a slight, rugose rim where it meets the ventral margin of the nasal, thus the nasal does

not participate in the antorbital fossa unlike the condition in gracilisuchids (Butler et al., 2014).

The lateral surface of the maxilla includes one foramen per alveolus. A large anteroposteriorly oriented ridge (= maxillary ridge of Irmis, Parker, et al., 2007) divides the body of the maxilla into two parts: the antorbital fossa lies dorsal to the ridge, and a ventral portion below the ridge. The ventral portion is inset medially to create a tooth row well medial of the lateral extent of the maxilla (= buccal emargination), a characteristic that is unique to *R. callenderi* among pseudosuchians and convergent with early-diverging ornithischian dinosaurs (Butler et al., 2008; Irmis, Parker, et al., 2007; Nesbitt, 2011). In lateral view, the ventral margin bows so that the ventral edge adjacent to the middle maxillary alveoli is more ventral than the ventral edge adjacent to the anterior and just slightly more ventral than the posterior alveoli.

The articulation of the maxilla with the premaxilla is preserved in PEFO 38609 and can be inferred from isolated elements. The anterior portion of the maxilla contacts the premaxilla anteriorly and anteroventrally where it fits between the posterodorsal surface of the premaxilla and the ventrolateral surface of the nasal. Medially, the palatal process of the maxilla projects anteriorly to dorsally overlap the medial process of the premaxilla. The medial surface of the maxilla bears a long anteroposteriorly trending sulcus, bounded by distinct ridges, which extends from the anterior end of the maxilla to ventral to the posterior end of the antorbital fenestra; this sulcus articulates with the palatine.

The posterior portion of the maxilla articulates with the jugal and the lacrimal. The exact articulation of the posterior portion of the maxilla and the anterior portion of the lacrimal is unclear. However, PEFO 34561 also preserves these elements in articulation, and although the maxilla-lacrimal contact is not clear (Figure 4c), the anterior border of the jugal is distinct enough to establish that the lacrimal and the maxilla exclude the jugal from participating in the margin of the antorbital fossa or the antorbital fenestra. This differs from the condition in many archosauriforms (e.g., *Proterosuchus fergusi*, *A. ferratus*, *E. okeeffeae*), but is similar to what is present in *G. stipanicorum* (MCZ 4117), where a posterodorsal process of the maxilla meets the lacrimal, excluding the jugal (Butler et al., 2014). The articulation of the maxilla with the jugal is complex in *R. callenderi*; a posteriorly projecting process of the lateral side of the maxilla fits into a slot on the lateral side of the jugal, and a posteriorly projecting process of the medial side of the maxilla fits into a slot on the ventromedial surface of the jugal and abuts posteriorly with a medially expanded area

where the jugal meets the ectopterygoid. The last alveolus of the maxilla is surrounded by the jugal on its lateral and medial sides.

5.2.4 | Lacrimal

Both lacrimals are preserved in PEFO 34561, the left still in articulation with the jugal and maxilla, but the element is best preserved in PEFO 34274 (Figures 4c, d). The pillar-like main body is mediolaterally thicker relative to the rest of the element and forms much of the anterior margin of the orbit. The orientation of the pillar is nearly dorsoventral. The ventral portion is expanded anteroposteriorly and has a broad posteroventral contact with the anterodorsal edge of the jugal. In particular, the lateral surface of the jugal bears a small basin that receives a rounded projection of the lacrimal. Anteriorly, the ventral portion of the lacrimal pillar contacts the maxilla posterior to the antorbital fenestra.

The dorsal portion of the lacrimal consists of a dorsoventrally broad, but mediolaterally thin, sheet of bone that projects anteriorly forming the dorsal border of the antorbital fenestra (Figure 4c). Anteriorly, this thin process contacts the ascending process of the maxilla and has a beveled dorsal surface that underlies the ventrolateral edge of the nasal. PEFO 34274 shows that the medial lip of this beveled edge forms the thin dorsal border of the antorbital fossa. Indeed, the antorbital fossa covers most of the lateral side of the lacrimal. The posterodorsal portion of the rim that defines the antorbital fossa gently arcs from the dorsal and near-horizontal portion to the posterior and vertical portion, whereas in gracilisuchids (e.g., *G. stipanicorum*), this transition has a much sharper angle. The posterodorsal edge of the lacrimal has a shallow, but distinct, concave embayment for the articulation with the prefrontal. Dorsal to this is a short posterior projection that fits into a slot on the medial side of the prefrontal (Figure 3b). The dorsal portion of the medial side of the lacrimal bears a sharp anteroposteriorly directed ridge that meets the thickened posteroventral edge of the nasal. Ventral to this ridge is a small, but distinct posteroventrally opening fossa.

Overall, the lacrimal of *R. callenderi* is similar to that of aetosaurs, in particular the isolated element from the holotype of *Stagonolepis olenkae* (ZPAL AbIII/1967; Sulej, 2010: fig. 2j–k). Similarities include the mediolaterally thickened posterior pillar that forms much of the orbital margin, and the anterior portion is a flat sheet of bone that bears a large portion of the antorbital fossa. A similar lacrimal with the thickened posterior pillar is in *G. stipanicorum* (MCZ 4117) and possibly the other gracilisuchids (Butler et al., 2014). The lacrimal of *R. callenderi* differs from that of *P. kirkpatricki* (TTU P-9000; Weinbaum, 2011) in that

the prefrontal-lacrimal contact is much more extensive in *P. kirkpatricki* limiting the contribution of the lacrimal to the orbit.

5.2.5 | Frontal

The frontals are often found articulated together in preserved specimens (e.g., PEFO 33787; PEFO 33874) or often with the articulated parietal and postfrontal (e.g., PEFO 34561; Figures 4i, j). The frontal is dorsoventrally thickened (~5 mm thick at the midline versus minimum width at the orbit = 12 mm in PEFO 34561) and anteroposteriorly elongate (three times longer than wide), and the dorsal surface is ornamented with pits and grooves that tend to be deeper and more subcircular than those present on the nasal. A mediolaterally thin, raised, longitudinal ridge is present on the dorsal surface for the entire length of the medial edge. A similar feature is present in loricatans (e.g., *Dromicosuchus grallator*, *P. kirkpatricki*; Nesbitt, 2011). There is no distinct raised rim (= orbital ridge of Stocker, 2010) outlining the dorsal margin of the orbit as in phytosaurs.

The anterior part of the lateral edge of the frontal tapers medially where it contacts the nasal, a condition also shared with paracrocodylomorphs (Nesbitt, 2011). A rugose articular surface for the prefrontal occurs immediately posterior of the nasal contact. The lateral edge is slightly concave where it forms the dorsal margin of the orbit immediately posterior to the prefrontal articulation. Posterior to the orbital margin of the frontal in medial view, a triangular articular surface marks the contact with the postfrontal. In dorsal view, the medial edge of the frontal is straight and bears faint striations on the midline surface; a raised ridge extending along this surface on the left frontal fits into a groove on the right element. Posteriorly, the frontal articulates with the equally wide parietal in an interdigitating suture just posterior to the articulation with the postfrontal (Figures 4i, j). Ventrally, the frontal is mostly smooth except for a large distinctly rimmed orbital fossa that occupies much of the medial surface (Figure 4j), and faint longitudinal striations at the anterior end. These striations may indicate slight underlapping of the frontal by the nasal that also occurs in *Longosuchus meadei* (TMM 31185-98). The ventral surface of the frontal is slightly concave anteromedial to the orbital fossa, representing the position of the olfactory bulbs.

5.2.6 | Parietal

The parietal is a dorsoventrally thick, “sickle-shaped” bone (in dorsal view) with an ornamented dorsal surface

bearing a patterning of incised grooves and pits similar to that on the frontal (Figures 4i, j). The parietal articulates with the frontal in a mediolaterally oriented interdigitating suture. The paired parietals are fully or partially coossified in larger specimens (e.g., PEFO 33787), whereas in smaller specimens (e.g., PEFO 34561, PEFO 34269) the parietal sutures are open.

Anterolaterally, the parietal barely contacts the postfrontal posterior to a continuous articulation surface between the frontal and postfrontal, and the postorbital also has a very slight contact with the parietal (Figure 3a). The midline margin of the parietal is straight with a thickened articular surface for its sister element, with striations and a raised ridge and groove contact between the elements, as seen on the frontal. The medial longitudinal ridge on the dorsal surface of the frontal continues posteriorly along the medial margin of the parietal. Thus, the dorsal surface at the midline of the parietals has a low longitudinal furrow flanked by two ridges that border the medial margins of the supratemporal fenestra similar to what is present in crocodylomorphs such as *D. grallator*; however, unlike the condition in *D. grallator* there is no supratemporal fossa present on the dorsal surface of the parietal. Lateral to the midline, dorsally expanded ridges mark the supratemporal edge. This ridge originates at the parietal–frontal border and extends onto the posterolateral processes.

When the parietals are articulated (Figure 3a), the occipital margin is V-shaped in dorsal view. Posterior to the edge of the medial margin articular surface, the parietal curves sharply laterally, providing the “sickle-shape” described above; this laterally curved process rapidly thins and tapers to a point. This distal point fits into a distinct groove on the posteromedial portion of the squamosal. The posterior margin of the process has a concave fossa contributing to the occipital plate. The conjoined parietals form an arch in posterior view that articulated with the supraoccipital. *R. callenderi* does not possess a parietal foramen.

The lateral margin of the parietal is smooth, forming the medial and posteromedial margins of the supratemporal fenestra. Anteriorly, the ventral surface is flat and has the same thickness as the frontal. The largely concave ventral surface bears a sharp, lateral ridge anteriorly that articulates with the laterosphenoid. Posterior to this, where the element begins to sharply curve laterally, this lateral ridge is deeply notched ventrally adjacent to a subrectangular embayment of the ventral surface of the main parietal body. This is the articulation surface for the supraoccipital and is very similar to what is present in *B. kupferzellensis* (SMNS 80260; Gower, 1999).

Larger specimens of *R. callenderi* (e.g., PEFO 33787) also have fully coossified parietals even when the frontals are separated along the midline in the same specimen.

Thus, PEFO 33787 appears to have fully coossified parietals, coossified frontal–parietal sutures, but open frontal–frontal sutures. Interestingly, other smaller specimens (e.g., PEFO 34269; PEFO 33898) have fused frontal–parietal sutures, but unfused parietals and unfused frontals. The smaller PEFO 34561 has separate parietals and frontals, but the frontal–parietal suture of the left side is coossified, whereas the frontal–parietal suture of the right side is not. The largest specimen in the collection (PEFO 33074) has coossified frontals with the suture apparent as only a thin line on the ventral surface. This specimen also appears to have had coossified parietals, although they have been broken away and are not completely preserved. Thus, it appears that through ontogeny the frontal–parietal sutures coossify first, followed by the parietals and then the frontals. Nesbitt et al. (2011) noted that in some non-crocodyliform crocodylomorphs (e.g., *Sphenosuchus acutus*) and in crocodyliforms (e.g., *P. richardsoni*) the parietals are completely coossified in presumed adult individuals.

5.2.7 | Postfrontal

The postfrontal is a small, thickened, triangular element with a sculptured dorsal surface marked with grooves and pits, that is often recovered articulated with the frontal (Figures 4i, j). In medial view, there is a triangular and rugose articular surface that articulates with the frontal and parietal; this suture is straight in dorsal view. On the posterior side, an articular surface for the postorbital forms a right angle with the frontal–parietal articular edge. The anterolateral edge in this triangular element is smooth and deeply concave as it forms a portion of the orbital margin and the associated orbital fossa on the ventral surface. The postorbital is excluded from the supratemporal fenestra by the junction of the parietal and the postorbital (Figures 3a, b).

5.2.8 | Prefrontal

The prefrontal is shaped like the number “7” in lateral view with a distinct rugose dorsal rim that articulates medially with the anterior portion of the frontal (Figure 4i). The posterior portion of the ventral process forms the anterodorsal margin of the orbit and has a smooth, posterolaterally facing, and slightly concave surface forming a distinct orbital fossa. The anterior margin of the ventral process is rugose and contacts the posterior portion of the lacrimal. There is a distinct groove for the reception of a posterior projection of the lacrimal ventral to the grooved dorsal rim. The dorsal rim projects slightly

anterior to this articulation. The prefrontal of *R. callenderi* lacks the ventromedial process that extends to the ectopterygoid found in crocodylomorphs and at least some aetosaurs (e.g., *L. meadei*, *S. robertsoni* Gower & Walker, 2002; Nesbitt, 2011).

5.2.9 | Jugal

The jugal is triradiate with anterior, posterodorsal, and posterior processes (Figures 4m, n). The lateral surface of the jugal is ornamented with a rugose pattern of pits and elongate grooves, and the most distinct ornamentation is located on the main body of the jugal on a broad anteroposteriorly trending ridge. This broad ridge on the lateral face is a continuation of the maxillary ridge and extends from the anteriormost portion to the posterior tip. The anterodorsal margin is concave in lateral view and forms the entire posteroventral edge of the orbit (Figure 4n). The ventral margin is straight in lateral view. The anterior process possesses a triangular slot on the lateral surface that receives the posterior process of the maxilla (see above); this slot is located on the broad ridge on the lateral surface. Dorsal to the small slot is a small dorsolaterally facing basin that receives the ventral margin of the lacrimal, thus excluding the jugal from participation with the antorbital fenestra (Figure 4n).

The posterior process of the jugal tapers and fits into a slot in the lateral surface of the quadratojugal. The dorsal surface of this process forms the anteroventral margin of the lateral temporal fenestra, and the posterior tip of the jugal is present at the level of the posterior margin of the lateral temporal fenestra.

The posterodorsal process forms the tallest portion of the jugal with the tapering apex being slightly recurved posteriorly. This projection underlies the posterior part of the margin of the postorbital; this slight overlap almost excludes the postorbital from entering the lateral temporal fenestra (Figure 3b). The lateral surface of the posterodorsal process bears a faint longitudinal sulcus that is nearly dorsoventrally oriented, which is a continuation of the sulcus on the lateral surface of the postorbital (Figure 3b). The anterior portion of the posterodorsal process meets the ventral surface of the postorbital, receiving an elongate anteroventral process of the postorbital in a distinct groove on the medial surface of the jugal. A ventrally projecting ridge originates from the ventral portion of this groove and meets the distinct posterolaterally facing pedicel that articulates with the ectopterygoid (Figure 4n). A shallow dorsal fossa is located dorsal to the surface of articulation with the ectopterygoid.

Overall, the jugal of *R. callenderi* is a very robust element, differing significantly from the more gracile, dorsolaterally thinner element found in the majority of archosauriforms and close relatives (e.g., gracilisuchids) with the exception of the rauisuchids (sensu Nesbitt, 2011; e.g., *P. kirkpatricki*, *Saurosuchus galilei*). *R. callenderi* also shares with *P. kirkpatricki* the broad and distinct maxillary ridge ventral to the antorbital fossa that extends posteriorly across much of the jugal. However, the jugal of *R. callenderi* differs from that of rauisuchids in possessing the triangular anterior projection that inserts into the lateral face of the maxilla.

5.2.10 | Quadratojugal

The L-shaped quadratojugal is covered laterally by a rugose pattern similar to that of the squamosal and jugal (Figure 4o). A slight ridge on the posterodorsal margin of the dorsal process articulates in a slot on the anteroventral margin of the squamosal. Posterior to this there is a shallow fossa that is overlapped by the anterolateral edge of the quadrate. The ventral tip of the fossa is the anterior border of the quadrate foramen. The posteroventral corner of the quadratojugal forms a continuous surface with the lateral portion of the quadrate, fitting into a fossa on the lateral margin of the latter element. The quadratojugal forms the posteroventral corner of the lateral temporal fenestra in *R. callenderi*.

Anteriorly, the tapered posterior process of the jugal inserts into a triangular slot on the lateral surface of the quadratojugal (Figure 4o). This style of articulation is also present in *P. kirkpatricki* (TTU P-9002; Weinbaum, 2011: fig. 13). A similar articulation style occurs in *A. ferratus* and *Paratypothorax andressorum* (SMNS 19003; Schoch & Desojo, 2016), where a sub-triangular posterior process of the jugal inserts into an embayment in the anteroventral margin of the quadratojugal ventral to the lateral temporal fenestra. In these taxa, a small anteroventral process of the quadratojugal underlaps the jugal (Schoch, 2007). A similar articulation also occurs in the doswelliid archosauriform *Rugarhychos sixmilensis* (Wynd et al., 2020) suggesting this character state may be plesiomorphic.

5.2.11 | Postorbital

The postorbital is a triradiate bone with an ornamented lateral surface and three distinct processes (Figures 4q, r). The anterodorsal process has a distinct lateral slot that receives the ventral and posterior portion of the postfrontal, the posterodorsal process articulates with the

anterodorsal margin of the squamosal, and the ventral process fits into a slot on the anterior and medial surface of the posterodorsal process of the jugal. The dorsal margin is broadly curved and possesses a distinct ridge that forms the anterolateral margin of the supratemporal fenestra. The curved anterior margin has a weaker ridge, forming the posterodorsal margin of the orbit. The strong dorsal ridge, which extends posteriorly onto the squamosal, is not found in aetosaurs (e.g., *Desmatosuchus smalli*, TTU P9024-; *T. coccinarum*, PEFO 38001). It is also probably absent in *A. geoffreyi* (UCMP 156046), which does not preserve the postorbital, but does have the squamosal and lacks this ridge. *D. grallator* has a similar dorsal ridge on the postorbital and squamosal (Sues et al., 2003).

The anteroventral portion of the squamosal and posterodorsal process of the jugal nearly meets along the posteroventral edge of the postorbital, almost excluding this element from participation in the lateral temporal fenestra (Figure 3b). This near exclusion is not unique to *R. callenderi* because it also occurs in *P. kirkpatricki* (Weinbaum, 2011), and the participation is extremely limited in aetosaurs (e.g., *A. ferratus*) and the crocodylomorph *D. grallator* (Nesbitt, 2011; Schoch, 2007).

The triangular element originally interpreted as the lacrimal by Parker et al. (2005: fig. 2) is actually an isolated postorbital recovered with the skull of PEFO 33787. The anterior portion of the left squamosal in Parker et al. (2005: fig. 2b) is actually an articulated postorbital.

5.2.12 | Quadrate

The quadrate is preserved in PEFO 34561 (Figure 4s, t), and the quadrates are obscured in PEFO 38609 (Figures 3c, d). The quadrate body is a solid, dorsoventrally tall bone that lacks fenestration and slopes posteroventrally, differing from the condition in shuvosaurids and aetosaurs where the quadrate slopes anteroventrally (Nesbitt, 2007).

A deep dorsoventrally oriented fossa is present posterolateral to the lateral flange (Figure 4s). The pterygoid flange is not well-preserved in PEFO 34561, but the thickened base of the flange occurs on the right element just dorsal to the medial condyle along the medial edge of the quadrate.

A thin and elongate crest projects anteroventrally and laterally from the dorsal end of the quadrate, and its beveled medial edge underlies the ventral surface of the squamosal providing a secondary squamosal/quadrate contact. As a result, we hypothesize that the quadrate was immobile. The anterior edge of this crest arcs posteriorly when it contacts the quadratojugal and inserts into a distinct fossa on the posterodorsal portion of the

quadratojugal. A quadrate foramen is located on the lateral margin of the quadrate (Figures 4s, t), just dorsal to an elongate fossa on the lateral side of the distal condyles that receives a tongue of the quadratojugal.

The ventral articular surface bears two convex surfaces divided by a concave surface. The medial condyle is large and expanded anteromedially compared to the lateral condyle.

5.2.13 | Squamosal

The morphology and laterally facing orientation of the squamosal is extremely similar to that of aetosaurs such as *S. robertsoni*, *A. ferratus*, *P. andressorum*, and *D. spurensis* (Figure 4u, v; Walker, 1961: fig. 2; Small, 2002: fig. 2; Schoch, 2007: fig. 8; Schoch & Desojo, 2016: fig. 4). The oddly-shaped squamosal (described as “sword-like” for *A. ferratus* by Schoch, 2007) forms the posterodorsal margin of the supratemporal fenestra. *T. ruthae* also has a laterally oriented squamosal; however, *R. callenderi* and aetosaurs lack the pronounced ventral projection found in that taxon (Ezcurra et al., 2017).

The squamosal bears three processes, an anterior process, a posterodorsal process, and a posteroventral process. The mediolaterally thin anterior process is the largest of the three and articulates ventrally with the quadratojugal, forms a small portion of the posterodorsal margin of the lateral temporal fenestra, and articulates dorsally with the posteroventral edge of the postorbital. A lateral ridge on the dorsal portion of the squamosal bounds the supratemporal fenestra laterally and continues anteriorly onto the dorsolateral margin of the postorbital. A small anteriorly pointing apex of the anterior process of the squamosal underlies a posterodorsal projecting prong of the dorsal process of the jugal. This contact excludes the postorbital from participation in the margin of the infratemporal fenestra as mentioned previously, similar to the condition in *P. kirkpatricki* (Weinbaum, 2011), and differing from the condition in aetosaurs (e.g., *P. andressorum*, Schoch & Desojo, 2016). A small slot on the anteroventral surface of the anterior process fits a thin dorsal process of the quadratojugal.

The posterior portion of the squamosal extends posterior to the head of the quadrate and divides into a posteroventral and an anterodorsal process. The head of the quadrate fits into a distinct ventrally facing fossa that extends onto the anterior part of the posteroventral process (Figure 4v); thus, the posteroventral process and the lateral edge of the articulation surface hides the head of the quadrate from lateral view. Additionally, on the posteroventral margin of the squamosal, there is a flat, posteriorly facing shelf that accepts the thin anterodorsal

margin of the quadrate. The posterior surface of the posteroventral process has a small facet that articulates with the paroccipital process of the opisthotic (Figure 4v). Unlike most archosauriforms, this facet is thickened mediolaterally and rounded into a knob similar to the condition in *T. dabanensis* (IVPP V3237) and aetosaurs (Nesbitt, 2011). The posterodorsal process bears a slit on its posterior edge that fits the posterolateral process of the parietal.

Among the bones of the palate, the vomers are not recognized from any known specimen. However, the ectopterygoid, pterygoid, and palatine are preserved in PEFO 34561 and an additional ectopterygoid is known (PEFO 33857); the palate is complete but obscured in PEFO 34089 (Figure 3d).

5.2.14 | Pterygoid

Although none are completely preserved (Figure 5a), the pterygoid consists of the anterior process, lateral process, and posterior process. The anterior process is triangular in cross-section with a tall dorsal ridge that delineates the element at the midline. The ventral surface of this process is concave. It tapers anteriorly but the contact with the palatine is unknown. The lateral process consists of a posteriorly pointed wing that slopes posteroventrally. The lateral portion of the ventral surface possesses a large facet along the entire length of the lateral process that articulates with the dorsal surface of the ectopterygoid (Figure 5a). The pterygoid body is a thin, vertically oriented blade. The ventral surface bears a rounded anteroposteriorly oriented ridge that continues onto the anterior process. Pterygoid teeth are absent. The posterior process (= quadrate process) is broken in all specimens (e.g., PEFO 34561) posterior to the articulation point with the semi-circular fossa for the basiptyergoid process of the parabasisphenoid. The anteroposterior length of the pterygoid is similar to that in archosauriforms such as *Erythrosuchus africanus* (Gower, 2003) and *P. kirkpatricki* (TTU P-9000), rather than the anteroposteriorly abbreviated pterygoids of aetosaurs (e.g., *L. meadei*, TMM 31185-98; *Neoetosauroides engaeus*, PVL 5698).

5.2.15 | Ectopterygoid

The anteroposteriorly elongate ectopterygoid (Figure 5b) possesses an anterior articular head abutting the medial pedicel of the jugal (Figure 4n). The ectopterygoid is single-headed with a flat articulation surface with the jugal as in aetosaurs (e.g., *L. meadei*, TMM 31185-98), differing from the condition in *B. kupferzellensis*, rauisuchids, and

Crocodylomorpha, where the ectopterygoid is double-headed with a split articulation surface on the jugal (Nesbitt, 2011; Weinbaum & Hungerbühler, 2007). The anterior portion of the body expands anteromedially and then expands posteroventrally. The near dorsoventrally compressed ectopterygoid body tapers and thins posteriorly. The lateral side of the ectopterygoid body is a thickened and flattened surface, which forms part of the medial margin of the suborbital fenestra; the edge thins posteriorly with the rest of the element. There is a distinct ridge that projects a short distance from the head along the dorsolateral edge of the ectopterygoid marking the lateral extent of the articular surface with the pterygoid. A small projection on the anteromedial side delineates the anterior border of the articulation with the pterygoid and fits into a small groove in the pterygoid (Figure 5b). The pterygoid lies on the dorsal surface of the ectopterygoid as in non-ornithodiran archosaurs (Nesbitt, 2011). The ventral surface of the ectopterygoid body is convex in *R. callenderi* (PEFO 34561), whereas it is concave in the aetosaur *L. meadei* (TMM 31185-98). The anteroposterior length of the ectopterygoid in *R. callenderi* (PEFO 34561) is proportionally similar to that of *Saurosuchus galilei* (PVL 32) and *P. kirkpatricki* (TTU P-9000) rather than the anteroposterior short ectopterygoid of *L. meadei* (TMM 31185-98).

5.2.16 | Palatine

A fragment of the palatine is present in PEFO 34561 (Figure 5c). The element is relatively flat, and its articulations with the pterygoid and maxilla are not apparent. An elongate hemielliptical concave margin on what is interpreted as the medial surface may represent the internal choana.

The disarticulated braincase of PEFO 34561 includes a nearly complete basioccipital, parabasisphenoid, otoccipital, and prootic (Figure 6). This is supplemented with the well-preserved basioccipital and well-preserved, but slightly crushed, otoccipital of PEFO 34269, a beautifully preserved otoccipital (PEFO 35000), and a badly weathered partial basicranium (PEFO 34570) from PFV 231. Isolated otoccipitals are known from PEFO 36875 and PEFO 36876. The supraoccipital is currently known only from a single crushed specimen (PEFO 38609), and its anatomy is obscured by other bones (Figure 3c).

5.2.17 | Parabasisphenoid

The basisphenoid and parasphenoid are coossified into a parabasisphenoid that is well-preserved and nearly

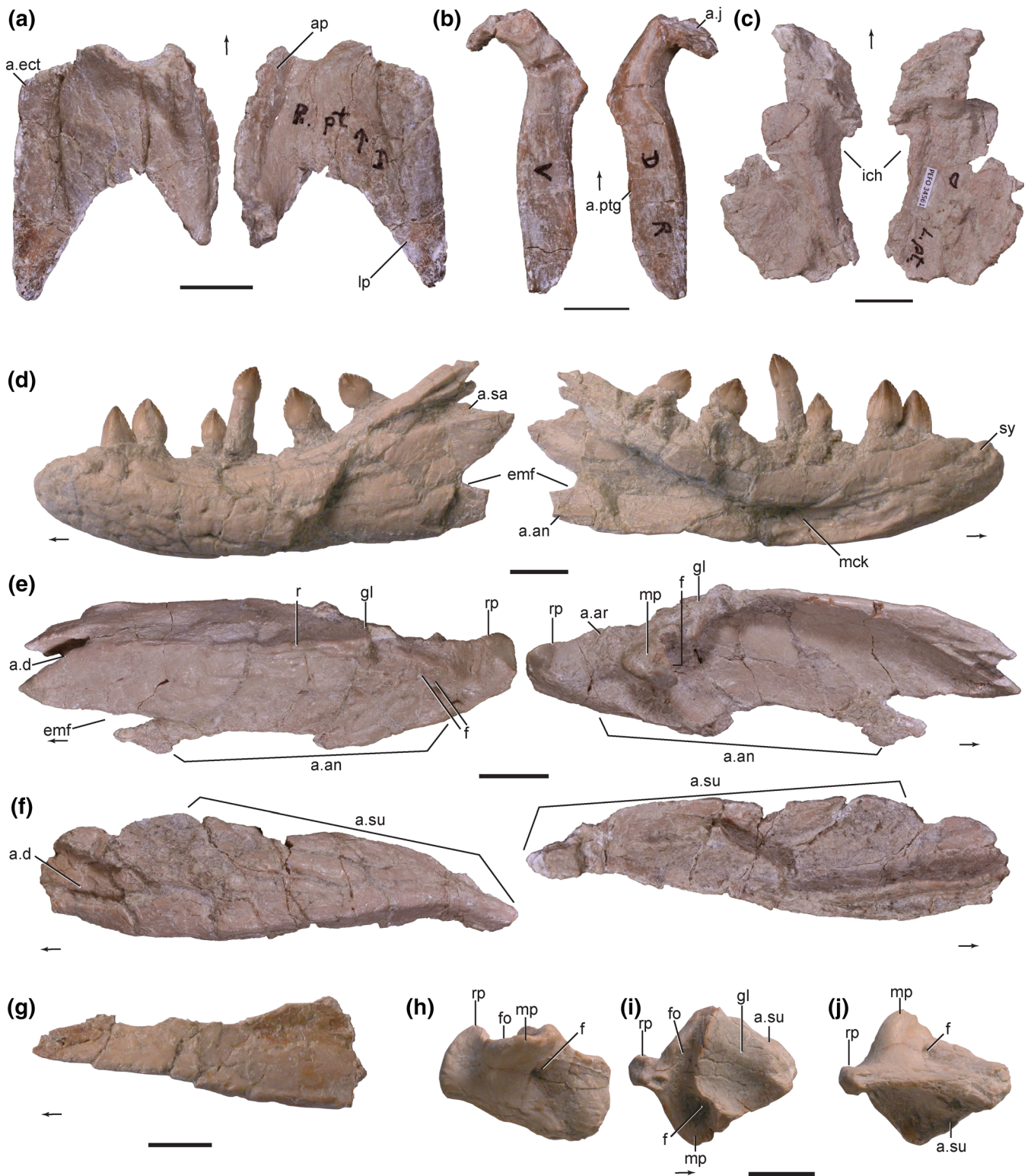


FIGURE 5 Palatal and mandibular elements referred to *Revueltosaurus callenderi* (PEFO 34561). Right pterygoid (a), right ectopterygoid (b), left palatine (c), left dentary (d), left surangular (e), left angular (f), left splenial (g), and left articular (h-j). Ventral view (left) and dorsal view (right) is visible in a-c and lateral view (left) and medial view (right) is visible in d-f. Splenial (g) is in medial view. Articular is visible in lateral (h), dorsal (i), and ventral view (j). a, articulates with; an, angular; ap, anterior process; ar, articular; d, dentary; ect, ectopterygoid; emf, external mandibular fenestra; f, foramen; fo, fossa; gl, glenoid; ich, internal choana; j, jugal; lp, lateral process; mck, Meckelian canal; mp, medial process; ptg, pterygoid; r, ridge; rp, retroarticular process; sa, surangular; su, surangular; sy, symphysis. Scale bars equal 1 cm, arrows point in anterior direction

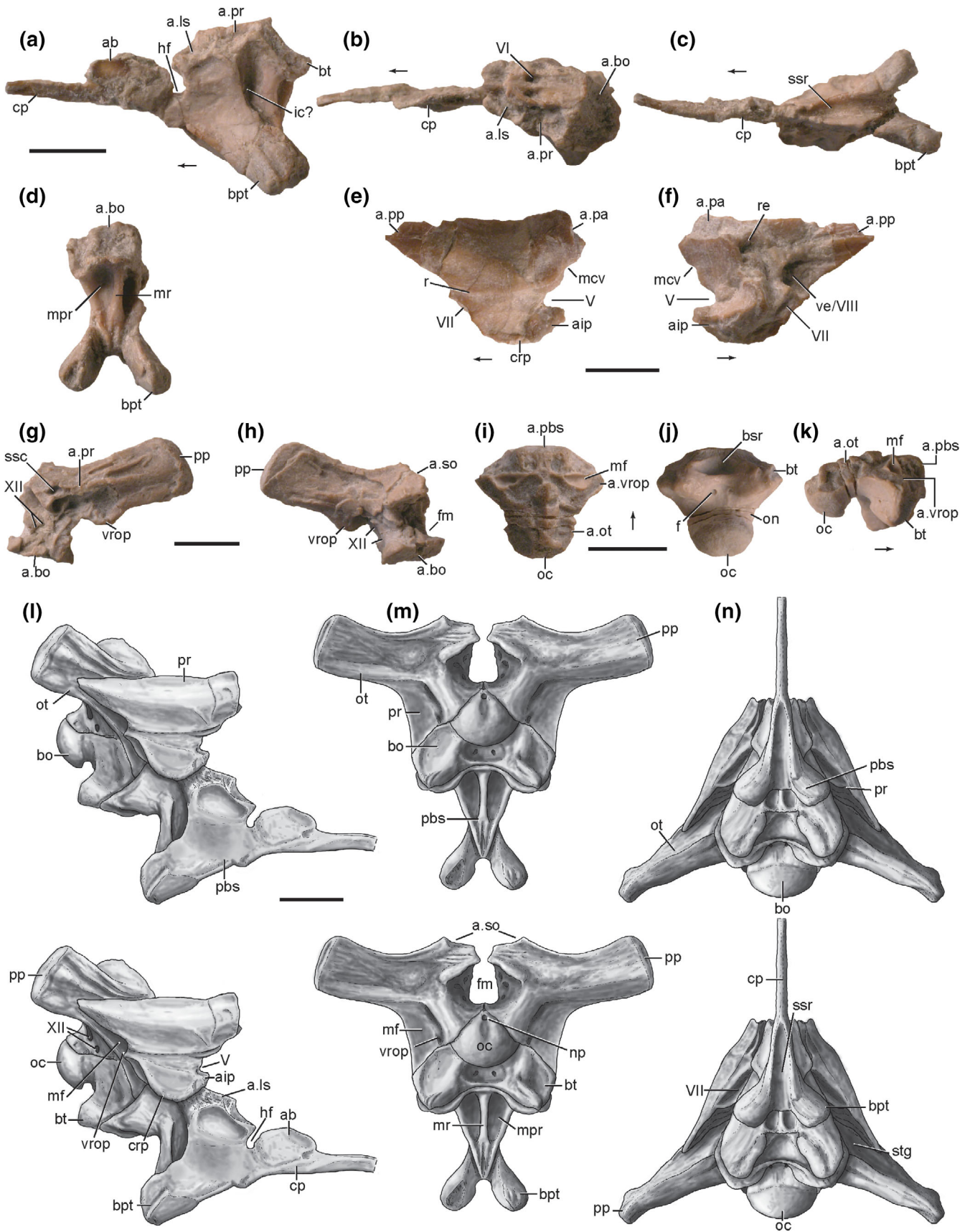


FIGURE 6 Legend on next page.

complete in PEFO 34561 (Figures 6a-d). The parabasisphenoid is strongly verticalized (i.e., the basiptyergoid processes are clearly ventral to the basitubera; Figures 6d, l), as in *B. kupferzellensis* (Gower, 2002), *P. kirkpatricki* (Chatterjee, 1985), *G. stipanicorum* (MCZ 4117), and *S. acutus* (Walker, 1990), differing from the moderately verticalized condition found in aetosaurs (e.g., *D. spurensis* and *S. robertsoni*, Small, 2002; Walker, 1961), phytosaurs (Camp, 1930; Stocker, 2010; Stocker et al., 2017), and *Arizonasaurus babbitti* (Gower & Nesbitt, 2006), where the basiptyergoid processes and basal tubera are roughly in the same anteroposterior plane.

The articular surface for the basioccipital in PEFO 34561 is mostly broken away, but the posterior and left lateral margins of the broken area are separated from the ventral portion of the parabasisphenoid by a sharp ridge. On the posterior side, ventral to this ridge, is another sharp but vertical ridge on the midline that divides two triangular, posterolaterally facing depressions (Figure 6d). This ridge is unique to *R. callenderi* and divides what is usually a single depression referred to as the median pharyngeal recess (Martz & Small, 2006; Nesbitt, 2011; Witmer, 1997) or hemispherical fontanelle (Heckert & Lucas, 1999; Parrish, 1994). In *R. callenderi*, these depressions are each bounded laterally by sharp ridges that slope ventromedially and converge ventrally between the posteroventrolaterally projecting basiptyergoid processes. A ventrally elongated trough-like depression (= median pharyngeal recess) is shared only with some rauisuchids (Gower, 2002; sensu Nesbitt, 2011), *G. stipanicorum* (MCZ 4117), some aetosaurs (e.g., *D. smalli*; Small, 2002, Parker, 2005a), and with crocodylomorphs (Nesbitt, 2011; Parrish, 1993), but is undivided in those taxa.

In ventral view (Figure 6c), the basiptyergoid processes diverge posterolaterally and extend posteriorly beyond the posterior margin of the main body of the parabasisphenoid. Anteriorly, two ventral ridges extend from these processes and converge medially below the hypophyseal fossa (= sella turcica) to form the ventral margin of the cultriform process of the parabasisphenoid. The ventral surface of the parabasisphenoid has a groove

between these ridges (subsellar recess, Figures 6c, n) as in an aetosaur braincase assigned to *D. spurensis* (UCMP 27408; Small, 2002); however, this groove is not present in the holotype skull of *D. spurensis* (UMMP 7476).

On the lateral surface of the parabasisphenoid (Figure 6a) a ventromedially deep triangular depression is present. Although it is not possible to see into the bottom of this depression, it is likely to have housed the main portion of the palatine branch of the facial nerve (VII) and the entrance of the internal carotid artery based on other aetosaurs and pseudosuchians (Gower, 2002; Gower & Walker, 2002; Nesbitt, 2011; Parrish, 1993). The crest bordering this groove anteriorly is the otosphenoidal crest (e.g., Witmer, 1997). The lateral surface of the parabasisphenoid between the cultriform process and the lateral depression for the internal carotid artery and facial nerve (VII) is smooth and slightly concave; this surface is called the alaris basisphenoidei (Säve-Söderbergh, 1947). Dorsal to this region is a small ridge for articulation with the anterior inferior process of the prootic.

The dorsal surface of the parabasisphenoid floors the anterior endocranial cavity as in *S. acutus*, *D. elaphros*, and *C. niloticus*, (Gower, 2002; Walker, 1990) and differs from some aetosaurs (e.g., MNA V3633), *B. kupferzellensis*, *A. babbitti*, and *P. kirkpatricki* where the prootic floors the cavity (Gower, 2002; Gower & Nesbitt, 2006). The exits for the abducens (VI) nerve are restricted to the parabasisphenoid and situated on the dorsal surface (Figure 6b) and close together medially as in Crocodylomorpha (Walker, 1990). The abducens are separated by a thin, low anteroposterior ridge and bounded laterally by two other distinct ridges. These three ridges meet just anterior to the abducens, forming a raised shelf.

Anterior and just ventral to this shelf is another short median anteroposterior ridge that divides the dorsal surfaces of the clinoid processes into paired facets; the anterior termination of the ridge forms the dorsal margin of the hypophyseal fossa. In most archosaurs, including other suchians, the prootics contact each other dorsal to

FIGURE 6 Braincase of specimens referred to *Revueltosaurus callenderi* (PEFO 34561). Parabasisphenoid (a-d), right prootic (e, f), left otoccipital (g, h), basioccipital (i-k), and reconstructed basicranium (l-n) in lateral (a, e, k, l), medial (f), dorsal (b, i), ventral (c, j, n), anterior (g), and posterior view (d, h, m). a., articulates with; ab, alaris basisphenoidei; aip, anterior inferior process; bo, basioccipital; bpt, basiptyergoid process; bt, basitubera; cp, cultriform process; crp, crista prootica; f, foramen; fm, foramen magnum; fo, fossa; hf, hypophyseal fossa; ic?, entrance of internal carotids?; ls, laterosphenoid; mcv, middle cerebral vein; mf, metotic foramen; mpr, median pharyngeal recess; mr, median ridge; np, notochoral pit; oc, occipital condyle; on, occipital neck; ot, otoccipital; pa, parietal; pbs, parabasisphenoid; pp, paroccipital process; pr, prootic; r, ridge; re, recess; so, supraoccipital; ssc, semicircular canal; ssr, subsellar recess; stg, stapedial groove; ve, vestibule; V, notch for trigeminal nerve; VI, canal for abducens nerve; VII, canal for facial nerve; VII, canal for vestibulocochlear nerve; XII, canal for hypoglossal nerve; vrop, ventral ramus of the otoccipital. Scale bars equal 1 cm, arrows point in anterior direction

the hypophyseal fossa to form the ossified pila antotica (e.g., Gower, 2002; Gower & Walker, 2002). However, in articulation, the prootic of PEFO 34561 probably did not reach this far anteriorly (see below), so the laterosphenoid likely contacted the parabasisphenoid; if so, this character is shared among *R. callenderi*, aetosaurs, and crocodylomorphs (Nesbitt, 2011; Walker, 1990).

The hypophyseal fossa opens anteriorly. The dorsum sellae, which forms the posterior wall of the fossa, is deeply concave and divided by a dorsoventrally oriented midline ridge, which meets the ridge roofing the dorsum sellae between the clinoid processes. The anterior exits of the abducens open anteriorly within the hypophyseal fossa, but it is not clear if the exits of the internal carotids are present in the same area.

A crest rises from the posterior end of the cultriform process immediately anterior to the hypophyseal fossa; this is the crista trabecularis, which is formed by the ossification of the trabecular cartilages (Oelrich, 1956). The cultriform process tapers anteriorly. A dorsally expanding, mediolateral flange is located on the posterior part of the process. Anterior to the crista trabecularis, the cultriform process is relatively slender, with faint longitudinal grooves along the dorsal margin and ventrolateral margin.

5.2.18 | Prootic

The right prootic is well preserved in PEFO 34561 (Figures 6e, f). The element appears to be complete, but the possibility exists that a portion of the anteroventral margin is broken away because the metotic foramen appears to be situated too far ventrally when articulated with the parabasisphenoid (compared to TMM 31185-98, *L. meadei*). If this is correct, then the prootic would be situated more anteriorly and dorsally than in our reconstruction (Figure 6l).

The anterolateral surface bears few features except a faint horizontal ridge that bisects the element. This ridge stretches from dorsal to the trigeminal foramen to the ventral surface of the posterolateral process of the prootic that articulates with the paroccipital process of the otoccipital. The posterior process of the prootic tapers posterolaterally and fits into a groove near the ventral edge of the anterolateral surface of the paroccipital process. The articulation is a simple contact, which differs from the intensely interdigitating suture in *B. kupferzellensis* (SMNS 80260), *A. babbitti* (MSM 4590), phytosaurs (e.g., *Wannia scurriensis* TTU P-00539), and *S. robertsoni* (Walker, 1990).

The dorsal edge of the posterolateral process is thin. A ventrally tapering facet on the medial side of the prootic contacts a similar facet on the anterior side of the

otoccipital (see below), and a pit on this surface presumably conducted the horizontal semicircular canal between the two elements. Anterior to this facet, the body of the prootic angles anteriorly as a buttress at the anterodorsal end of the element, and a deeply concave, well-defined facet for the parietal lies along the dorsomedial edge of this buttress, immediately above the trigeminal foramen; a pit on this surface probably conducted the anterior semicircular canal between the two elements (Figure 6f).

The otic capsule is exposed on the medial surface of the prootic, indicating that the wall of the otic capsule was incompletely ossified in *R. callenderi*, similar to *Euparkeria capensis* (Gower & Weber, 1998) and unlike most suchians (Gower, 2002; Nesbitt, 2011). A large concavity at the base of the posterolateral process, just above the posterior termination of the stapedial groove, probably represents the vestibule (Figure 6f); this is bordered anteriorly by the ventrally tapering surface interpreted here as the otoccipital contact. A smaller, anteroventrally inclined groove (which is more or less parallel to the stapedial groove) is ventral to and separated from the vestibule by a ridge; this is interpreted here as the cochlear recess. Anterior to the vestibule, cochlear recess, and ventrally tapering articular surface for the otoccipital, is a deep and somewhat complex recess, which is more difficult to interpret; this may represent the anterior ampullary recess (sensu Gower, 2002; = anterior osseus ampulla sensu Baird, 1970) and/or the exposed anterior semicircular canal.

The anterior part of the medial surface of the prootic is a broad, smooth surface just posterior to the trigeminal foramen and ventral to the deep facet for the laterosphenoid; this probably represents the auricular (flocular) recess (Gower, 2002). This surface contains a central foramen, the exit for cranial nerve VII (Figure 6f).

The posteroventral part of the foramen for the trigeminal nerve (V) is an embayment at the anterior edge of the prootic, and the sharp edge sloping anterodorsally away from it is probably the posterior border of the foramen. A small crest along this surface probably represents part of the partial division of the opening into an upper foramen for the middle cerebral vein, and a lower opening for the trigeminal nerve itself. Partial or complete division of the trigeminal foramen also occurs in crocodylomorphs, *S. robertsoni* (Walker, 1972, 1990), *L. meadei* (TMM 31185-98), and some non-crocodylomorph loricatans such as *P. kirkpatricki* and *B. kupferzellensis* (Gower, 2002). The ridge extending across the lateral surface of the prootic originates just above this crest, to that the two enclose a small groove.

A small hook of bone lies ventral to the trigeminal foramen and forms part of its ventral border; this is the

anterior inferior process of the prootic (Oelrich, 1956). The base of the anterior inferior process contacts the parabasisphenoid, probably just lateral to the exit foramina for the abducens nerve (VI) on the parabasisphenoid. The anterior inferior process is unlikely to have contacted the facets above the clinoid process and dorsum sellae (see above); this would place the prootic too far anteriorly for the posterior process to meet the paroccipital process of the otoccipital, and also place the crista prootica and stapedia groove (see below) well anterior to the groove for the internal carotid artery and facial nerve (VII). If the articulation of the prootics advocated here is correct, then the prootics could not have met along the midline, and the facets above the dorsum sellae on the parabasisphenoid must therefore have contacted the laterosphenoid (discussed above).

The ventral edge of the anterior inferior process is thickened anteriorly, and this thickened surface is posteriorly split to form the stapedia groove. The crest bordering this groove laterally is the crista prootica, which in lateral view hides the exit of the facial nerve (VII; Figure 6e), which possibly exited at the dorsal extent of this groove. The crista prootica is part of the otosphenoidal crest (sensu Witmer, 1997) and in articulation, the crista prootica is continuous with the part of the otosphenoidal crest on the parabasisphenoid.

5.2.19 | Otoccipital

The opisthotics and exoccipitals are indistinguishably coossified in specimens from the quarry (but see below), and the combined element (otoccipital sensu Kley et al., 2010; Bever et al., 2005) is best preserved in PEFO 34269; the following description is mostly taken from that specimen. Largely complete but less well-preserved otoccipitals are also known for PEFO 34561 (Figures 6g, h) and PEFO 35000. The main body of the exoccipital portion is a robust pillar bordering the foramen magnum laterally, and the metotic foramen posteriorly; the opisthotic portion forms the posterolaterally projecting paroccipital process, contacts the supraoccipital dorsally and prootic anteriorly, and contains part of the osseous labyrinth.

The otoccipital contacts the basioccipital in a broad, rugose-surfaced contact at the foot of this pillar, and a posterior tongue (sensu Gower & Weber, 1998) contacts the dorsal surface of the occipital condyle. Dorsomedial to the posterior tongue, on the lateral wall of the foramen magnum, are two foramina (see PEFO 35000); one is located along the lateral edge of the base of the otoccipital, and the other is directly beneath the paroccipital process. Both of these represent the internal exits for the hypoglossal (XII)

nerve. Medial to the pillar, a thin crest separates the wall of the foramen magnum from the vestibule.

The pillar of PEFO 35000 bears a lateral exoccipital ridge (sensu Gower, 2002; Gower & Walker, 2002; = crista tuberalis sensu Sulej, 2010) that does not continue onto the basioccipital. This ridge occurs in all suchians except *A. babbitti* and *Xilousuchus sapingensis* and is plesiomorphically absent in early-diverging archosaurs (Gower, 2002a, 2002b; Gower & Walker, 2002; Gower & Nesbitt, 2006; Nesbitt, 2011). The hypoglossal (XII) foramina are posterior to the lateral exoccipital ridge (Figure 6h) as in some aetosaurs (e.g., *L. meadei*, TMM 31185–98), some loricatans (e.g., *P. kirkpatricki*), and crocodylomorphs (Gower, 2002; Gower & Walker, 2002; Nesbitt, 2011).

A posteriorly projecting process on the opisthotic portion of the otoccipital borders the foramen magnum dorsolaterally and contacted the proatlas. This process is slightly inclined laterally, with a concave dorsal surface. The medial surface of this process forms part of the supraoccipital contact, suggesting that the supraoccipital contributed to the dorsal margin of the foramen magnum. A foramen is present on the medial side of the base of the proatlas process, just below the supraoccipital suture. A deep pit on the supraoccipital sutural contact probably conducted the posterior vertical semicircular canal from the posterior ampullary recess into the supraoccipital.

The paroccipital process of the otoccipital is only slightly expanded laterally. The lateral end is rounded and convex in posterior view. A broad, laterally shallowing groove near the ventral edge on the anterior side of the paroccipital process was covered by the posterolateral process of the prootic. This groove is bordered dorsally by a crest that flattens distally; two smaller and slightly more dorsolaterally inclined crests occur just dorsal to the crest bordering the groove.

The posterior and dorsal part of the vestibule is the largest concavity in the opisthotic portion of the otoccipital, located just anteroventral to the supraoccipital suture. As in the prootic, the vestibule is fully exposed in medial view (Figure 6g), and the vestibule communicates with the metotic foramen, indicating that the walls of the otic capsule were incompletely ossified. The deepest part of the vestibule preserved in the opisthotic portion lies in the dorsal part of the concavity, and probably represents the posterior ampullary recess (e.g., Gower, 2002; = posterior osseus ampulla sensu Baird, 1970). Just anterior to the vestibule, at the medial end of the groove on the paroccipital process that contacts the prootic, are two small but deep pits separated by a thin crest. The upper of these probably conducted the lateral semicircular canal into the prootic (Figure 6g).

The ventral ramus of the opisthotic portion of the otoccipital (sensu Gower, 2002; Gower & Sennikov, 1996; Gower & Walker, 2002; = crista interfenestralis sensu Säve-Söderbergh, 1947; Oelrich, 1956; Chatterjee, 1978; Walker, 1990; Sulej, 2010), which separates the fenestra ovalis from the metotic foramen, is extremely thin and incompletely preserved in all specimens. What is preserved indicates that the descending process would have been hidden in posterior view by the lateral ridge of the otoccipital.

5.2.20 | Basioccipital

In smaller individuals (e.g., PEFO 34269), the basioccipital is disarticulated from the otoccipitals and parabasisphenoid, but these elements are coossified later in other specimens (e.g., PEFO 34570). The occipital condyle (e.g., PEFO 34269) is composed primarily of the basioccipital with a minor contribution from the two otoccipitals. In PEFO 34561 and PEFO 34269 there is a distinct notochordal pit on the midline near the articulation with the otoccipitals (Figure 6m). Ventrally, a mediolaterally broad condylar stalk separates the occipital condyle from the basitubera of the basioccipital (Figure 6j), which are connected by a narrow transverse ridge. Anterior to the intertuberal ridge and incising its anterior margin, is a distinct anteriorly directed triangular basioccipital recess. The anterolateral edges of this recess are delineated by a sharp ridge and the apex terminates at a broad, vertical surface where the basioccipital meets the parabasisphenoid. In posterior view, the single-lobed basioccipital basitubera differ from the bi-lobed tubera of *B. kupferzellensis* (Gower, 2002: fig. 1). The anterior surfaces lateral to the basioccipital recess form slightly concave, rugose articular surfaces for the parabasisphenoid portion of the basitubera. The dorsal edges of the basitubera are flattened surfaces confluent with the contact surface for the otoccipitals. When in articulation, the lateral ridge of the otoccipital contacts this surface, obscuring the descending process of the otoccipital in posterior view, and as in other suchians, the ridge extends onto the basioccipital (Gower, 2002; Gower & Walker, 2002). At the posteromedial base of each tuber in PEFO 34269 is a small foramen of unknown function.

The rugose dorsal surface of the occipital condyle and the condylar stalk are divided by a midline ridge into two dorsolaterally facing articular surfaces for the otoccipitals (Figure 6i). The presence of only a single midline ridge suggests that the otoccipitals contacted each other along this line. The absence of contact of the otoccipitals was used as a potential synapomorphy by Gower (2002; Gower & Walker, 2002) to link crocodylomorphs to

aetosauroids. Nonetheless, it is clear that the exoccipitals touch in *R. callenderi*, an aetosauroid braincase (MNA V3633), *Tecovasuchus chatterjeei* (TTU P-545, Martz & Small, 2006), *L. meadei* (TMM 31185–98), and *P. kirkpatricki* (TTU P-9000). In contrast, the exoccipitals are widely separated in *E. okeeffeae*, Crocodylomorpha, and Dinosauria (Nesbitt, 2007, 2011; Walker, 1990). The surface dorsal to the basioccipital tubera is incised by two mediolaterally elongate, sharp-rimmed fossae that are the ventral portion of the metotic foramen. Just anterior to the medial margin of this foramen are two distinct, but shallow pits, the ventral portions of the cochlear recesses, which anteriorly contact the articular surface for the parabasisphenoid. The ventral ramus of the otoccipital would have contacted the dorsolateral surface of the basioccipital between the floor of the metotic foramen and the cochlear recess.

5.3 | Mandible

Nearly the entire mandible is represented in PEFO 34561 (Figures 5d–j) and PEFO 38609 (Figure 3d), including both articulars, angulars, surangulars, splenials, and dentaries. A prearticular and coronoid have not been recovered for *R. callenderi*.

5.3.1 | Dentary

Complete dentaries are present in PEFO 34561 (Figure 5d). Teeth are present to the anteriormost margin like the plesiomorphic condition in archosaurs and unlike the edentulous margin in aetosauroids. The dentary tooth count varies between 10 and 11. The mesial-most alveoli have the smallest diameter in the element and are slightly constricted labiolingually; the alveolar diameters generally increase distally. In dorsal view and starting mesially, the tooth row curves medially so that it is lingual of the lateral wall of the dentary. Tooth roots are exposed predominantly on the lingual side of the mandible and interdental plates are present. At least in the right dentary of PEFO 34561, these are fused in the mesial alveoli.

Anteriorly the dentary tapers to a rounded point in lateral view (Figure 5d). The weakly developed dentary symphysis forms a rounded “chin,” and the ventral margin of the dentary is broadly rounded near the symphysis; it becomes a sharper edge more posteriorly. Small foramina cover the lateral surface of the anterior portion, and these decrease in number posteriorly. A row of particularly large foramina occurs near and parallel to the dorsal margin; it is difficult to determine whether or not these have a one-to-one relationship with the alveoli.

The medial surface is excavated by a Meckelian groove that extends for much of the length of the element (Figure 5d). The groove is tallest and deepest posteriorly, where it covers virtually the entire medial side of the dentary, and constricts anteriorly, becoming a shallow groove at about the sixth dentary tooth and then completely disappears at the third or fourth alveolus.

Posteriorly, three distinct tapering processes extend beyond the posterior margin of the tooth row (Figure 5d). The central and dorsalmost processes articulate with distinct grooves on the anterolateral surface of the surangular, whereas the lower process fits into a groove on the anterolateral surface of the angular. The most dorsal and central processes bracket an anteriorly tapering sulcus on the lateral surface of the dentary that held the central anterior process on the surangular (see below). The more dorsal process has two prominent sharp ridges on the lateral surface; the dorsalmost one is continuous with a lateral ridge on the surangular (see below). The central process covers all or most of the area where the external mandibular fenestra would be located in other archosaurs; thus, the external mandibular fenestra was small and occurs ventral to the central process.

5.3.2 | Surangular

The surangular forms the dorsal part of the lateral wall of the hemimandible, and a rugose ornamentation covers the lateral surface (Figure 5e). A sharp ridge extends anteroposteriorly across the dorsolateral edge of the lateral surface (= surangular ridge) of the surangular as in many other archosaurs, including phytosaurs, *P. kirkpatricki*, *A. babbitti*, and *B. kupferzellensis* (Gower, 1999; Nesbitt, 2005a, 2005b; Stocker, 2012; Weinbaum, 2011).

The anterior edge of the surangular has three anterior projections (Figure 5e). The central projection is the largest and fits lateral to an anteriorly tapering sulcus between the dorsal and central posterior processes on the dentary (see above). A deep concavity between the dorsal and central processes of the surangular holds the dorsal posterior projection on the dentary. The more ventral anterior process of the surangular is set further posteriorly along the ventral edge of the element and has a thin ventral flange that may have been covered laterally by the angular.

In medial view at the posterior margin, a process projects medially and the anterodorsal surface of this process contributed to the articular surface of the glenoid. The posterior side of this medial projection is convex, fitting into a concavity on the anterolateral surface of the articular; the anterior side of the projection is a deep fossa. Just posterior to this projection, the surangular is slightly overlapped by the lateral lip of the articular. The

posterior end of the surangular is mediolaterally flattened and forms the lateral surface of the retroarticular process.

A small foramen is present just ventral to the posterior end of the dorsolateral ridge, on the posterolateral surface of the surangular. This foramen opens posteriorly as evidenced by a well-defined, posteriorly widening channel. The foramen passes anteromedially through the surangular to exit within the deep fossa on the anterior side of the medially projecting process. The medial expression of the foramen is larger than the lateral expression as in *E. okeeffeae*, *S. inexpectatus*, aetosaurs (e.g., *L. meadei* and *D. spurensis*), *Euparkeria capensis*, *H. ischigualastensis*, *P. kirkpatricki*, and *Crocodylomorpha* (Gower & Weber, 1998; Nesbitt, 2007, 2011; Small, 2002; Weinbaum, 2011).

Another foramen is located anterodorsal to the one just described on the posterolateral surface of the surangular, also below the dorsolateral ridge, but anterior to the glenoid. On the medial surface of the surangular, the probable exit for this foramen occurs in another anteriorly facing concavity just anterior to the large foramen on the anterior side of the medial projection; these two medial foramina are separated by a small crest. The medial surface of the surangular is concave anterior to these foramina.

The angular at least contacted the posterior part of the ventral edge of the surangular and may have contacted most of the ventral edge and partially overlapped the ventral anterior projection of the surangular. The small external mandibular fenestra is present between the central and ventral anterior projections of the surangular, with the central projection of the dentary forming the anterodorsal border, and the angular forming the ventral border.

5.3.3 | Angular

The robust angular forms the posteroventral portion of the hemimandible. The medially expanded ventral edge has a facet for the prearticular on the anterior portion (Figure 5f). The posterior part of the dorsal margin has a thin tongue of bone that fits into a slot on the ventral margin of the surangular. Like the surangular, the lateral surface bears a rugose pattern. Anteriorly, the lateral surface of the surangular has a triangular slot that accepts the ventral posterior process of the dentary along the ventral margin of the jaw.

5.3.4 | Splenial

The mediolaterally thin splenial (Figure 5g) covers the entire Meckelian groove of the dentary. The tapering

anterior portion does not participate in the mandibular symphysis (Figure 3d) as it does in some aetosaurs (e.g., *P. andressorum*, Schoch & Desojo, 2016). The ventral margin has a flattened articular surface for the ventral margin of the dentary. A similar surface on the dorsal margin articulates with the dentary just above the Meckelian groove and ventral to the shelf containing the tooth row.

5.3.5 | Articular

The articular (Figure 5h–j) is the most commonly recovered isolated cranial element in the *Revueltosaurus* Quarry (PFV 297). In articulation with the surangular, the glenoid surface is oriented anteromedially/posterolaterally. The medial part of the glenoid is slightly concave to fit the large medial condyle of the quadrate, and the lateral part of the glenoid is convex to fit the concavity between the condyles on the quadrate. The anterior boundary of the glenoid is not distinct in contrast to the posterior boundary, which has a very sharp and prominent rim. The anteriormost part of the lateral surface of the articular bears a distinct fossa, which receives the medial process of the surangular (see below).

Posterior to the posterior boundary of the glenoid on the dorsal surface of the retroarticular process, there is an arcuate, laterally tapering, and deeply concave fossa (Figure 5i). The lateral and medial ends of the fossa lie dorsal to dorsoventrally thickened edges that overhang the medial and lateral sides of the articular. The lateral one of these overlaps the dorsal edge of the surangular. The medial portion of the arcuate fossa contains a distinct foramen that pierces the articular, exiting anteroventrally out the medial wall on the anterior side of the medial edge. This foramen may be homologous with a similar feature in raiusuchids, phytosaurs (Nesbitt, 2011), and other archosauriforms (Sookias et al., 2020). Posterior to the arcuate fossa, there is a prominent mediolaterally compressed crest at the posterior end of the retroarticular process. The ventral surface of this crest is confluent with a pronounced median ridge that extends along the ventral surface of the articular.

5.4 | Dentition

The teeth of *R. callenderi* have been well-described (Heckert, 2002; Hunt, 1989; Hunt & Lucas, 1994; Padian, 1990). However, these descriptions were based on isolated teeth and the positional data were hypothesized using ornithischian dinosaurs as a model. Having multiple tooth bearing elements with in-situ teeth now allows a

refinement of previous work. Hunt (1989) was correct in differentiating premaxillary teeth from maxillary teeth. Yet, teeth like those in the premaxilla (Figures 4e, f), characterized by being symmetrical mesiodistally and lingually curved at the apex, are also found in the anterior portion of the dentary. Maxillary (Figures 4g, h) and dentary teeth (Figure 5d) in positions posterior to the third tooth are nearly symmetrical mesiodistally, but sometimes are lingually curved at the apex, labiolingually compressed, and have large expanded crowns. The shape of the maxillary and dentary teeth varies positionally without a discernable pattern, possibly related to tooth replacement.

5.5 | Postcrania

Isolated and associated postcranial elements are common in the quarries at PFV 297 and PFV 414. The best-preserved skeleton is that of PEFO 34561, which will provide the basis for the reconstruction (Figure 7) and description, with other specimens supplementing the description where noted.

5.6 | Axial skeleton

5.6.1 | Atlas-axis complex

The atlantal pleurocentrum, intercentrum, and neurapophysis are present (Figures 8a–c). The prezygapophysis of the atlantal neurapophysis is a small anteriorly-projecting rounded projection (Figure 8a). In phytosaurs (e.g., PEFO 31219) and crocodylomorphs (Brochu, 1992), the prezygapophysis expands more laterally. The postzygapophysis is long and spike-like and projects posterodorsally. Extending medially from the zygapophyses is a broad thin flange that forms the roof of the neural canal.

The atlantal pluerocentrum (Figure 8b) is crescentic in anterior and posterior views, unlike in phytosaurs, where it is rectangular in anterior view (e.g., PEFO 31219). Both the anterior and posterior surfaces are convex, though the anterior articular face is slightly flatter and wider than the posterior articular face. The posterior articular face possesses a shallow dorsoventrally trending sulcus that is also found in phytosaurs (e.g., PEFO 31219). The dorsal surface of the atlantal pleurocentrum is concave and mediolaterally twice as wide as anteroposteriorly long. Proportionally, the atlantal pleurocentrum of *R. callenderi* is anteroposteriorly shorter than the same element in *L. meadei* (TMM 31185–97) and *T. coccinarum* (AMNH 7634), otherwise they are very similar.

The anterior face of the atlantal intercentrum is broken away, but the posterior half of the element is well

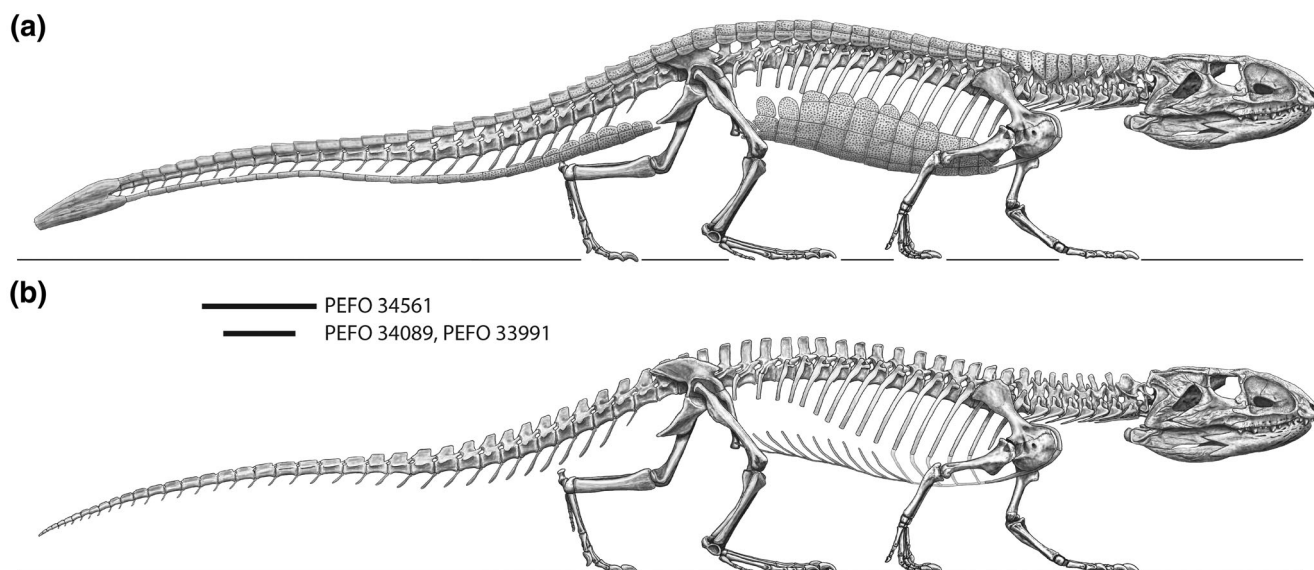


FIGURE 7 Reconstruction of the skeletal anatomy of *Revueltosaurus callenderi* based off of PEFO 34561, PEFO 34089, and PEFO 33991 with osteoderms (a) and without osteoderms (b). Scale bars equal 10 cm

preserved. In posterior view (Figure 8c), the element is subrectangular with slight dorsoventral constrictions along the midline. The atlantal intercentrum is concave dorsally where it articulates with the atlantal pleurocentrum. It articulates with the axial pleurocentrum with a flat saddle-shaped surface (Figure 8d). The ventral surface of the atlantal intercentrum is excavated by a deep depression bordered by a sharp anterior ridge. The lateral surface is incised by a deep dorsoventrally oriented sulcus that curves anteriorly at its dorsal extent. Both the lateral and ventral depression are not found in phytosaurs (e.g., *Mach-aeropsopus mccauleyi*, PEFO 31219), where the atlantal intercentrum is otherwise very similar to that of *R. callenderi*.

The axial intercentrum is not known from any specimen. The axial pleurocentrum (Figure 8d) of *R. callenderi* is approximately equant in its dimensions. The anterior articular face is dorsally concave where it articulates with the atlantal elements; ventral to this area the articular face is flat and slopes posteroventrally where it would articulate with the axial intercentrum. The lateral edges of the anterior articular face of the axial pleurocentrum are expanded because the margins abut with the parapophyses. The parapophyses have flat articular surfaces, are raised on distinct pedestals, and face posterolaterally. The diapophyses form a rounded point that faces posterolaterally and slightly ventrally. The lateral surface of the centrum possesses a deep fossa posterior to the parapophysis. This fossa is proportionally deeper than in *L. meadei* (TMM 31185-97) or *T. coccinarum* (AMNH 7634), though the depth of this fossa changes through ontogeny in other archosaurs (Irmis, 2007) and is absent in a number of aetosaurs (Desojo et al., 2012). The ventral

surface of the axis centrum possesses a sharp median ventral keel. This is absent in *L. meadei*.

Like most archosaurs, the neural spine of the axial pleurocentrum is triangular in lateral view (Figure 8d) with a much more dorsally expanded posterior portion. It projects anteriorly beyond the centrum face. Posteriorly, the neural spine possesses a shallow dorsoventral groove, possibly for reception of ligaments. The prezygapophysis is positioned low on the neural arch; its articular surface is oriented approximately 55° from lateral. The postzygapophysis is positioned midway on the neural spine and the articular surface projects approximately 50° from lateral. The dorsal part of the postzygapophysis is a sharp ridge and ends in a well-developed epiphysis that overhangs the articular surface posterodorsally. Axial epiphyses are known in other pseudosuchians such as *B. kupferzellensis* (Gower & Schoch, 2009; Langer & Benton, 2006), and probably at least in some aetosaurs where Case (1922, p. 36) describes it as a “decided prominence” on the postzygapophysis in *D. spurensis* (UMMP 7504). Laterally, a well-developed lamina connects the prezygapophysis and postzygapophysis; this may be homologous to a combined prezygadiapophyseal and postzygadiapophyseal laminae of archosauriform cervical vertebrae (Desojo et al., 2002; Nesbitt, 2005a; Wilson, 1999), but the lamina in the axis of *R. callenderi* does not contact the diapophysis.

5.6.2 | Postaxial cervical vertebrae

PEFO 34561 does not preserve any post-axial anterior cervical vertebrae, so this description mainly is based on

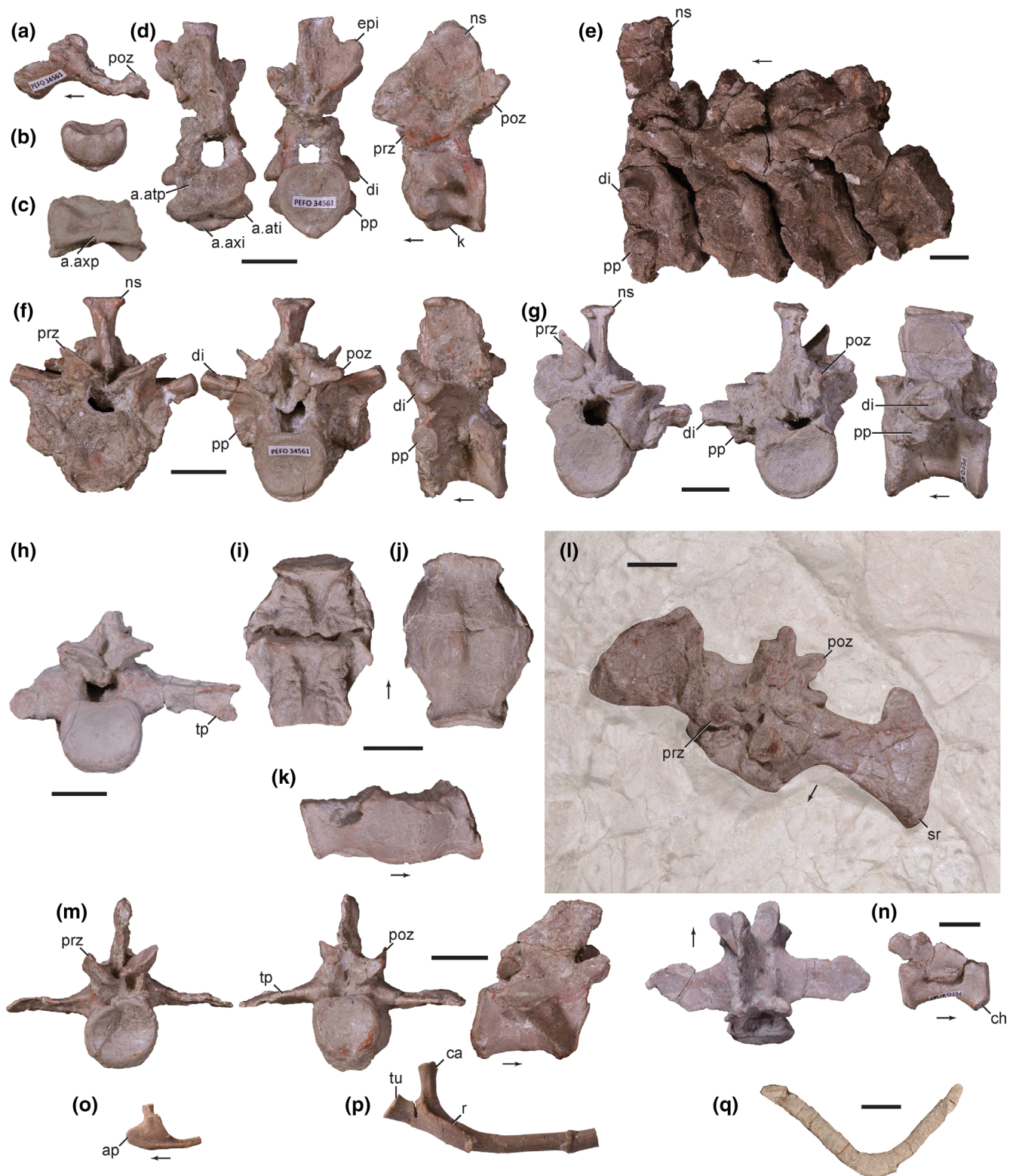


FIGURE 8 Axial skeleton of specimens referred to *Revueltosaurus callenderi*. Atlantal neurapophysis (a, PEFO 34561), atlantal pleurocentrum (b, PEFO 34561), atlantal intercentrum (c, PEFO 34561), axis pleurocentrum (d, PEFO 34561), anterior cervical vertebrae (e, PEFO 34833), posterior cervical vertebra (f, PEFO 34561), anterior trunk vertebra (g, PEFO 41387), last trunk vertebra (h, PEFO 34561), coossified sacral centra (i-k, PEFO 36876), second sacral vertebra (l, PEFO 34269), anterior caudal vertebra (m, PEFO 34561), posterior caudal vertebra (n, PEFO 41387), cervical rib (o, PEFO 34561), trunk rib (p, PEFO 34561), and gastralium (q, PEFO 33847) in lateral (a, e, k, n, o, p), anterior (b), posterior (c, h), dorsal (i, l), and ventral view (j, q). Vertebrae in d, f, g, and m are shown in anterior, posterior, and lateral view from left to right. a., articulates with; ap, anterior process; ati, atlantal intercentrum; atp, atlantal pleurocentrum; axi, axial intercentrum; axp, axial pleurocentrum; ca, capitulum; ch, chevron facet; di, diapophysis; epi, epiphysis; k, keel; ns, neural spine; poz, postzygapophysis; pp, parapophysis; prz, prezygapophysis; r, ridge; sr, sacral rib; tp, transverse process; tu, tuberculum. Scale bars equal 1 cm, arrows point in anterior direction

PEFO 33861, PEFO 34269, and PEFO 34833 (Figure 8e). The articular faces of the centra are amphicoelous and are oriented parallel to each other. The centra are anteroposteriorly short; the anteroposterior length of the centrum is two-thirds its height. The diapophysis is situated on the dorsolateral surface of the centrum whereas the parapophysis is located on the ventrolateral surface. In between there are moderately to well-developed non-pneumatic fossae. Ventrally, all the centra possess well-developed keels. The neural arch and spine are dorsoventrally taller than the centrum; comparison of PEFO 33861 and PEFO 34833 suggests that the neural spine displays positive allometry relative to the centrum. The neural spine is posteriorly placed and slightly overhangs the centrum. It is laterally compressed and anteroposteriorly narrow, with a very slight expansion at the dorsal tip. The zygapophyses are oriented 50°–55° from lateral. The postzygapophysis possesses a well-developed epipophysis through at least the fourth cervical vertebra (based on PEFO 34833). The presence of post-axial epipophyses is important because this character has a restricted distribution in archosaurs, and they are only present in *R. callenderi*, saurischian dinosaurs, *B. kupferzellensis*, *V. campi* (e.g., PEFO 33978), *X. sapingensis* (IVPP V6026), *E. okeeffeae* (AMNH FR 30587), and *Hesperosuchus agilis* (AMNH FR 6758; Langer & Benton, 2006; Nesbitt, 2011).

The morphology of the middle to posterior cervical vertebrae is similar to the more anterior cervical vertebrae than the trunk vertebrae in that they have faint ventral keels and lack distinct vertebral laminae; however, the centrum is more equant in its dimensions (Figure 8f). Furthermore, the diapophysis is present on the neural arch, the zygapophyses are proportionally larger than more anterior vertebrae, the postzygapophyses lack epipophyses, and the transverse expansion of the dorsal margin of the neural spine is better developed. Thus, the posterior cervical vertebrae are transitional in morphology between the anterior cervical and the mid-trunk vertebrae.

5.6.3 | Trunk vertebrae

Continuing the trend seen in the cervical series, the first two trunk vertebrae (determined by the associated rib type) are also transitional in morphology (Figure 8g) between the cervical vertebrae and the trunk vertebrae closer to the sacrum. The centra are anteroposteriorly longer than dorsoventrally tall, and the centrum faces are amphicoelous. The trunk centra lack ventral ridges on the midline (= ventral keels). The prezygapophysis is oriented 30° from horizontal, whereas the postzygapophysis is oriented only 20° from horizontal. The neural spine is more expanded anteroposteriorly than in the cervical

vertebrae; this expansion is a result of well-developed dorsoventral laminae on the anterior and posterior edges of the neural spine. The dorsal portion of the neural spine is expanded laterally into an extensive “spine table” with a flat dorsal surface, similar to that of aetosaurs (e.g., *D. spurensis*, MNA V9300). In dorsal view, these spine tables are heart-shaped with the apex of the heart pointing posteriorly. The diapophysis and parapophysis are connected by a well-developed paradiapophyseal lamina; this lamina is found in other archosaurs (e.g., Nesbitt, 2005b), but it is particularly large in these vertebrae of *R. callenderi*. The parapophysis is located on the neural arch, but it is not dorsal to the dorsalmost extension of the centrum. The first two trunk vertebrae have moderately developed centroprezygapophyseal, centropostzygapophyseal, spinoprezygapophyseal, spinopostzygapophyseal, prezygodiapophyseal, postzygodiapophyseal, and intrapostzygapophyseal laminae differentiating them from the cervical vertebrae (Wilson, 1999).

The remaining trunk vertebrae possess centra that are even more anteroposteriorly longer than tall with a ratio ~1.25. Compared to the first two trunk vertebrae, the parapophysis is much closer to the diapophysis; the parapophysis is just anteromedial to the diapophysis and they are connected by a small paradiapophyseal lamina. The centrozygapophyseal and spinozygapophyseal laminae are not as pronounced in the more posterior trunk vertebrae, though the intrapostzygapophyseal lamina remains distinct, and an intraprezygapophyseal lamina is present. The neural spines are heart-shaped like the transitional vertebrae, but they are slightly more anteroposteriorly elongate.

The posteriormost trunk vertebra is slightly shorter anteroposteriorly than the sacral centra. The anterior and posterior centrum faces are offset dorsoventrally by 10°. The transverse process consists of a fused rib and synapophysis composed of the diapophysis and parapophysis (Figure 8h). This combined structure points posterolaterally and is grooved on the anterior and posterior faces. The process ends laterally in a bifurcated fork, and it is not clear if this contacted the ilium. Most of the laminae are not well-developed except for the intrazygapophyseal laminae. The neural spine is broken off on this specimen.

5.6.4 | Sacral vertebrae

Both PEFO 34561 and PEFO 34269 preserve partial second sacral vertebrae. Several isolated sacral centra were collected (e.g., PEFO 33875 and 33819), but the sacral rib and neural arch are broken off. The number of sacral vertebrae is determined to be two based on: (a) two distinct sacral rib scars on ilia of *R. callenderi*; (b) two ankylosed centra (PEFO 36876) with clear articulations for ribs and neural arches (Figures 8i–k); and (c) there appear to be

only two morphologies of sacral vertebrae among the isolated specimens. The two ankylosed centra demonstrates that some specimens of *R. callenderi* may coossify their sacral vertebrae and that this character is variable within the taxon. As all the specimens from PFV 297 are of similar size, this coossification in some specimens does not appear to be size related. Alternatively, because in ventral view the lateral expansions of the centra around the ankylosed area are not perfectly symmetrical, this fusion could represent a pathology and additional specimens are needed to confirm this.

The sacral centra are elongate and mediolaterally wider than dorsoventrally tall, and the centrum faces are amphicoelous (Figures 8i–k). The second sacral rib articulates with most of the lateral surface of the centrum and part of the ventrolateral surface of the neural arch (PEFO 36876). In dorsal view, the sacral rib of the second sacral vertebra expands greatly into an anteroposteriorly elongate articulation with the ilium (Figure 8l). In lateral view, this articulation surface is cigar-shaped; this articulates with most of the length of the postacetabular process of the ilium. The anterior portion of the articulation is slightly convex with a slight dorsomedial expansion. The rest of the articular surface is concave. The articular surface of the centrum and the second sacral rib is circular in lateral view (Figure 8k). A transverse ridge separates the articular surface into two parts, a lower part that fits into a slot on the lateral side of the second sacral centrum, and an upper part that articulates with the neural arch. The neural arch is not well-preserved in any specimen; the prezygapophysis is oriented 60° from lateral and the postzygapophysis is oriented only 10° from lateral (though they might be slightly crushed).

The total number of caudal vertebrae present in *R. callenderi* is unknown; however, there are at 34–36 caudal vertebrae in the aetosaurian *A. ferratus* (J.B. Desojo, personal communication, 2021), and a similar number may have been present in the aetosauriform *R. callenderi* (Figure 7; Nesbitt, 2011; Marsh et al., 2020).

5.6.5 | Anterior and mid-caudal vertebrae

Anterior caudal vertebrae (Figure 8m) possess hourglass-shaped centra in ventral view that are anteroposteriorly longer than mediolaterally wide and deeply grooved ventrally (e.g., PEFO 34561). This groove expands at the anterior and posterior ends and is marked by distinct ridges. The anterior end merges with two posteriorly inclined faces, which serve as the articulation surfaces for the chevrons. These differ from the hook-like chevron facets of some rauisuchids (e.g., UCMP 124890; Long & Murry, 1995: fig. 130c). Because the anteriormost caudal vertebra is not preserved, it is not clear at which position

the chevrons start. The articular faces are round and amphicoelous with sharp rims. The neural arch is low, or around half the height of the centrum articular face. The prezygapophysis is well-developed forming a posteroventrally, and medially oriented flat articular surface. The distal margins of both prezygapophyses merge together and are confluent with the anterior edge of the neural spine. The spine is anteroposteriorly broad with a straight posterior edge and an anteroventrally sloping anterior edge. The apex is not expanded into a well-developed spine table. The postzygapophysis is much taller (roughly twice the height) than the prezygapophysis. Its lateral margin is nearly straight, and the articular surface is inclined ventromedially about 45° and faces slightly posteriorly.

Well-developed transverse processes are flat, wing-like blades that extend laterally and curve slightly anteriorly (Figure 8m). As in most aetosaurus (e.g., *D. spurensis*, MNA V9300), the transverse processes originate at the base of the neural arch and are fully coossified in all specimens recovered for *Revueltosaurus*. This differs from the condition in phytosaurs where the attachment for the transverse process crosses the neurocentral suture. Mid-caudal vertebrae are similar except that they are proportionally anteroposteriorly longer and the transverse processes are reduced relative to the more anterior. Overall, the morphology of these vertebrae is very similar to that of aetosaurus (e.g., MNA V9300, *D. spurensis*; Parker, 2008: fig. 16), but less robust overall.

5.6.6 | Posterior caudal vertebrae

The centra of the posterior caudal vertebrae (Figure 8n) are anteroposteriorly elongate and strongly amphicoelous. Chevron facets are present but are less distinct than in the mid-caudal vertebrae and no distinct groove on the midline of the ventral surface is present. The transverse processes are short laterally, dorsoventrally flattened projections from the posterior half of the base of the neural arch. The zygapophyses project slightly beyond the centrum face and are small tab-like processes. Compared to the previous vertebral series the neural spine is reduced to a thin median ridge connecting the prezygapophyses and postzygapophyses.

5.6.7 | Ribs

Cervical and trunk ribs are known from the associated specimens and within the bonebeds at PFV 297 and PFV 414. A nearly complete cervical rib from PEFO 34561 is well-preserved and is missing only its posterior tip and the tuberculum (Figure 8o). The anterior process of the rib forms a rounded projection and tapers posteriorly to

form a thin process. In anterior and posterior view, the capitulum and the base of the tuberculum are separated by deep grooves. In medial view, the posterior process curves anterodorsally and forms a ridge that becomes the capitulum. Shallow fossae occur on either side of this ridge. The length of the rib is short, being about the same length as the length of a cervical centrum.

Several anterior trunk ribs are also preserved in PEFO 34561 (Figure 8p). All are missing the distal half of the element. The tuberculum is raised on a pedestal that is oval in cross section and well separated from the capitulum. The capitulum is raised on an elongate pedestal that is circular in cross section and oriented approximately 45° from the tuberculum. A sharp dorsoventral ridge is present distal to the convergence of the capitulum and tuberculum on the anterior side of the rib. In between the ridge and the shaft in medial view is a moderately deep fossa. In posterior view, there is a very shallow fossa just distal to the convergence of the capitulum and tuberculum. The rest of the rib shaft is convex anteriorly and flat posteriorly and forms a medially curved rod.

A more posterior trunk rib (PEFO 33848) is similar except that the rib shaft curves more strongly medially. Also, the capitulum and tuberculum are not separated on elongate pedestals; they are connected by a thin ridge and the capitulum extends more medially than the tuberculum. The anterior ridge is slightly less projected than the more anterior trunk rib, and the posterior fossa just distal to the capitulum and tuberculum is slightly deeper. The rest of the rib shaft is more oval in cross section than the more anterior trunk rib. The distal end is slightly expanded and is concave in distal view.

5.6.8 | Gastralium

A single gastralium is known from the bonebed (PEFO 33847; Figure 8q). The element has two shafts that form an open “V.” The apex of the gastralium is rounded and does not form a sharp point. The shaft is oval in cross-section, giving the element a flattened appearance. The lack of many preserved gastralia suggests that *R. callenderi* had few gastralia like other aetosaurs (e.g., *Typhothorax coccinarum*, Heckert et al., 2010) rather than the greater number in other pseudosuchians (e.g., the loricate *Prestosuchus chiniquensis*, Desojo et al., 2020).

5.6.9 | Chevrons

Strangely, no chevrons have been recovered from the two quarries. It seems quite unlikely that *R. callenderi* lacked chevrons given their common occurrence in other

archosauromorphs, so this most likely is a taphonomic effect given the tail “club” formed by osteoderms along the tail (see below). Furthermore, the caudal vertebrae possess distinct chevron facets on their ventral surface.

5.7 | Appendicular skeleton

For non-podial limb girdle elements and long bones, directional terms are applied as though the long axes of the elements were oriented dorsoventrally, so that the surfaces that always face anteriorly are referred to as “anterior” and the surfaces that always face posteriorly are referred to as “posterior”; proximal and distal are therefore equivalent to dorsal and ventral, respectively. Podial elements are described as if the long axes are oriented anteroposteriorly.

5.7.1 | Scapula

PEFO 34561 preserves a complete right scapula (Figures 9a, b) and most of the left scapula, the latter missing its dorsal apex. The scapula and coracoid in *R. callenderi* (e.g., PEFO 33789, PEFO 36875) are nearly always found coossified independent of size; however, both the scapulae and coracoids of PEFO 34561 are separate elements (Figures 9a, b). When the glenoid of the scapula and coracoids are combined, the glenoid is oriented posteroventrally with a lateral component like that of phytosaurs and aetosaurs (Long & Murry, 1995).

The posteroventrally oriented glenoid rim of the scapula is slightly smaller than its counterpart of the coracoid and projects less posteriorly. In ventral view, the area of the glenoid is roughly hemispherical and projects posterolaterally. The coracoid articulation is comma-shaped in proximal view, with the broad part of the “comma” being deflected medially and abutting the glenoid, whereas the thin, mediolaterally compressed part of the comma extends anteriorly. The thin part of the coracoid articulation forms the ventral margin of a mediolaterally compressed anterior process, which makes up one-fourth of the dorsoventral length of the anterior edge of the scapula. The dorsal edge of the acromion process is raised laterally from the rest of the scapula and slopes anteroventrally from the anterior edge of the shaft. In *A. mississippiensis*, this area is the origin of the *M. deltoideus scapularis inferior* (Brochu, 1992).

The shaft of the scapular blade is mediolaterally compressed and teardrop-shaped in cross-section, with a tapered anterior edge. Two-thirds the distance to the dorsal end the shaft the element gradually begins to expand anteroposteriorly into a pointed, posterodorsal apex



FIGURE 9 Pectoral girdle and forelimb specimens referred to *Revueltosaurus callenderi*. Right scapula and coracoid (a, b, PEFO 34561), interclavicle (c, d, PEFO 34561), left humerus (e–h, PEFO 34561), right ulna (i–l, PEFO 34561), right radius (m–p, PEFO 34561), partial right manus (q, r, PEFO 33870), and isolated manual ungual (S, T, PEFO 34582) in lateral (a, t), medial (b), dorsal (d, q), ventral (c, r), anterior (e, j, n), posterior (f, i, m), proximal (g, k, o, s), and distal view (h, l, p). acp, acromion process; btu, biceps tubercle; cf, coracoid foramen; dc, distal carpals; dpc, deltopectoral crest; ef, ectepicondylar foramen; fo, fossa; g, glenoid; glr, glenoid rim; gr, groove; hh, humeral head; k, kink; ms, muscle scar; ol, olecranon; rat, radial tuber; rc, radial condyle; uc, ulnar condyle. Roman numerals indicate metacarpals. Scale bars equal 1 cm, arrows point in anterior direction

(Figures 9a, b) as in some aetosaurs (e.g., *N. engaeus*, PVL 3525). The dorsal edge of the scapula is dorsally convex in lateral view. A “kink” on the posterior edge of the scapula is the origin of the *M. thoraciscapularis superficialis* in

A. mississippiensis (Brochu, 1992). *R. callenderi* lacks the tear-drop shaped prominent tuber found on the posterolateral edge just dorsal to the glenoid, a character present in some aetosaurs (e.g., *L. meadei*, TMM 31185-97) and

Batrachotomus kuperfezellensis (SMNS 80271; Nesbitt, 2011), but there is a clear homologous muscle scar in the same location (Figure 9a).

5.7.2 | Coracoid

The right coracoid of PEFO 34561 is complete (Figures 9a, b). The posterolaterally oriented glenoid rim is the thickest part of the coracoid. The scapula articulation on the coracoid mirrors the coracoid articulation on the scapula, with the thickest part being proximal adjacent to the glenoid, and the anterior part of the articulation being mediolaterally compressed.

Posteroventral to the rim of the glenoid and along the posterior rim of the coracoid, there is a distinct notch separating the main body of the coracoid from the glenoid fossa as in other crown archosaurs (Nesbitt, 2011). The posterior, ventral, and anterior edges of the coracoid form a semicircular arc in lateral view, with the posterior margin being slightly thicker than the rest of this edge (= biceps tubercle; Figure 9a). Anterior to the glenoid fossa, just ventral to the articulation with the scapula on the lateral surface of the coracoid, is a depressed area where the element thins. Just anterior to this depression is the coracoid foramen, which angles ventrolaterally through the element. The medial surface of the coracoid is strikingly concave. The coracoid did not have an elongated postglenoid process as in crocodylomorphs, but is deeper, more similar to other suchians, especially aetosaurs (e.g., *S. robertsoni*, Walker, 1961). There is no deep groove on the posteroventral edge as in loricatans such as *P. kirkpatricki* (e.g., TTU P-9000) and *D. grallator* (NCSM 13733).

5.7.3 | Interclavicle

Although clavicles have not been identified from the preserved specimens, complete and partial interclavicles are preserved. The interclavicle (Figures 9c, d) is dorsoventrally compressed, thins posteriorly, and is convex on the ventral side and slightly concave dorsally. Shallow grooves and a few small foramina litter the dorsal surface. The posterior (distal) half of the element is mediolaterally wider and dorsoventrally thinner than the anterior half of the element. The element narrows and thickens anteriorly into the most mediolaterally constricted region (neck); the anterior portion is slightly expanded mediolaterally from the neck. The head and neck are rounded in cross-section. The anterior apex of the head lacks any lateral processes and two distinct subrectangular concave sockets face anterolaterally for

reception of the clavicles. The lack of lateral processes is similar to *A. scagliai* (PVL 2073) and other pseudosuchians such as *Batrachotomus kuperfezellensis* (SMNS 80271).

5.7.4 | Humerus

The humerus (PEFO 34561, Figures 9e–h) has an expanded proximal head as well as an expanded distal end; both ends are asymmetrically more expanded medially than laterally, so that the medial margin of the humerus is arched. The expanded proximal articular head bears three expanded articular surfaces: medial, central (= humeral head), and lateral (Figure 9g). The apex of the deltopectoral crest, located about one-third distal on the shaft, is short in lateral view and pointed anteriorly. The anterior surface of the proximal head is concave. The midshaft is oval in cross-section.

The long axis of the proximal end and the long axis of the distal end are twisted about 30°. A distinct ectepicondylar foramen is present on the lateral side of the distal end (Figure 9f). The small process of bone that encloses the ectepicondylar foramen laterally contacts the lateral distal end so that the foramen is totally enclosed; however, the end of this small process of bone is not fully coossified to the lateral portion of the distal end of the humerus. In *D. spurensis*, this process is fully coossified so that the lateral border of the foramen is continuous (Long & Murry, 1995; Small, 1985). A deep ventral notch separates the two rounded distal articular surfaces. The more lateral articular surface is 20% thicker anteroposteriorly than the more medial articular surface (Figure 9h). A large, deep fossa is located on the anterior surface just proximal to the distal articular surface. The depth of this fossa is very similar to that of aetosaurs (e.g., *L. meadei*, TMM 31185-84a).

5.7.5 | Ulna

The complete right ulna of PEFO 34561 (Figures 9i–l) is 84% of the length of the humerus. The proximal end is mediolaterally expanded as in aetosaurs (e.g., *T. coccinarum*, AMNH FR 2713; *S. olenkae*; Parker, 2013; Drózdź, 2018), not compressed as in phytosaurs (Long & Murry, 1995), and bears a well-developed proximally expanded olecranon process (Figures 9i, k). The olecranon has a mediolaterally broad dorsal process separated by a “sigmoid notch” (Brochu, 1992) from the more mediolaterally constricted anterior process. The surface between the processes is concave to receive the distal end of the humerus. A pronounced radial tuber is present on the dorsolateral surface of the ulna between these two processes

(Figure 9k). This tuber is also present in *B. kupferzellensis* (SMNS 80275) *Fasolasuchus tenax* (PVL 3850), and aetosaurs (e.g., *T. coccinarum*, AMNH FR 2713). The shaft is mediolaterally compressed. The distal end expands mediolaterally and the convex distal articular end is slightly twisted anteriorly. This is similar to aetosaurs (e.g., *A. ferratus*, SMNS 5770, Specimen 6) and differs from the “squared off” distal end found in loricatans (Nesbitt, 2011).

5.7.6 | Radius

A well-preserved right radius (PEFO 34561; Figures 9m–p), which corresponds with the ulna just described, is much shorter than the humerus (~69% of the proximodistal length of the humerus). It has a mediolaterally expanded proximal head, the proximal surface is concave, typical for suchians (e.g., *B. kupferzellensis*, SMNS 80275; *S. olenkae*, Drózdź, 2018), and is surrounded by a small rim. The shaft is subcircular in cross section. The distal end thickens both anteroposteriorly and mediolaterally. The distal articular surface is convex with a shallow longitudinal groove on the posterior edge as in *P. kirkpatricki* (e.g., TTU P-9002) and *H. agilis* (AMNH FR 6758; Nesbitt, 2011). This distal groove does not appear to be present in aetosaurs, at least not in *S. olenkae* for which the forelimb is well documented (Drózdź, 2018).

5.7.7 | Manus

An incomplete right manus (PEFO 33870; Figures 9q, r) was reassembled from broken, but partly articulated fragments. The preserved manus consists of two distal carpals and four metacarpals. The manus can be identified as from the right side: digit I can be identified by the shortness of the metacarpal compared to the others, and the presence of one phalanx and an ungual. The proximal ends of the metacarpals overlap each other in dorsal view, as in other archosaurs (e.g., *S. robertsoni*, Walker, 1961: fig. 14g), such that metacarpal I overlaps the anteromedial surface of metacarpal II, which overlaps the anteromedial surface of metacarpal III, etc. The metacarpals are not dorsoventrally flattened as in *S. olenkae* (Drózdź, 2018).

Metacarpal I is slightly disarticulated from the rest of the metacarpus. It has one attached (but slightly disarticulated) phalanx and ungual. The proximal portions of metacarpals II–IV are in articulation; metacarpals II and III are almost complete except for missing segments of the midshaft, whereas only the proximal end of metacarpal IV is present. The expanded distal ends of the metacarpals have distally flat articular ends and deep flexor pits on the dorsal surfaces.

A rounded carpal, possibly distal carpal 3, lies on the proximal surface in between metacarpal II and III. A thin, partial carpal sits on distal carpal 3 and metacarpal IV.

The manual unguals arc anteroventrally. The unguals are slightly mediolaterally compressed, but not to the same degree as the pedal unguals. The dorsal edges of the unguals are more constricted than the ventral edges. An isolated ungual (PEFO 34582, Figures 9s, t) is both larger and better preserved than the ungual on digit I. The ventral surface of this ungual is covered with fine pits, and faint grooves cover the lateral and medial surfaces. The proximal articular end of the ungual is subcircular and concave.

5.7.8 | Ilium

The ilium (Figure 10a, b) is well represented both from within (PEFO 33892, PEFO 33894, PEFO 33845, PEFO 34056, PEFO 33876, PEFO 34561) and outside (PEFO 33791, PEFO 33991) the two quarries. The rugose dorsal margin is markedly convex and mediolaterally thin. The short preacetabular process projects anteriorly and slightly medially, but does not project further than the anterior extent of the articulation with the pubis as in aetosaurs (e.g., *T. coccinarum*, UCMP V2816/122683; *A. ferratus*, Schoch, 2007) and some suchians (e.g., *Pop. gracilis*, YPM VP 57100). The angle between the body of the ilium and the preacetabular process is about 90° and slightly more acute in larger specimens (e.g., PEFO 33991). The preacetabular process is mediolaterally expanded at its anterior extent, and slightly expands laterally at its dorsal margin. This expansion is not the same as the laterally expanded crest dorsal to the supraacetabular crest in *Pos. kirkpatricki* (TTU P-9002) and *Pop. gracilis* (PEFO 34865). The dorsal margin of the ilium is convex in lateral view.

The acetabulum is concave laterally and dorsoventrally deep. The sharp supraacetabular crest (Figure 10a) is not as well developed as in *Pos. kirkpatricki* (TTU P-9002) and *Pop. gracilis* (PEFO 34865), but more similar to phytosaurs (e.g., *Machaeroprotopus mccauleyi*, PEFO 31219), aetosaurs (e.g., *D. spurensis*, MNA V9300), and non-archosaur archosauriforms (e.g., *Euparkeria capensis*, Ewer, 1965). The crest stretches anteriorly to the pubic peduncle. The articular surfaces with the pubis and ischium meet at a ventrally directed point like that of phytosaurs (e.g., PEFO 31219, *M. mccauleyi*), *B. kupferzellensis* (Gower & Schoch, 2009), *E. capensis* (Ewer, 1965), and aetosaurs (e.g., *Lucasuchus hunti*, TMM 31100-1). However, the high angle (~150°) between the pubic and ischial peduncles in *R. callenderi* differs from the typically lower angle (~90°) in most phytosaurs, aetosaurs, and paracrocodylomorphs (see above). Both articular surfaces, the pubic and ischial peduncles, have an elongated teardrop-shape where the tapering

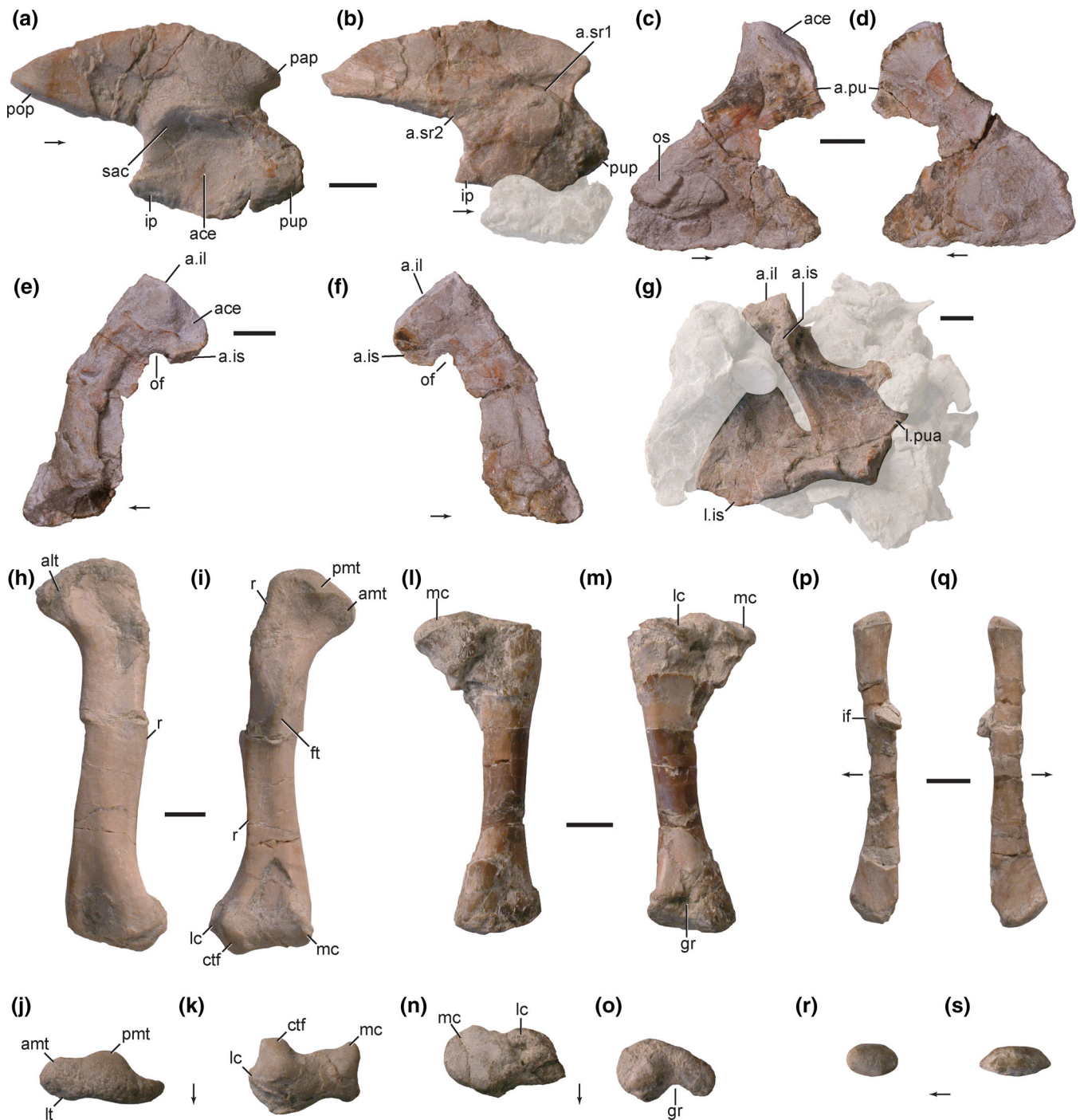


FIGURE 10 Pelvic girdle and hindlimb specimens referred to *Revueltosaurus callenderi*. Right ilium (a, PEFO 34561) and left ilium (b, PEFO 34561), right ischium (c, d, PEFO 36875), left pubis (e, f, PEFO 36875), left pubis and ischium (g, PEFO 34561), left femur (h-k, PEFO 34561), left tibia (l-o, PEFO 34273), and left fibula (p-s, PEFO 34561) in lateral (a, c, e), medial (b, d, f), anterior (h, l, p), posterior (g, i, m, q), proximal (j, n, r), and distal view (k, o, s). a. articulates with; ace, acetabulum; alt, anterolateral tuber; amt, anteromedial tuber; ctf, crista tibiofibularis; ft, fourth trochanter; gr, groove; il, ilium; if, iliofibularis scar; ip, ischial peduncle; is, ischium; lc, lateral condyle; lt, lateral tuber; mc, medial condyle; of, obturator foramen; os, osseoderm; pap, preacetabular process; pmt, posteromedial tuber; pop, postacetabular process; pu, pubis; pua, pubic apron; pup, pubic peduncle; r, ridge; sac, supraacetabular crest; sr, sacral rib. Scale bars equal 1 cm, arrows point in anterior direction

points meet at the ventrally directed point. Nearly all of the acetabulum is located anterior to the ventral margin of the postacetabular process. The ventral margin of the postacetabular process is mediolaterally

thick and is continuous with the anteroposterior trending ridge that articulates with the second sacral rib. The postacetabular process terminates in an acute point.

The medial surface bears articulations for two sacral ribs (Figure 10b). The anteriormost sacral rib attachment, for primordial sacral rib one, is a downturned triangle that extends from the anterior process to the second sacral rib scar. The second sacral rib scar is located at the posterior extent of the acetabulum and trends posterodorsally, ventral to the medial ridge of the postacetabular process. The region dorsal to the medial ridge of the postacetabular process is concave and the surface medial to the acetabulum is convex.

5.7.9 | Ischium

A strong acetabular rim delineates a pronounced ventral acetabular margin. The articular surface is teardrop-shaped corresponding to the ischial peduncle of the ilium. None of the ischia preserves the articulation with the pubis. The shaft is mediolaterally compressed anteriorly and twists posteriorly to form a dorsoventrally compressed ischial plate (Figures 10c, d). The thin ventral edge is sharp and there appears to be a gap at the posterior edge of the articulated ischia. The anterodorsal surface bears a fossa on the proximal portion that is elongated anteroposteriorly and opens dorsally. It stretches from near the articular surface with the ilium to where the ischium thins into the ischial blade. The ischia meet along the thin medial edge.

5.7.10 | Pubis

The left pubis from PEFO 34561 is preserved but crushed into a small block of diagenetically crystallized material that cannot be mechanically separated (Figure 10g) and a partial right pubis from PEFO 34269 preserves the proximal end. The best-preserved pubes are from PEFO 36875 (Figures 10e, f) where the elements are distorted but separate from other material and incomplete. The proximal articular surface is teardrop-shaped in cross-section corresponding to the pubic peduncle of the ilium. Just ventral to the articulation with the ilium is a thickened articular surface for the proximal portion of the ischium, thus the contact between the two elements is ventrally expanded. The medial surface of the proximal head of the pubis is flat. The left pubis of PEFO 36875 shows that a single obturator foramen was present just ventral to the acetabular portion of the element. The thin posterior margin is broken away but enough is preserved of the anterior margin to show that the foramen was large and circular (Figure 10e). In lateral view, the pubic shaft arcs anteroventrally and slightly tapers. Distally the shaft thins significantly and flares mediolaterally, forming a

broad pubic apron as in other pseudosuchians. The apron is mediolaterally broad (Figure 10g) as in aetosaurs (e.g., *D. spurensis*, MNA V9300), and it differs from the narrower pubic aprons of paracrocodylomorphs (e.g., *P. gracilis*, PEFO 34865). The medial margin is straight for contact with the opposite pubis. The anteromedial border of the apron is posteriorly deflected. The distal end of the pubic shaft does not expand distally, forming a knob as in the aetosaur *D. spurensis* (Parker, 2008) and in *A. scagliai* (PVL 2073).

5.7.11 | Femur

The femoral head is distinct from the shaft (Figures 10h, i) and possesses two rounded medial tubera and one anterolateral tuber (Figure 10j). The well-defined posteromedial tuber is similar to that of *D. smalli* (TTU-P9024), *T. coccinarum* (AMNH FR 2710), *A. scagliai* (PVL 2073), and the ornithosuchid *R. tenuisiceps* (PVL 3827) in that it is the largest of the proximal tubera. There is no sulcus on the proximal surface as in juvenile phytosaurs and aetosaurs, *E. okeeffeae* (Nesbitt, 2007), *Prestosuchus chiniquenensis* (SNSB-BSPG AS XXV), and some avemetatarsalians (Nesbitt et al., 2017). Instead, the proximal surface is strongly concave and rugose. In proximal view, the lateral margin is broadly concave, with one weakly developed anterolateral tuber. There is no anterior trochanter. The large, bulbous, and strap-like “fourth trochanter” (ridge of attachment for the *M. caudifemoralis*; Nesbitt, 2011) begins just distal of the femoral head and extends distally to about to mid-shaft (Figure 10i). The enlarged “fourth trochanter” is similar to that of aetosaurs (e.g., *T. coccinarum*, AMNH FR 2710) in robustness. Additionally, a large, rugose pit lies anteromedially of the “fourth trochanter.” A proximodistally oriented ridge lies on the posteromedial edge of the proximal head. A small ridge is present on the posterolateral surface of the femur and is likely the attachment location for the *M. iliofemoralis* (see Nesbitt, Butler et al., 2018) and a similar ridge is present in *A. scagliai* (PVL 2073) and *T. coccinarum* (AMNH FR 2710). A sharp ridge is located on the posterior edge of the shaft that stretches from midshaft to the lateral condyle of the distal femur. The ridge proximally terminates in a distinct point at the midshaft.

The distal end expands to a mediolateral width equal to that of the long axis of the proximal head. In proximal view, the distal condyles are offset approximately 45° from the femoral head. The distal femoral condyles are separated by a broad shallow depression on the posterior side (Figure 10i). The posterior projections of the crista tibiofibularis and the medial condyle diverge posteriorly (Figure 10k). The pointed lateral condyle is separated

from the *crista tibiofibularis* by a laterally opened shallow notch. The distal articular surface is convex. The medial margin of the medial condyle is slightly concave in distal view (Figure 10k). This differs from the condition in aetosaurs (e.g., *T. coccinarum*, AMNH FR 2710) where the surface is convex in distal view. It is closer to what is seen in *A. geoffreyi* (PEFO 38763) where the medial margin is flat.

5.7.12 | Tibia

The best-preserved tibia is an isolated left element from the PFV 297 (PEFO 34273; Figures 10l–o). The proximal head of the tibia is significantly expanded similarly to aetosaurs; Parrish (1986) suggested that the expanded tibial head may be a synapomorphy of the aetosaurs. Like aetosaur tibiae, the proximal surface of the tibia in *R. callenderi* is divided by a ridge into two equal sized slightly concave medial and lateral condyles (Figures 10l–o). The proximal surfaces of the medial and lateral condyles are concave, and a distinct lip is present where the two condyles meet. The proximal head of the tibia is greatly expanded mediolaterally relative to the diameter of the shaft with the greatest expansion medially (Figure 10n). The shaft is subrounded in cross section. The tibia length is approximately two-thirds the length of the femur (Data S2). A vertical ridge is located on the posterolateral side of the shaft.

The distal end is also mediolaterally expanded but not as strongly as the proximal end and strongly resembles the suchian condition (Figure 10o). The medial portion of the articular surface projects distally and is convex. The lateral portion is less distally expanded along its posterior edge and a posterior groove divides the two articulation surfaces.

5.7.13 | Fibula

In PEFO 34561, the fibula is fairly straight (Figures 10p–s), differing from that of aetosaurians, which have a pronounced “kink” (e.g., *N. engaeus*; PVL 3525; *L. meadei*, TTM 31185-97). The proximal end is anteroposteriorly expanded and rounded in proximal view. The small, rounded *iliofibularis* crest is located one-third the distance distally from the lateral surface of the shaft (Figure 10p). Its external surface is smooth, barely raised above the surface of the shaft differing from the more pronounced rugose crest found in aetosaurs (Parrish, 1986) that is more distally positioned. The distal end is mediolaterally compressed and expanded anteroposteriorly relative to the shaft. The distal

articular surface is smooth and beveled anteromedially as in phytosaurs (e.g., UCMP 122621).

5.7.14 | Astragalus

The astragalus (Figures 11a–f) is much like that of other suchians (e.g., aetosaurs). In anterior view, a large anterior hollow occupies much of the anterior surface (Figure 11a). The tibial and fibular surfaces meet at a peak in anterior view. Posteriorly, the astragalar peg (Figure 11b) is present on the posterodistal surface just ventral to the distolaterally trending posterior groove. The astragalar peg has a mediolateral length about twice the anteroposterior height of the element. The posterodistal surface of the peg has a shallow division, but this division is not reflected as a ridge on the articulating surface of the calcaneum. The fibular facet of the astragalus is concave and subrectangular (Figure 11e). The tibial articular facet (Figure 11c) is split into two concave regions with a small convex area separating a smaller lateral articular surface and a larger medial articular surface. The larger surface articulates with the ventral process of the tibia. The smaller articular surface is located on the entire dorsal surface of the fibular process. A thin ridge separates the tibial and fibular facets. The distal roller is convex and resembles those of other suchians (see Sereno, 1991; Nesbitt, 2011).

5.7.15 | Calcaneum

The calcaneum (Figures 11g–l) is generally similar to that of most early suchians (e.g., aetosaurs). The hemicylindrical articular surface is divided by an anteroposteriorly trending ridge into the fibular facet and astragalar facet. The astragalar facet is entirely medial to the fibular facet, unlike the condition in *E. okeeffeae* (AMNH FR 30857), *P. kirkpatricki* (e.g., TTU-P 9002), and crocodylomorphs (e.g., “*H. agilis*” YPM 41198), where the astragalar facet is located more ventrally (Nesbitt, 2011). The concave socket for the astragalar peg (Figure 11h) does not penetrate the medial wall of the hemicylindrical articular surface. The calcaneal tuber is directed posteriorly like that of nearly all early suchians. The calcaneal tuber is mediolaterally expanded and expanded dorsal and slightly in the ventral direction (Figure 11k). The tuber does not have an anteroposteriorly oriented groove as in *P. kirkpatricki* (e.g., TTU P-9002) and crocodylomorphs (e.g., “*H. agilis*,” YPM 41198). Instead, the posterior surface is concave as in aetosaurs (e.g., *Typothorax antiquum*; Lucas et al., 2002). The ventral surface bears a concave fossa. The articulation area with the

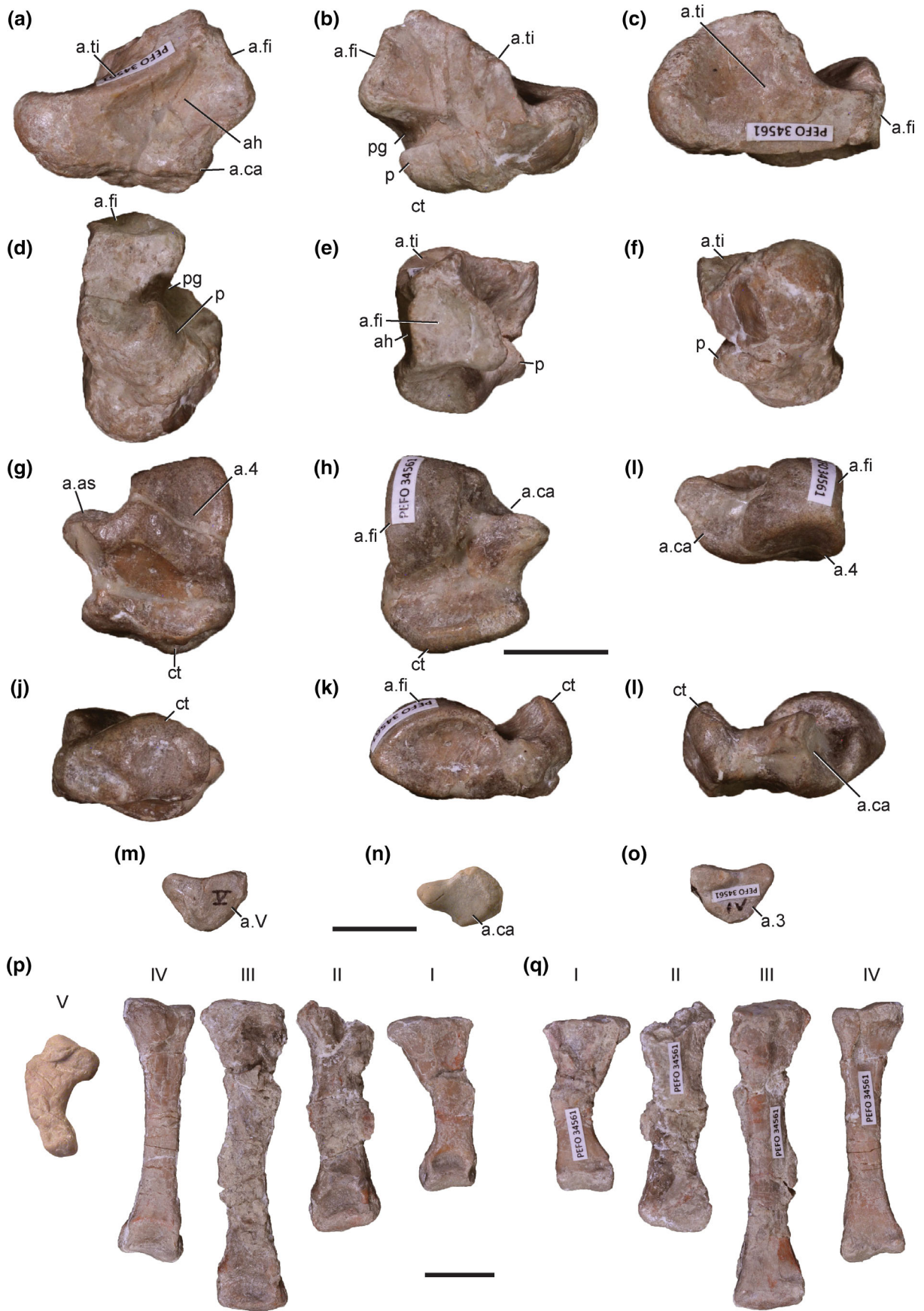


FIGURE 11 Legend on next page.

distal tarsal 4 is markedly concave and not flat as in phytosaurs and other suchians (Long & Murry, 1995).

5.7.16 | Pes

Disarticulated but associated pedes are known from multiple individuals. The right distal tarsal 4 (Figures 11m–o) is preserved and has a posteromedial process. The rounded proximal surface is slightly concave with a heel on the posterior portion. A clear facet is located on the posterolateral side that would articulate with the proximal portion of metatarsal V. Posterior to the facet for metatarsal V is a non-articular surface with fossae and foramina. The medial side is concave and articulated with metatarsal IV. Just dorsal to this articulation a concavity is present that may have fit the third tarsal. Distal tarsal 4 of *R. callenderi* is more similar to that of phytosaurs (e.g., AMNH FR 3001) than to paracrocodylomorphs (e.g., ‘*H. agilis*’, YPM 41198; Nesbitt, 2011).

The metatarsals (Figures 11p, q), exclusive of metatarsal V, share the following characters: proximal and distal expansions, convex distal ends, deep lateral ligament pits, and deep extensor pits on the dorsal surfaces as in most archosauriforms (Nesbitt, 2011). Additionally, the distal surfaces are rectangular-shaped, mediolaterally wider than dorsoventrally deep, with a gap in the middle of the posterior side. Metatarsal I has a lateral expansion at the proximal end that anterodorsally overlaps metatarsal II. In proximal view, metatarsal I is ellipsoid. Two of the metatarsals represent II and III, but because one is incomplete, it is difficult to assign these bones a position. Metatarsal II and III are the longest, thickest at the midshaft, and have the greatest distal expansion. Metatarsal IV is the thinnest at the midshaft and is the most gracile of the four metatarsals. The strongly hooked metatarsal V (Figure 11p), represented from PEFO 34269 (preserved dorsal side-up in a block of other elements), bears a large proximal surface for articulation with distal tarsal 4. The distal end tapers to a small articular surface for contact with the phalanges. Nearly all of the phalanges are known; however, because of disarticulation, the assignment to a digit and the order is impossible to reconstruct. It is probable that the phalangeal formula is 2-3-4-4-?, similar to that of other early-diverging archosaurs. The asymmetrical unguals have concave articular

facets and arc ventrally. The ventral side is flat and the unguals are triangular in cross-section. This morphology is similar to that of some aetosaurs (e.g., *A. ferratus*, SMNS 5771-S22; *A. scagliai*, PVL 2052; *N. engaeus*, PVL 3525), but differs from the mediolaterally compressed unguals of phytosaurs (e.g., UCMP 34239), *P. chiniquensis* (SNSB-BSPG XXV 11e), and *R. tenuisceps* (PVL 3827).

5.8 | Osteoderms

R. callenderi possesses an elaborate dermal skeleton of rectangular osteoderms that cover the dorsal and ventral surfaces of the animal (Figures 7b, 12h). The dorsal armor consists of two paramedian columns of plates that straddle the midline of the animal similar to the carapace of many pseudosuchians, and two columns of associated lateral osteoderms providing four dorsal osteoderms per row as in aetosaurs (Desojo et al., 2013). There is no evidence that *R. callenderi* possessed “sublateral” osteoderms like those found in *A. geoffreyi* (Marsh et al., 2020). Each row of osteoderms in *R. callenderi* corresponds to an underlying vertebra (Hunt et al., 2005). The ventral armor consists of at least four columns of square to rectangular (anteroposteriorly longer than mediolaterally wide) osteoderms that covers the thorax and tail. The posteriormost osteoderms of the tail co-ossify to form a tube-like caudal sheath. It is not clear if there are gular osteoderms as in phytosaurs (e.g., UCMP 27235). Nor is it clear if there were small appendicular osteoderms as in aetosaurs (e.g., *Coahomasuchus kahleorum*, NMMNHS P-18496; *A. scagliai*, PVL 2052) or in erpetosuchids (e.g., *T. ruthae*) (Ezcurra et al., 2017; Heckert & Lucas, 1999).

The dorsal paramedian osteoderms are extremely similar to those of aetosaurs in that they are mediolaterally wider than anteroposteriorly long, possess a dorsal ornamentation of random pattern of incised circular and oblong pits, and have a distinct raised anterior bar along the anterodorsal edge of the osteoderm (Parker et al., 2005). The anterior bar also possesses anterior and anteromedial projections as in non-desmatosuchin aetosaurs (e.g., *Scutarx deltalyus*, PEFO 34045; Parker, 2016b). One important difference between the paramedian osteoderms of *R. callenderi* and aetosaurs is that in the former (as well as in *A. geoffreyi*,

FIGURE 11 Tarsal and metatarsal specimens referred to *Revueltosaurus callenderi*. Left astragalus[NS1] (a–f PEFO 34561), left calcaneum (g–l PEFO 34561), left? distal tarsal 4 (m–o, PEFO 34561), right metatarsals I–IV (p, q, PEFO 34561), and metatarsal V (p, PEFO 34269) in anterior (a, i), posterior (b, j), proximal (c, h, n), distal (d, g), lateral (e, k, m), medial (f, l, o), dorsal (p), and ventral view (q). 3, distal tarsal 3; 4, distal tarsal 4; a, articulates with; ah, anterior hollow; ca, calcaneum; ct, calcaneal tuber; p, peg; pg, posterior groove; fi, fibula; ti, tibia. Roman numerals indicate metatarsals. Scale bars equal 1 cm, arrows point in anterior direction

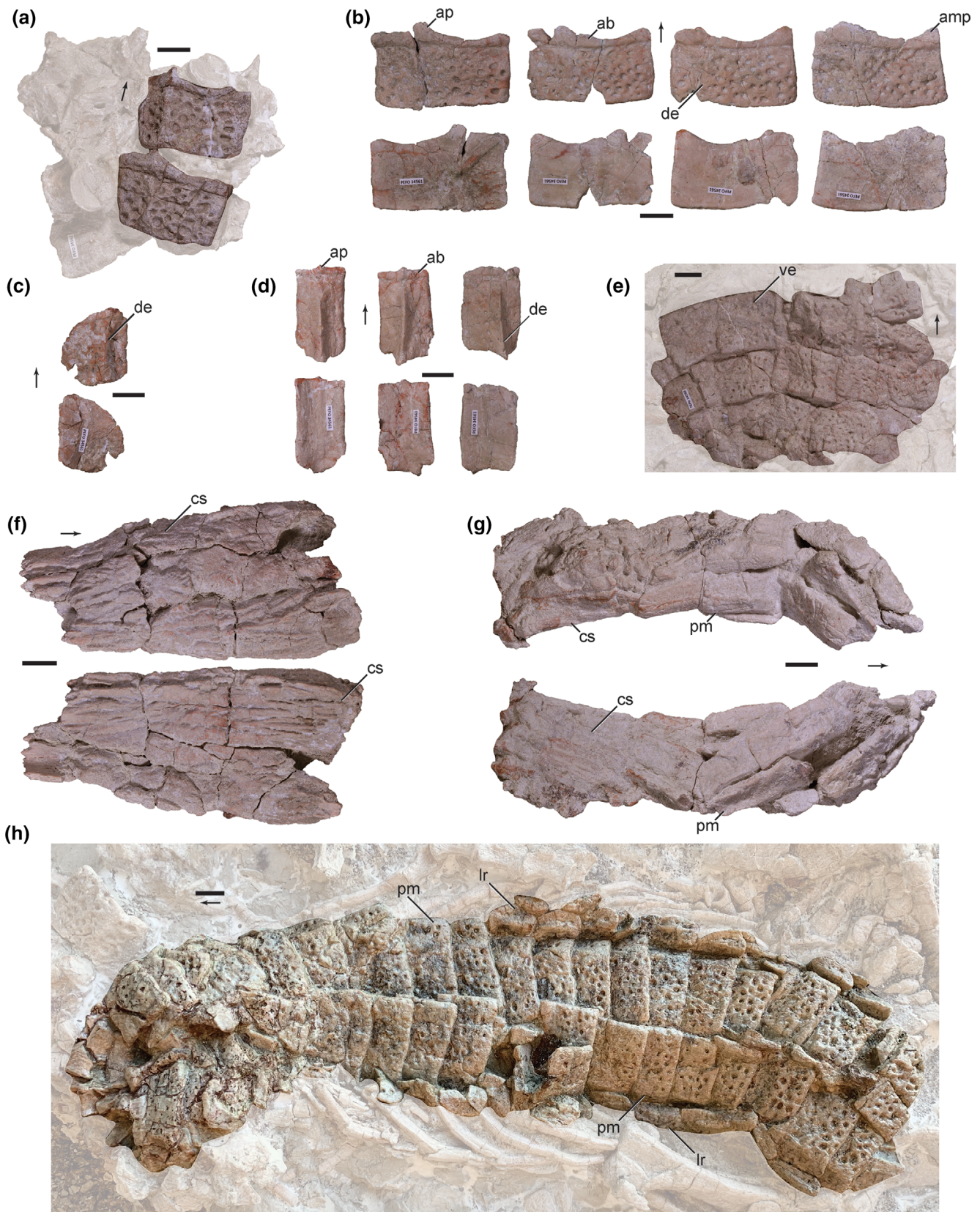


FIGURE 12 Dermal skeleton of specimens referred to *Revueltasaurus callenderi*. Articulated trunk paramedian osteoderms (a, PEFO 34561), four isolated trunk paramedian osteoderms (b, PEFO 34561), a trunk lateral osteoderm (c, PEFO 34561), three caudal paramedian osteoderms (d, PEFO 34561), articulated ventral osteoderms (e, PEFO 34269), articulated distal tail osteoderms (f, PEFO 33850; g, PEFO 38669), and articulated dorsal carapace (h, PEFO 42442/UWBM 116869). Dorsal view overlies ventral view in b, c, and d. ab, anterior bar; amp, anteromedial projection; ap, anterior projection; cs, caudal sheath; de, dorsal eminence; lr, lateral osteoderm; pm, paramedian osteoderm; ve, ventral osteoderm. Scale bars equal 1 cm, arrows point in anterior direction

for example, UCMP 139576) the dorsal eminence, and associated osteoderm flexion, occurs closer to the lateral margin of the osteoderm, whereas in aetosaurs the dorsal eminence and flexion occur closer to the medial margin (Marsh et al., 2020; Parker, 2007).

5.8.1 | Anterior cervical paramedian osteoderms

The first three paramedian rows of the right side are preserved in PEFO 34561, and several rows are preserved in PEFO 42442/UWBM 116869 (Figure 12h). The first osteoderm is roughly triangular in dorsolateral view with straight medial and posterior margins (Figure 7a). The ornamentation is weakly incised, and there is no anterior bar. Instead, on the anterior ventral surface there is a scalloped, rugose surface for articulation with the posterior margin of the skull. The second osteoderm is also triangular but wider than the first osteoderm. This osteoderm is similar to the first in its morphology except that it lacks the ventral articular surface and instead has a weak anterior bar along the narrow anterior margin. The third osteoderm is rectangular (mediolateral width:anteroposterior length ratio of 2.0), with a dorsal ornamentation of small pits. This osteoderm is arched near its lateral edge, and there is a pronounced anterior bar with a triangular anterior projection at the point of arching. The ventral surface of the plate is smooth. In dorsal view, the medial margin is straight, whereas the lateral margin is gently rounded and lacks an articular surface for a lateral osteoderm.

5.8.2 | Middle and posterior cervical paramedian osteoderms

Cervical paramedian osteoderms are wider than long (mediolateral width:anteroposterior length ratio of 2.5 excluding the anterior bar) and appear to widen slightly in each subsequent posterior row (Figure 12h). The dorsal pitting is smaller and weakly incised. The anterior bar makes up one-fifth of the total length of the osteoderm. The anterior margin of the osteoderm is straight and lacks anteromedial and anterior projections. The osteoderm is slightly arched near the lateral edge, two-thirds the distance from the medial edge. There is no dorsal eminence associated with the point where the osteoderm is arched. In dorsal view the medial margin of the osteoderm is straight, whereas the lateral edge is weakly curved. The lateral margins taper and possess no signs of an articular surface for a lateral osteoderm. Thus, there is presently no evidence for cervical lateral osteoderms in *R. callenderi*.

5.8.3 | Dorsal trunk paramedian osteoderms

Dorsal paramedian osteoderms are termed such because they cover the trunk vertebral series (Long & Ballew, 1985). These osteoderms (Figures 12a, b, h) have mediolateral width:anteroposterior length ratios of approximately 2.2 excluding the anterior bar. The dorsal pitting on these plates is larger and more incised than on the cervical paramedians. In dorsal view, the medial margin is straight, and the lateral edge slightly rounded. As in the cervicals, these osteoderms are transversely arched close to the lateral margin; however, in many of these osteoderms there is a dorsal eminence in the form of an anteroposterior ridge that lacks pitting and contacts the posterior margin of the osteoderm. This ridge is more pronounced in the more posteriorly situated osteoderms, but the exact position of this change is not clear in the existing materials. The anterior bar is well-developed but comprises less than one-fifth of the total length of the osteoderm, in contrast to the cervical osteoderms. Furthermore, there are two distinct processes on the anterior bar, a triangular anterior process anterior to the dorsal eminence and a triangular anteromedial projection. The anterior margin of the osteoderm between these two projections is concave in dorsal view. Similar projections and the concave margin occur in the paramedian plates of non-desmatosuchin aetosaurs (e.g., *Scutarx deltatylus*, PEFO 34045). The ventral surface of the osteoderm is smooth.

5.8.4 | Lateral trunk osteoderms

The articulated specimen PEFO 42442/UWBM 116869 (Figure 12h) preserves some of the lateral osteoderms in articulation (seven on the right side and six on the left), and they were present through at least the mid-trunk to sacral area. Cervical and caudal lateral osteoderms are not preserved. There is only a single set of lateral osteoderms per row as in aetosaurs, differing from *A. geoffreyi*, which in some regions has distinct external and internal lateral osteoderms (Marsh et al., 2020). The lateral osteoderms of *R. callenderi* are markedly oblong (subrectangular or oval, longer than wide), with a raised central keel and a surrounding ornamentation of shallow pits as in the other osteoderms (Figure 12c). There is no strong medial articulation surface for the corresponding paramedian; however, the medial edge is straight, whereas the lateral edge is rounded. The lateral osteoderms are slightly flexed in anterior and posterior views, thus the element is divided into distinct medial and lateral flanges as in aetosaurs (Parker, 2007). These flanges are of roughly equal dimensions, and overall the osteoderms are very narrow in comparison with other aetosauriforms, differing significantly from the lateral

osteoderms of *A. geoffreyi*, and aetosaurs that are much broader in dorsal view and either square or wider than long rectangles (Desojo et al., 2013; Marsh et al., 2020). Furthermore, the laterals of *R. callenderi* lack pronounced dorsal eminences that form elongate spines in many other aetosauriforms (e.g., desmatusuchin aetosaurs sensu Parker, 2016a). Instead they look more like the appendicular osteoderms found in aetosaurs and erpetosuchids (e.g., Ezcurra et al., 2017; Heckert & Lucas, 1999).

5.8.5 | Pelvic and anteriormost caudal paramedian osteoderms

These osteoderms are associated with pelvic and hindlimb elements in PEFO 34561 and PEFO 42442/UWBM 116869 and are very similar to the dorsal paramedian osteoderms (W:L ratio of 2.0) except that the pitting is larger and more deeply incised and the dorsal eminence is more pronounced.

5.8.6 | Anterior and middle caudal paramedian osteoderms

Many of these osteoderms were found in association with caudal vertebrae in PEFO 34561 (Figure 12d). They can be distinguished from the cervical, dorsal, and pelvic paramedian osteoderms because they are longer than wide, possess a weak ornamentation of tiny pits, and have a strongly developed dorsal eminence that consists of a sharp, raised keel that originates behind the anterior bar and continues to the posterior plate margin. These keels appear to be situated more medially in contrast to the more laterally positioned eminences of the dorsal series. An anterior bar is present on these plates and possesses the triangular projection anterior to the dorsal eminence. These plates are sharply angulated along the line of the keel; more anterior osteoderms flex at approximately 40°–50°, whereas the more posterior caudal osteoderms have angles of 80°–90°. The caudal osteoderms get narrower and more elongate posteriorly corresponding with the lengthening of the caudal vertebrae.

5.8.7 | Posterior caudal paramedian osteoderms

The posteriormost caudal paramedian osteoderms are simple elongate strips of bone as in aetosaurs (Jepsen, 1948), coossified into a hollow tube structure at the end of the tail (Figure 12f, g). This coossification is different from what is seen in aetosaurs (e.g., *T. coccinarum* (MCZ 1488) and

L. meadei (TMM-31185-97) where the strip-like osteoderms remain distinct from each other.

PEFO 36875 preserves much of the tail including osteoderms and vertebrae. A partially articulated portion from the mid-section of the tail preserves two rows of dorsal paramedian osteoderms, and at least two rows of ventral osteoderms demonstrating that the tail was sheathed in osteoderms as in aetosaurs (Figure 7a). The ventral osteoderms are rectangular, longer than wide, and possess faint ornamentation of numerous small circular pits. At the distal end of the tail, the dorsal and ventral osteoderms are greatly elongated narrow osteoderms that are fused together forming a sheath around the end of the tail (e.g., PEFO 33850; Figure 7a).

5.8.8 | Ventral osteoderms

An articulated region of ventral osteoderms is preserved in PEFO 34269 (Figure 12e). At least four columns of osteoderms formed the ventral carapace of *R. callenderi* with two types of osteoderms, rectangular and sub-rectangular. Hindlimb material associated with this armor suggests that the armor is from the posterior trunk (and possibly cloacal) region. The rectangular ventral osteoderms are similar to the caudal paramedian osteoderms in that they are longer than wide; however, they are flat rather than angulated and lack an eminence. In ventral view, all margins are straight and the medial and lateral margins possess thickened, slightly rugose articular surfaces for adjacent osteoderms along the row. A short anterior bar is present, and the pitting is tiny and not deeply incised. The dorsal surface of the osteoderm is smooth.

The elliptical ventral osteoderms are also longer than wide but lack articular surfaces for adjacent osteoderms. No anterior bar is present and a central pronounced anteroposterior keel extends the entire length of the osteoderm. PEFO 34269 demonstrates that these osteoderms were positioned lateral to the rows of rectangular osteoderms and thus were marginal. In pseudosuchians, ventral osteoderms are only known in non-desmatusuchin aetosaurs (Parker, 2016a) and *A. geoffreyi* (Marsh et al., 2020).

5.9 | Histological description

5.9.1 | Femur

The bone surface at the mid-diaphysis of the femur (PEFO 33843) is still encased in matrix (Figure 13a, b). The original bone surface is preserved in some areas, and bone fragments that became separated from the surface

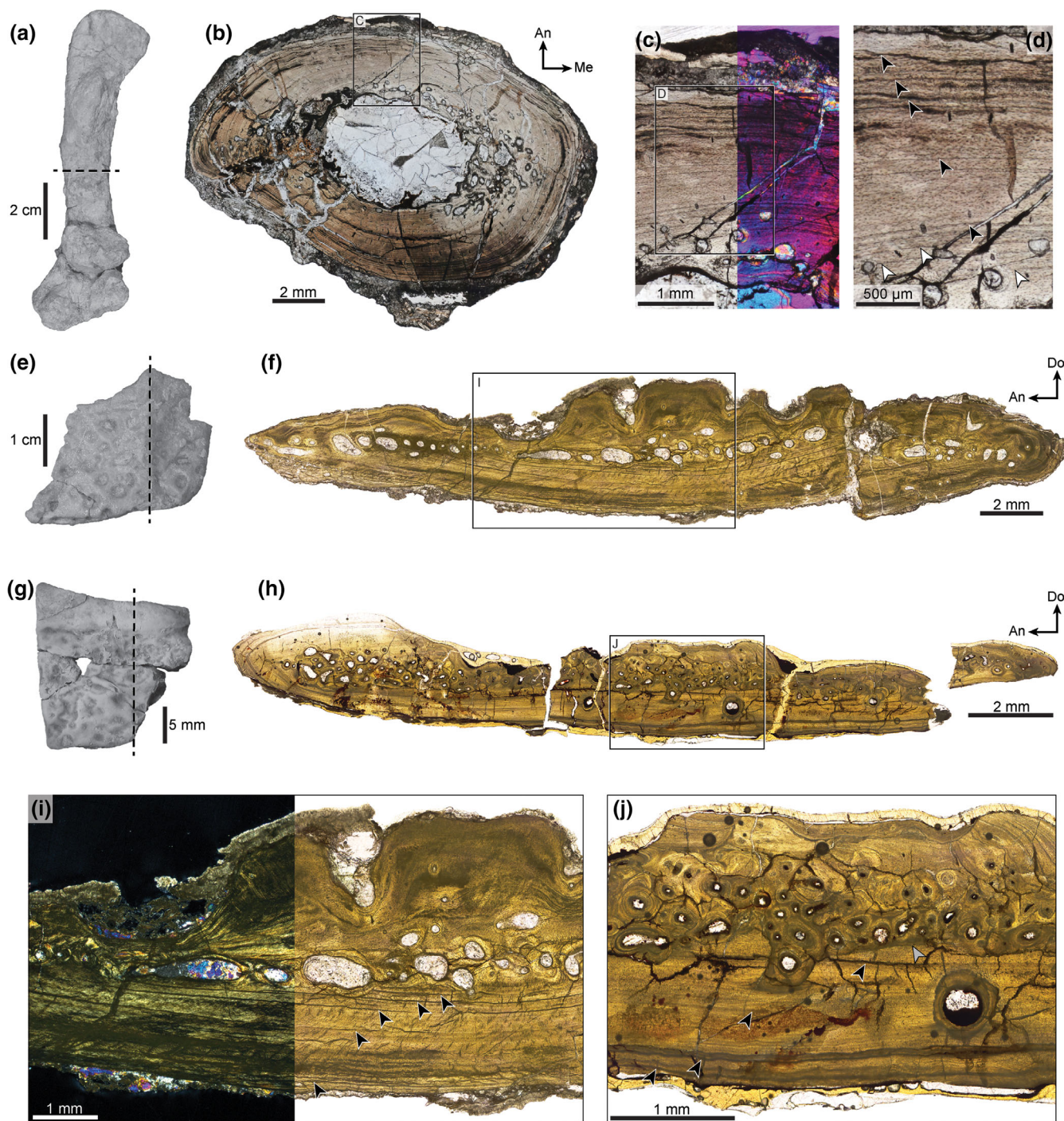


FIGURE 13 Osteohistology of *Revueltosaurus callenderi* (a–f, i) and *Krzyzanowskisaurus hunti* (g–h, j). Left femur of *R. callenderi* (PEFO 33843) in posterior view (a) and transverse section (b–d), paramedian osteoderm of *R. callenderi* (PEFO 33940a) in dorsal view (E) and longitudinal section (f, i), and paramedian osteoderm of *K. hunti* (UCMP 175058) in dorsal view (g) and longitudinal section (h, j). Dashed lines in a, e, and g indicate plane of histological section. Black arrows in d, i, and j indicate growth marks, white arrows in d indicate possible growth marks, and gray arrow in j indicates resorption line. All histological photographs are imaged in plane light except for the right side of c (purple hues), which is cross-polarized with a quartz plate, and the left side of i (black background), which is cross-polarized. Surrounding epoxy has been cropped out for clarity; see Morphobank Project P620 for original full resolution histological images. Specimen in g was coated with ammonium chloride sublimate for clarity. An, anterior; Do, dorsal; and Me, medial

after fossilization are also found within the matrix. Numerous cracks are visible in cross-section, some of which subsequently were expanded and infilled by

mineral crystals (Figure 13b). It is difficult to determine how much of the bone surface is missing because several pieces of varying thickness have broken off in different

areas. Because of this, the measurement of the circumference of the periosteal surface as preserved (and the area it encompasses) is an underestimate.

The femur of PEFO 33843 is suboval or almond-shaped in cross-section (Figure 13b). It is squared off posteromedially and shows a slight pinching posterolaterally. At the point it was sampled, the femur has an external circumference of 41.23 mm, a major axis diameter of 15.07 mm, and a minor axis diameter of 9.44 mm. The medullary cavity is oval and centrally located (Figure 13b), with a major axis diameter of 6.50 mm and a minor axis diameter of 4.10 mm. Many erosion rooms are visible, but these are largely confined to the internal cortex in a band along the major axis (mediolateral width of the cross-section; Figure 13b). Although the endosteal margin has been destroyed in places by crystal growth in the medullary cavity, 2–12 lamellae are visible lining the preserved parts of the endosteal margin (Figure 13b, bottom of image). These lamellae are secondarily deposited; they cut at angles across the primary tissues of the inner cortex.

Five LAG “packets” (groups of associated LAGs) punctuate the cortex (Figures 13b, c, and black arrows in Figure 13d). In subsequent discussion, these LAGs are numbered 1–5, from innermost to outermost. The exact paths of the LAGs and periosteal surface used for circumference measurements can be seen in Figure 13b (also see a traced version which is available in MorphoBank as image M95080) (O’Leary & Kaufman, 2007). In this section, we refer to the area of the cortex endosteal to (internal to) LAG 1 as the inner cortex, the cortex between LAGs 1 and 2 as the midcortex, and all bone periosteal to (external to) LAG 2 as the outer cortex.

Each LAG is a packet of 2–5 annuli and rest lines, some of which grade into parallel-fibered tissue at one or more points around the circumference (white arrows and innermost black arrow in Figure 13d). The zones between the LAG packets decrease in width periosteally, but no external fundamental system (EFS) is visible. The LAGs reveal an ontogenetic shift in cross sectional shape. Early in ontogeny (e.g., LAG 1), the mid-diaphysis was more oval, and it became progressively more flattened (compressed anteroposteriorly), more pinched posterolaterally, and more squared-off posteromedially with age (Figure 13b).

The cortex is fairly uniform in appearance throughout the section, which consists of poorly vascularized, largely unremodeled parallel-fibered bone (Figures 13b–d; note overall lack of secondary osteons). The erosion rooms are confined to the inner cortex (Figures 13b–c). Most of these are small (0.1–0.2 mm diameter), but some reach 0.8 mm in diameter. These vary in stages of maturity; some are lined with 1–3 lamellae, and others are unlined. However, there is no clear relationship between the size of the erosion room and the number of lamellae.

Primary canal density in the inner cortex is very low, with only a few longitudinal simple canals (Figure 13b). Some are oriented slightly oblique relative to the long axis of the bone and resemble very short radial canals (Figures 13c–d). Secondary osteons are absent from the inner cortex. The primary bone tissue type in the midcortex is parallel-fibered bone. The medial and posterior regions of the midcortex is slightly better vascularized compared to the inner cortex, except for the anterior side of the bone, which is poorly vascularized. Nearly all of the canals are isolated longitudinal primary simple canals, but very short anastomoses may connect two canals. These anastomoses are usually radial but may be circumferential or oblique. The canals are arranged circumferentially. The outer cortex shows more organized parallel-fibered bone compared to the midcortex, and locally may be lamellar. Vascular density is extremely low, and the longitudinal (or very slightly oblique) simple primary canals resemble those of the inner cortex. The outermost cortex is nearly avascular and composed of highly organized parallel-fibered bone (*sensu* Stein & Prondvai, 2014) or lamellar bone (Figures 13b–d).

The osteocytes of the inner cortex are generally round in cross-section and oriented parallel or oblique to the long axis of the bone. They are not spaced evenly, and do not change orientation or arrangement with proximity to the vascular canals. However, they are more disorganized in the primary tissue between erosion rooms. In the midcortex, osteocytes occur in similar densities compared to the inner cortex, but they are better organized. In the outer cortex, the osteocytes are not evenly spaced, but they are arranged more centripetally compared to the midcortex.

The bone tissues of PEFO 33843 suggest moderately slow growth and low levels of bone turnover. Vascularity is always low, and the bone tissue never shows a level of disorganization (i.e., of collagen fibers or osteocytes) suggestive of fast depositional rates. This condition is similar to what is observed in previously sampled aetosaurs and phytosaurian archosauriforms, though these larger-bodied animals show slightly higher vascularity (de Ricqlès et al., 2003). In contrast, most sampled early archosauriforms and paracrocodylomorph archosaurs show a significantly greater degree of vascularity and tissue disorganization (e.g., woven bone tissue), suggesting relatively faster growth rates in those taxa (Arcucci et al., 2019; Botha-Brink & Smith, 2011; de Ricqlès et al., 2003; de Ricqlès et al., 2008; Garcia Marsà et al., 2020; Klein et al., 2017; Nesbitt, 2007; Ponce et al., 2017; Schachner et al., 2020). Indeed, annual bone deposition rates at the time of fastest growth preserved in this section (the time represented in the zones between LAGs 1 and 2, and 2 and 3) were ~ 21.9 and 21.5 mm²/year, respectively. Later in life, these rates

slowed dramatically ($\sim 7.6 \text{ mm}^2/\text{year}$ between LAGs 3 and 4 and $\sim 12.5 \text{ mm}^2/\text{year}$ between LAGs 4 and 5). These growth rates are similar to those reported for aetosaurs, but considerably slower than those reported for avemetatarsalian archosaurs (Cubo et al., 2012; Legendre et al., 2013; Padian et al., 2001). Independent of evolutionary changes in life history strategy among early archosaurs, the slower growth of *Revueltosaurus* is not a surprise because of its small body size (cf. Case, 1978). No secondary osteons are present, and although there are numerous erosion rooms, many are in a state of non-resorption (they are lined with several lamellae), suggesting low levels of bone turnover. Despite a lack of extensive secondary remodeling, the cortical tissue shows increased organization moving periosteally, and thus it is unlikely that bone depositional rates would have increased dramatically had the animal lived longer. In the absence of an EFS, we do not make conclusions about the lifespan of this taxon, but this individual certainly lived several years.

The evidence of slowing growth, but no EFS, is broadly consistent with the size range of femora from the PEFO *R. callenderi* sample, whose mid-diaphysis major axis diameter ranges from 14.4 (PEFO 34561) to 22.1 mm (PEFO 33991). The sampled femur (PEFO 33843) has a diameter of 15.1, which is just below the mean (16.4 mm) and similar to the median size (15.4 mm) of the sample. Though size is not a perfect proxy for ontogeny (Griffin et al., 2020), the presence of substantially larger femora (PEFO 33991 and 35318) and the lack of an EFS in PEFO 33843 both indicate that the latter individual was not fully grown, though it had likely passed the point of inflection in its growth curve. Thus, we can hypothesize that most of the specimens in this study are neither early juveniles or adults from a skeletal maturity perspective.

5.9.2 | Paramedian osteoderms

In comparing the osteohistology of the sampled paramedian osteoderms of *R. callenderi* and *Krzyzanowskisaurus hunti*, it is important to note that some observed variation may be due to positional effects, both in terms of the osteoderm's exact location in the carapace and where along the osteoderm the histological section was taken. Below, we describe the two osteoderms together, explicitly noting where they differ.

Like the femur, the sampled paramedian osteoderm of *R. callenderi* (PEFO 33940a) has a thin coating of sparry calcite (Figures 13f, i), whereas the osteoderm of *K. hunti* (UCMP 175058) has a coating of amber-colored adhesive, possibly shellac (Figures 13h, j). Cracks and internal spaces of both elements are permineralized by

calcite spar. Small zones of UCMP 175058 are permineralized by an opaque reddish-brown mineral (Figures 13h, j), likely an iron mineral such as siderite or hematite. Both specimens display a small number of large cracks with displacement and greater number of smaller hairline cracks (Figures 13e–j) but are otherwise well-preserved.

Both osteoderms are predominantly compact cortical bone with a relatively small number of moderately sized vascular spaces (Figures 13f–j); these spaces are smaller than those observed in the aetosauriform *A. geoffreyi* (Marsh et al., 2020: fig. 8), but much larger than the densely-packed small spaces that comprise internal cancellous tissue in aetosaurs (Cerda et al., 2018; Cerda & Desojo, 2011; Parker et al., 2008; Scheyer et al., 2014). As observed by Scheyer et al. (2014: pg. 255) for a small paramedian osteoderm of *R. callenderi*, these endosteal spaces are rimmed by secondary lamellar tissue; the secondary tissue filling these spaces is more extensive in the osteoderm of *K. hunti* (Figures 13h, j). In the specimen of *K. hunti*, the ventral boundary of this remodeled zone forms a marked discontinuity between the secondary tissue and primary tissue of the basal cortex (gray arrow in Figure 13j) that is similar to the resorption line Cerda et al. (2018) described for aetosaurs, but this boundary is less distinct in *R. callenderi* (Figure 13i). In contrast, the basal cortex in both specimens is almost completely avascular, save for a few widely spaced simple canals and primary osteoderms, similar to what Scheyer et al. (2014) observed for *Revueltosaurus* and the condition in *A. geoffreyi* (Marsh et al., 2020), whereas aetosaurs appear to be slightly more vascular in this region (Cerda et al., 2018; Scheyer et al., 2014). This primary bone of the basal cortex comprises parallel-fibered tissue, but lacks the laminar texture described for *A. geoffreyi* (cf. Marsh et al., 2020, p. 16). The basal cortex of the *R. callenderi* osteoderm possesses relatively abundant Sharpey's fibers at a high angle to the long axis of the cross-section (Figure 13i, similar to the condition observed in some aetosaurs (cf. Cerda et al., 2018: fig. 7g–h), whereas they appear to be absent in *K. hunti* (Figure 13j).

Similar to other pseudosuchian archosaur osteoderms, the basal cortex also preserves the clearest record of growth marks (e.g., Cerda et al., 2018; Cerda & Desojo, 2011; Games, 1990; Hutton, 1986; Marsh et al., 2020; Parker et al., 2008; Scheyer et al., 2014). Like the femur, these growth marks also occur in “packets” in the paramedian osteoderms of both *R. callenderi* and *K. hunti* (Figures 13i–j). Using the same criteria applied to the femur, we conservatively estimate that these growth marks comprises 4–5 LAGs/annuli in either specimen (black arrows in Figures 13i–j). In *R. callenderi*, there are 2–3 LAGs just

ventral to the endosteal spaces that are partly destroyed by secondary tissue (Figures 13f,i), whereas only a single LAG is apparent in the same position in *K. hunti* (Figures 13h,j). Both osteoderms display a widely spaced single LAG midway through the basal cortex, and 1–2 LAGs near the periosteal (ventral) margin. No EFS is present in either specimen. Scheyer et al. (2014, p. 255, fig. 10a) described and figured 11 LAGs in the *R. callenderi* osteoderm they sampled, but this count appears to include individual growth marks from LAG packets, and possibly other laminae (e.g., their growth mark #3 appears to curve around secondary tissue rimming a vascular canal), so it may be an overestimate of the number of LAGs/annuli present.

The cortex dorsal to the endosteal spaces underlies the dorsal ornamentation of the osteoderms. It is dominated by the “cut and fill” structure observed in aetosaurs and crocodyliforms (Cerda et al., 2018; Cerda & Desojo, 2011; de Buffrénil, 1982; de Buffrénil et al., 2015; Hua & de Buffrénil, 1996; Scheyer et al., 2014), where primary tissue is resorbed and filled pockets of secondary lamellar-zonal tissue whose centroid drifts with the location of overlying ornamentation; this feature is absent in the aetosauriform *Acaenasuchus geoffreyi* (Marsh et al., 2020, p. 16). Similar to the endosteal remodeling, secondary lamellar tissue in this part of the cortex is more extensive in the specimen of *K. hunti* (Figures 13f, h, i–j).

The osteoderm histology of both *R. callenderi* (PEFO 33940a) and *K. hunti* (UCMP 175058) is consistent with the observations from the femur of *R. callenderi* (PEFO 33843) in their evidence for relative growth rate and skeletal maturity. The predominance of nearly avascular parallel-fibered primary cortical tissue indicates a relatively slow growth rate (Cubo et al., 2008; de Margerie et al., 2002; de Margerie et al., 2004; Francillon-Vieillot et al., 1990). The presence of a minimum of 4–5 LAGs/annuli indicates these specimens are not from young juveniles, but the lack of an EFS indicates they were still actively growing. In the case of the *K. hunti* osteoderm, the presence of at least two more closely spaced LAGs near the periosteal surface (Figure 13j) could suggest that growth is starting to slow, but we cannot make the same inference for the osteoderm of *R. callenderi*. The more extensive remodeling of the *K. hunti* osteoderm might also indicate a more advanced skeletal maturity than that of the *R. callenderi* specimen, though we have a limited understanding of how remodeling rates vary across the pseudosuchian carapace (Cerda et al., 2018; Taborida et al., 2013). Nonetheless, similar to the conclusions for *A. geoffreyi* (Marsh et al., 2020, p. 17), these data generally contradict the hypothesis that osteoderms with this morphology and size represent young juveniles of large-bodied aetosaurs such as *Calyptosuchus wellsi* (cf. Heckert & Lucas, 2002b).

6 | DISCUSSION

6.1 | The phylogenetic relationships of *R. callenderi*

The resulting strict consensus tree of our phylogenetic analysis (Figure 2e) (648 most-parsimonious trees of 1,457 steps, Consistency Index = 0.356, Retention Index = 0.762) has a generally similar structure of that of previous iterations of the Nesbitt et al. (2011) dataset for pseudosuchian archosaurs (Figure 2). *R. callenderi* is found as a suchian in an unresolved position with *A. geoffreyi* + *E. olseni* and Aetosauria; together *R. callenderi*, *A. geoffreyi* + *E. olseni*, and Aetosauria comprise Aetosauriformes (see above).

R. callenderi was identified as a pseudosuchian based on the presence of a crocodylian-normal ankle joint between the astragalus and the calcaneum and the presence of mediolaterally wide osteoderms with an anterior articular facet (Parker et al., 2005) after the initial discovery of skeletons of the taxon from PFV 297. Parker et al. (2005) also hypothesized that the architecture and arrangement of the squamosal was similar to that of aetosaurs. Brusatte et al. (2010) were the first to include *R. callenderi* in a phylogenetic analysis, recovering it as sister taxon of Ornithosuchidae within Suchia. Nesbitt et al. (2011) also included *R. callenderi* in a phylogenetic analysis, utilizing the new material described here, and hypothesized that it is the sister taxon to Aetosauria (Figure 2a), an arrangement recovered in most subsequent analyses (e.g., Butler et al., 2014; Figure 2b); more recently, Marsh et al. (2020) found *R. callenderi* in a clade with *A. geoffreyi* + *E. olseni* that is the sister taxon to Aetosauria (Figure 2d). We also recover this topology, and name, define, and diagnose this clade Aetosauriformes (see Systematic Paleontology section). Despite the somewhat labile relationships of Ornithosuchidae, Erpetosuchidae, and Phytosauria, Aetosauriformes has remained consistent in its placement as an early-diverging clade of suchians (Nesbitt, 2011; Butler et al., 2014; Ezcurra et al., 2017; Marsh et al., 2020; Figure 2).

The skull of *R. callenderi* and aetosaurs share striking unambiguous synapomorphies (Figures 3a, b): (a) a posterior process of the maxilla articulates into a slot on the lateral side of the anterior portion of the jugal; (b) the postorbital-squamosal contact continues ventrally for much or most of the ventral length of the squamosal; (c) the posterior process of the jugal splits the anterior process of the quadratojugal; and (d) the external foramina for abducens nerves within the parabasisphenoid only. Among early-diverging archosaurs, the four character states listed above are only observed in *R. callenderi* and aetosaurs. The second and third characters comprise

drastic changes in the shape and structure of the posterior portion of the skull of *R. callenderi* and aetosaurs relative to other early-diverging archosaurs. Plesiomorphically, the supratemporal fenestrae of early-diverging archosaurs are dorsally oriented, whereas the supratemporal fenestrae in aetosaurs (e.g., *D. smalli*, TTU P-9024) are oriented laterally. The change in orientation of the fenestra in aetosaurs is related to the alteration of the postorbital and squamosal in *R. callenderi* - an intermediate condition between that of early diverging archosaurs and all other aetosauriforms. In particular, the postorbital and squamosal are shifted ventrally exposing the supratemporal fenestrae in lateral view in *R. callenderi*. The postorbital and squamosal are further shifted ventrally in aetosaurs, thus exposing the supratemporal fenestrae completely in lateral view and reducing the size of the infratemporal fenestra (e.g., *D. smalli*, TTU P-9024). In addition, a rounded and thick facet for the paroccipital process on the medial side of the posterior process of the squamosal is also apomorphic for *R. callenderi* and other aetosauriforms.

The first three character states reinforce the articulations between the facial elements associated with jaw musculature (Schumacher, 1973). The location of the abducens nerve foramen was originally hypothesized as a potential synapomorphy supporting a crocodylomorph + aetosaur clade exclusive of other pseudosuchians (Gower, 2002), but more recent phylogenetic analyses, including ours, suggest this apomorphy evolved at least twice—once in aetosauriforms and once in crocodylomorphs. Although not quantified in this analysis, a dorsoventrally thickened skull roof (i.e., nasals, frontals, and parietals) is also shared by *R. callenderi*, erpetosuchids, and aetosaurs.

Postcranially, *R. callenderi* and aetosaurs share similarities in the proportions of the hindlimb to forelimb and shape of the humerus and proximal ankle elements, even though those similarities were not unambiguous synapomorphies. Specifically, *R. callenderi* and aetosaurs share a shortened radius relative to the humerus, and a concave posterior surface of the calcaneal tuber, though these apomorphies have a more widespread distribution among Archosauria. *R. callenderi* and aetosaurs share middle trunk vertebrae that have diapophyses and parapophyses that expand laterally where both articulations originate on a transverse process. Large aetosaurs (e.g., *D. spurensis*, MNA V9300; *T. coccinarum*, NMMNH P-12964; Parker, 2008; Heckert et al., 2010) expand these processes laterally and partially or completely coossify them to the respective rib to form a broad dorsal surface. The expansion of the transverse processes in *R. callenderi* and other aetosaurs seems to correlate with the presence of wide osteoderms. Additionally, although not quantified in the phylogenetic analysis, *R. callenderi* and aetosaurs share a hypertrophied fourth trochanter of the

femur, a character state previously considered unique to aetosaurs (Small, 2002).

The similarities of the osteoderms of *R. callenderi*, aetosaurs, and *A. geoffreyi* give additional support to the new clade, Aetosauriformes, presented here. According to our analysis, *R. callenderi*, *A. geoffreyi*, and aetosaurs share the following carapacial synapomorphies (Figure 12): (a) the presence of lateral osteoderms at least in the trunk region (also present in erpetosuchids); (b) an anterior bar located on the anterior edge of the osteoderm (also shared with *E. olseni* and crocodylomorphs); (c) a ventral carapace in the trunk area; and (d) presacral dorsal osteoderms that are wider than long. Covered with a full set of paramedian, lateral, and ventral osteoderms, the osteoderm arrangements of *R. callenderi* and *A. geoffreyi* both resemble that of aetosaurs (Marsh et al., 2020).

Clearly there is still a large morphological gap between the skeletal morphology of *R. callenderi* and that of aetosaurian members of Aetosauriformes given the high support for the monophyly of all other aetosaurs in this analysis and others (e.g., Marsh et al., 2020; Nesbitt, 2011). After the divergence of *R. callenderi* + *A. geoffreyi* and aetosaurs from their common ancestor, the skull, carapace, and postcranial skeleton of aetosaurs underwent further evolutionary transformations relative to other diapsids. The skulls of aetosaurs exhibit modifications of the anterior portion of the skull by elongating the premaxillae to form an anteroposteriorly enlarged external naris; the supratemporal fenestra became laterally oriented, and in the mandible the anterior dentition is reduced and became “slipper-shaped” (Desojo et al., 2013; Reyes et al., 2020). The carapace of aetosaurs became even more extensive, covering even the ventral portion of the tail (Heckert et al., 2010). The postcranial skeleton was further modified to compensate for the heavy carapace with hypertrophied limb elements (similar to ankylosaur dinosaurs) such as the robust humeri and tibiae as well as a pronounced olecranon process of the ulna. With a nearly identical armor carapace is it not surprising that these same elements in *R. callenderi* are extremely similar in their degree of robustness.

6.2 | *R. callenderi*, *Revueltosaurus*-like taxa, and the isolated tooth problem

The discovery of non-dental cranial and postcranial material referable to *R. callenderi* removed the ornithischian record of the Late Triassic Epoch in current-day North America and beyond and has called into question the utility of taxa based on isolated teeth for use in phylogenetic and biogeographic studies (Butler et al., 2006; Irmis et al., 2010; Irmis, Parker, et al., 2007; Nesbitt et al., 2007; Parker et al., 2005). Furthermore, the realization that

the teeth of *R. callenderi* belong to a pseudosuchian, rather than a dinosaur, has demonstrated the prevalence of convergent dental morphologies across disparate clades of archosauromorphs. This observation that “herbivorous-like” teeth evolved multiple times during the Triassic Period has further garnered support by the discovery of generally similar “herbivorous-like” teeth of silesaurids (Dzik, 2003; Ferigolo and Langer, 2007; Nesbitt et al., 2010; Martz & Small, 2019), and azendohsaurids (Flynn et al., 2010; Nesbitt et al., 2015), not to mention that those of ornithischian dinosaurs could still be present in the Triassic Period (Langer et al., 2017). Given the high rates of convergence in “herbivorous-like” teeth in Triassic archosauromorphs, we are hesitant to diagnose the genus *Revueltosaurus* based solely on the original type and referred species, each based on a single tooth holotype (e.g., “*Revueltosaurus*” *hunti*, “*Revueltosaurus*” *olseni*). Consequently, it is unclear whether many of the *Revueltosaurus*-like teeth are attributable to *Revueltosaurus* or represent other lineages that evolved a similar dental morphology. In the following paragraphs, we outline the problems and discuss possible solutions that can only be solved with the discovery of additional material.

6.2.1 | Diagnosing the Genus *Revueltosaurus*

The holotypes of *R. callenderi* (NMMNH P-4957), “*Revueltosaurus*” *hunti* (NMMNH P-29357), and the recently attributed species “*Revueltosaurus*” (= *Pekinosaurus*) *olseni* (YPM 7666; Heckert et al., 2012) each comprise a single isolated tooth that was the basis for their specific diagnosis. Most recently, Heckert et al. (2012) diagnosed the genus *Revueltosaurus* (comprising *R. callenderi*, *R. hunti*, and *R. olseni*) using the following combination of character states: size (tooth crowns approximately 7 to 15-mm tall); numerous small denticles (more than seven per carina) that are offset (sub-perpendicular) to the tooth margin; denticles proportionately short and often worn to the enamel by precise occlusion; lack of a true cingulum; premaxillary tooth crowns that are approximately twice as tall as maxillary/dentary tooth crowns and weakly recurved; and maxillary/dentary tooth crowns phylodont (leaf-shaped). This diagnosis relies on a combination of character states that are present in other Triassic archosauromorph lineages (e.g., Ezcurra, 2016). For example, the combination of the size of the teeth, the number of the denticles, and the orientation of the denticles overlap with other distantly related taxa (e.g., *Silesaurus opolensis*, Dzik, 2003; *Azendohsaurus madagaskarensis*, Flynn et al., 2010). The character “denticles proportionately short and often worn to the enamel by precise occlusion” lacks precision in terms of what is considered “short,” and the wear pattern is difficult to rule out in other taxa and relies on a certain age of tooth during the replacement cycle (i.e., young

teeth would not be diagnosable because there would not be worn). Furthermore, the absence of apomorphic character states (e.g., absence of cingulum) should not be used in a diagnosis, because they are symplesiomorphies. Additionally, the assignment of tooth position based on a single tooth (e.g., premaxillary tooth crowns are approximately twice as tall as maxillary/dentary tooth crowns and weakly recurved; maxillary/dentary tooth crowns leaf shaped) cannot be determined from the original type material, and even with additional teeth from the same locality, only craniodental material with teeth can provide the association of tooth shape and tooth position. Therefore, the proposed tooth position of the holotype teeth of *K. hunti* and *P. olseni* is assumed based on an inferred close relationship with *R. callenderi*, which is known from craniodental material with teeth (see above). In conclusion, the genus *Revueltosaurus sensu lato* cannot be adequately and sustainably diagnosed based on the type materials of *R. callenderi*, *K. hunti*, and *P. olseni* and we therefore restrict the genus to a single species, *R. callenderi*. As such, we propose that “*R.*” *hunti* retain the subjective junior synonym *Krzyzanowskisaurus hunti* as erected by Heckert (2005) and “*R.*” *olseni* retain the subjective senior synonym *Pekinosaurus olseni*. We further caution the assignment of any existing isolated tooth taxa to *Revueltosaurus*.

We do recognize that in the future, with more complete material, *R. callenderi*, *Krzyzanowskisaurus hunti*, and *Pekinosaurus olseni* may represent a monophyletic genus *Revueltosaurus*, but an assignment of all three species to a single genus is not currently possible because it makes an a priori assumption about relationships (see below) that is parallel to the original argument that the *Revueltosaurus* teeth were assignable to Ornithischia in the first place. This could have undesirable cascading effects on further macroevolutionary studies (e.g., biogeography and paleocology). Alternatively, it is also quite possible that these taxa may turn out to be distantly related.

6.2.2 | What is *Krzyzanowskisaurus hunti*?

Heckert (2002) described “*Revueltosaurus*” *hunti*, later assigned to the new genus *Krzyzanowskisaurus* (Heckert, 2005), based on isolated teeth from the Los Esteros Member of the Santa Rosa Formation (Dockum Group) in central New Mexico and the Blue Mesa Member of the Chinle Formation in eastern Arizona (type locality of *A. geoffreyi*—see Marsh et al., 2020), and has recently been recognized from the lower Chinle Formation in southeastern Utah (Marsh et al., 2020, p. 16). *Krzyzanowskisaurus hunti* teeth are distinguished from *R. callenderi* teeth by the presence of a ridge (“cingulum”) at the base of the tooth crown, which connects with the carinae and is often denticulated (Heckert, 2002, 2005;

Irmis, Parker, et al., 2007; Figures 14a, b). Originally, *Krzyzanowskisaurus* was named given the disparate morphology of the teeth between the two forms and the argument that the *Krzyzanowskisaurus* teeth still were assignable to an ornithischian rather than a pseudosuchian (Heckert, 2005). Irmis, Parker, et al. (2007) disagreed with the assignment of *Krzyzanowskisaurus hunti* to the Ornithischia based on the similar arguments detailing the difficulties of assigning isolated teeth to ornithischians as presented previously and the structure that Heckert (2002, 2005) identified as a “cingulum” was not homologous with similar structures in ornithischian dinosaurs. Furthermore, Irmis, Parker, et al. (2007) also noted that a *Revueltosaurus*-like squamosal, quadrate, and osteoderms were also found at the same Arizona locality as *Krzyzanowskisaurus hunti* teeth, just as had happened at the type locality for *R. callenderi* (Hunt et al., 2005).

These Arizona *Revueltosaurus*-like specimens (Figure 14) come from locality UCMP 7308 (not UCMP 7037/V7037/V7038, contra Long & Murry, 1995; Heckert, 2002, 2005), a diverse mixed assemblage microvertebrate site collected by Charles Camp in the 1920s in the Blue Hills near St. Johns, Arizona, and located in strata equivalent to the lower portion of the Blue Mesa Member at PEFO (Heckert, 2002, 2005; Heckert & Lucas, 2003; Irmis et al., 2011; Marsh et al., 2020; Parker & Martz, 2011). Camp's collections from UCMP 7308 were collected from small localized sandy zones he called “meal pots,” and included abundant small vertebrate remains (Heckert & Lucas, 2002a, 2002b; Long & Murry, 1995). These “meal pots” contain a disarticulated mix of a variety of different taxa and it is difficult to associate different individual elements, though Camp gave each collection area within the locality a separate field number, allowing us to reconstruct the general association of specimens across the broader locality.

Nearly all described teeth of *Krzyzanowskisaurus hunti* from UCMP 7308 come from field number CLC 36/8 (UCMP 139564 to 139,575), except for one tooth from CLC 36/10 (UCMP 139563). In the same volume in which Heckert (2002) named and described “R”. *hunti*, Heckert and Lucas (2002b) described ~50 small rectangular osteoderms from the same locality, assigning them to juveniles of the aetosaur *Calyptosuchus wellsi*. As noted by Irmis, Parker, et al. (2007), these osteoderms (Figures 14i, j) are indistinguishable from those of *R. callenderi*. All of the specimens possess a raised anterior bar and faintly incised widely spaced circular pitting with a random arrangement, a character state combination otherwise unique to *R. callenderi*. Heckert and Lucas (2002b) identified two osteoderm morphotypes: those that are wider than long, which they interpreted as paramedian osteoderms, and those that are longer than wide, which they interpreted as lateral osteoderms. Based on the associated and articulated

specimens of *R. callenderi* from PEFO, the former are paramedian osteoderms from the posterior cervical, dorsal, and anterior caudal regions of the body, whereas the latter morphology belongs to the more distal caudal region of the armor carapace. Many of the osteoderms described by Heckert and Lucas (2002b) possess the same field number as the *Krzyzanowskisaurus hunti* teeth, CLC 36/8.

In examining uncatalogued material from locality UCMP 7308, Irmis, Parker, et al. (2007) also identified two cranial elements referable to *Revueltosaurus* from field area CLC 36/8, a nearly complete left squamosal (UCMP 165205; Figure 14g) (erroneously listed as a right squamosal in Irmis, Parker, et al., 2007), and a partial quadrate (UCMP 165206; Figure 14f). The squamosal (UCMP 165205) is identical to the same element preserved in the PEFO *R. callenderi* specimens; it is triradiate, with a larger anterior process that broadens anteriorly, and short but distinct posterodorsal and posteroventral processes. Like *R. callenderi*, the dorsolateral surface is sculptured; this sculpturing is bounded medially by a distinct ridge that forms the lateral boundary of the supratemporal fossa. Although very similar to aetosaurs, both UCMP 165205 and *R. callenderi* squamosals are proportionally wider and shorter than the same element in aetosaurs (e.g., Desojo & Báez, 2007; Schoch, 2007; Small, 2002; Sulej, 2010). The isolated partial quadrate (UCMP 165206) cannot be formally referred to *Revueltosaurus* because the quadrate of *R. callenderi* does not possess any autapomorphies, but it is identical in shape and morphology to known examples of the element in *R. callenderi*, and shares with this taxon an enlarged medial condyle and vertical orientation. In contrast, aetosaur quadrates are oriented anteroventrally (e.g., Desojo & Báez, 2007; Schoch, 2007; Small, 2002; Sulej, 2010).

Further examination of uncatalogued material from UCMP 7308 by the authors has revealed additional skeletal material likely referable to *Krzyzanowskisaurus hunti* (Figures 14c–g), and all but one of these elements are also from field area CLC 36/8 (the only exception is parietal UCMP 195227, from CLC 36/26–80). A nearly complete left postorbital (UCMP 195217; Figure 14d) is nearly identical to that of *R. callenderi* and differs from most other archosauriforms (e.g., Nesbitt, 2011: figs. 7, 8, 11), including aetosaurs, in possessing a relatively short jugal process that is connected to the squamosal process by a broad web of thin, slightly ornamented bone. Two anterior portions of left parietals (UCMP 195227 and 195228) are unlike the relatively broad, flat condition of most archosaurs (e.g., Nesbitt, 2011: figs. 8, 11), and share with *R. callenderi* a narrow straight shape that broadens slightly towards the frontal articular surface, possesses a low median ridge, and a thin, dorsally-tall ridge on the lateral margin that borders the supratemporal fenestra

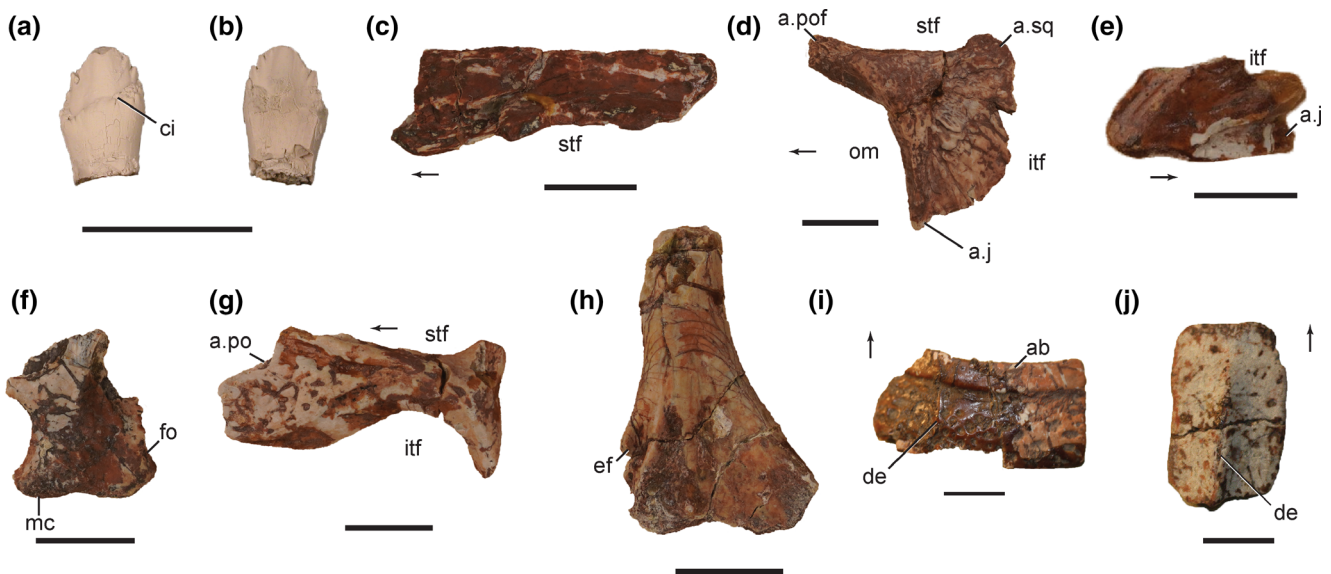


FIGURE 14 Select elements of specimens referred to *Krzyzanowskisaurus hunti* from the Blue Hills, AZ. Isolated tooth coated in ammonium chloride sublimate for clarity (a, b, UCMP 139573), left parietal (c, UCMP 195227), left postorbital (d, UCMP 195217), right quadratojugal (e, UCMP 194219), right quadrate (f, UCMP 165206), left squamosal (g, UCMP 165205), distal end of left humerus (h, UCMP 165207), trunk paramedian osteoderm (i, UCMP 175055), and caudal paramedian osteoderm (j, UCMP 175064) in lingual (a), labial (b), dorsal (c, i, j), lateral (d, e, g), and posterior view (f, h). Abbreviations: a., articulates with; ab, anterior bar; ci, “cingulum”; de, dorsal eminence; ef, ectepicondylar foramen; fo, fossa; itf, infratemporal fenestra; j, jugal; mc, medial condyle; om, orbital margin; pof, postfrontal; sq, squamosal; stf, supratemporal fenestra. Scale bars equal 1 cm, arrows point in anterior direction

(Figure 14c). A right quadratojugal missing its dorsal process (UCMP 195219; Figure 14e) is nearly identical in shape to that of *R. callenderi*, including the autapomorphic v-shaped articular slot for the jugal, though it lacks the heavy ornamentation on the lateral surface of specimens from PEFO. The distal portion of a humerus (UCMP 165207; Figure 14h) and two cervical vertebrae (UCMP 195222) cannot be formally referred to *Revueltosaurus* based on apomorphies, but they are identical to the same elements from *R. callenderi* and do not match the morphology of other archosauriform taxa known from this site (i.e., *A. geoffreyi* and *V. campi*).

The association of *Krzyzanowskisaurus hunti* teeth, *R. callenderi*-like osteoderms, and *R. callenderi*-like cranial elements from UCMP 7308 at the same exact sites (to the extent of the precision available from collection records) is intriguing, but no *Krzyzanowskisaurus hunti* teeth have been found directly associated with or articulated in craniodental material. Our previous work (e.g., Irmis, Nesbitt, et al., 2007; Irmis, Parker, et al., 2007) suggested the teeth, crania and postcrania, and osteoderms may be attributable to a single species and therefore support a close relationship between *Krzyzanowskisaurus hunti* (or even share the same genus) and *R. callenderi*. However, a number of factors make this hypothesis equivocal. First, it is clear that Camp’s “meal pots” contain a diversity of vertebrate remains (Heckert & Lucas, 2002a; Long & Murry, 1995; Marsh et al., 2020) and the association can be

coincidental. Second, the teeth of *Krzyzanowskisaurus hunti* do not share any unique character states with *R. callenderi* exclusive of other archosauromorphs with “herbivorous-like” teeth. Third, teeth identical to *R. callenderi* have now been found at similar stratigraphic levels this series of localities (see Geologic Setting above). Granted, *R. callenderi* teeth (*sensu stricto*) have not been found at the “meal pots” but, this should not rule out the possible presence of *R. callenderi* at the locality because they occur at roughly the same stratigraphic occurrence at the nearby Petrified Forest National Park. Given this information, we are hesitant to assign the *R. callenderi*-like non-dental cranial elements to *Krzyzanowskisaurus hunti* and maintain that *Krzyzanowskisaurus hunti* could possibly be distantly related to *R. callenderi*. The cranial and post-cranial skeletal material documented above do indicate that a *Revueltosaurus*-like taxon is present in the UCMP 7308 assemblage, but we must remain agnostic as to whether this is the same taxon as *K. hunti*. Only the discovery of *Krzyzanowskisaurus hunti* teeth unambiguously associated with cranial and/or postcranial remains will help phylogenetic affinities and alpha taxonomy of the species.

6.2.3 | Other *Revueltosaurus*-like taxa

A potential *Revueltosaurus*-like animal is present in the Wolfville Formation (Carnian; Sues & Olsen, 2015) of

Nova Scotia. Originally referred to an ornithischian dinosaur (Galton, 1983), Irmis, Parker, et al. (2007) argued that NSM 004 GF 012.001, a posterior portion of a left maxilla with much of a tooth in an alveolus, shares a number of character states with *R. callenderi* both in dental and maxillary morphology including a strong ridge along the ventral margin of the antorbital fossa, the well-developed buccal emargination of the tooth row in ventral view, and a denticled tooth crown lacking a basal asymmetrical swelling (Irmis, Parker, et al., 2007). An ilium from the Wolfville Formation (NSM 012 GF 032.021) is very similar to that of *R. callenderi* in having an anterior process of the iliac blade that does not extend anteriorly beyond the anterior extent of the pubic peduncle and has a broad, rounded dorsal margin to the iliac blade. This element also supports the presence of a *Revueltosaurus*-like taxon from the formation (Sues & Olsen, 2015).

6.3 | Biostratigraphic occurrences and implications

R. callenderi has only been recorded from two areas, the type locality in the Bull Canyon Formation (Dockum Group) of eastern New Mexico (Hunt, 1989; Hunt et al., 2005) and the Chinle Formation at Petrified Forest National Park (Padian, 1990; Beuhler et al., 2001; Parker et al., 2005; Atchley et al., 2013; Figure 1b). At the latter location, prior to finding voucher specimens of the taxon in the uppermost Blue Mesa Member and middle Sonsela Member, *R. callenderi* was thought to occur in a restricted stratigraphic range in the lower-middle Petrified Forest Member (Beuhler et al., 2001; Hunt, 2001; Parker & Martz, 2011). Based on this, Hunt (2001) argued that *R. callenderi* was of biochronological utility. In both the New Mexican type locality and Painted Desert localities in northern PEFO, *R. callenderi* cooccurs with the aetosaur *T. coccinarum* and mystriosuchine (= pseudopalatine) leptosuchomorph phytosaurs, taxa that have been used as index taxa for the Revueltian holochronozone (Lucas & Hunt, 1993; Martz & Parker, 2017). Loughney et al. (2011) argued that because at PEFO *R. callenderi* was found only in a specific facies (blue paleosols) at a single stratigraphic level (just above the Painted Desert 3 Sandstone), that these occurrences did not represent the true stratigraphic range of the taxon and instead reflected a preservation bias. Subsequent discoveries of *R. callenderi* material from the Owl Rock Member (Gordon et al., 2020; Whatley et al., 2013) and Sonsela Member (Atchley et al., 2013) supports this hypothesis, and these new specimens demonstrate that at least at PEFO, the stratigraphic range of *R. callenderi*

extends into the underlying Adamanian holochronozone. The absence of *R. callenderi* at other pencontemporaneous sites in the American Southwest is puzzling, particularly given how abundant it is at the sites where it does occur. For example, the vertebrate assemblage of the Petrified Forest Member at Ghost Ranch in northern New Mexico is geographically intermediate between the type locality of *R. callenderi* and PEFO, shares the presence a variety of Revueltian index taxa (Irmis, Nesbitt, et al., 2007; Whiteside et al., 2015), and has precise age constraints that show it overlaps in time with the lower Petrified Forest Member at PEFO (Irmis et al., 2011; Rasmussen et al., 2020). There is no obvious taphonomic reason why this well-sampled and diverse assemblage should not preserve *Revueltosaurus*, as it contains everything from small-bodied drepanosaurs to large-bodied phytosaurs and aetosaurs. Similarly, it is curious that *R. callenderi* has not been found at other Bull Canyon Formation sites or in equivalent strata in west Texas (e.g., Lehman & Chatterjee, 2005; Martz et al., 2013; Martz & Parker, 2017).

The presence of dental, cranial, and osteoderm elements referable to *R. callenderi* from the upper part of the Blue Mesa Member at PEFO now extends the stratigraphic range of the taxon even further, into the Adamanian (Figure 1b). The assemblage from the upper part of the Blue Mesa Member includes the aetosaur *D. spurensis* and non-pseudopalatine leptosuchomorph phytosaurs, which have been used as index taxa of the Adamanian holochronozone (Heckert et al., 2007; Lucas & Hunt, 1993; Martz & Parker, 2017). Thus, *R. callenderi* demonstratively occurs in Adamanian and Revueltian units, but it remains unclear if the stratigraphic ranges of *R. callenderi* and *K. hunti* overlap, as they have never been found in the immediate vicinity of each other. The lowest occurrences of *R. callenderi* at PEFO are in the uppermost Blue Mesa Member (Figure 1b) and date to between 218.5–216.5 Ma (Rasmussen et al., 2020), whereas the St. Johns *K. hunti* material from the upper Blue Mesa Member are only constrained to a maximum age of 219.39 ± 0.12 Ma (Ramezani et al., 2014). So, we cannot determine whether these *K. hunti* specimens are slightly older or the same age as the oldest PEFO specimens of *R. callenderi*. Arguably, if all of the St. Johns skeletal material belongs to the taxon *Krzyzanowskisaurus hunti* (see above), this taxon may be restricted to the lower Chinle Formation and Dockum Group, and *R. callenderi* would occur only in the Upper Chinle and Dockum. If *Pekinosaurus olseni* is more closely related to *R. callenderi* than to other archosauromorphs as suggested by Irmis, Parker, et al. (2007) and Heckert et al. (2012), *Revueltosaurus*-like taxa have a longer stratigraphic range than previously

recognized. *Pekinosaurus olseni* is from the Pekin Formation in the Deep River Basin of North Carolina, which is dated to the late Carnian (Olsen et al., 2015; Whiteside et al., 2011), and thus older than any occurrence from western United States. Finally, Heckert et al. (2012) report *Pekinosaurus olseni* from a microvertebrate assemblage in the overlying Cumnock Formation of the Deep River Basin in North Carolina, which is earliest Norian in age (Olsen et al., 2015; Whiteside et al., 2011), and therefore also older than *R. callenderi* or *K. hunti*. Thus, isolated teeth similar to *Revueltosaurus* from the eastern United States may suggest an even longer stratigraphic range for these potentially related taxa, beginning in the late Carnian and extending through the late Norian. Thus, the use of *Revueltosaurus* as an index taxon is questionable.

6.4 | Social grouping in Triassic Pseudosuchians

Mass death assemblages of the same species of pseudosuchians occur throughout the Triassic and have been found in paracrocodylomorphs (de França et al., 2011; Nesbitt et al., 2020) and in aetosauriforms. The *Revueltosaurus* Quarry (PFV 297) contains a minimum of 12 associated individuals, all of which seem to be juveniles or subadults based on overall size (specimens of *R. callenderi* from nearby PFV 231 are larger than those from PFV 297), and limb bone size distribution compared to osteohistology (see above section). In addition, PFV 297 specimens display incomplete ossification of the otic capsule, frontals and parietals, scapulocoracoid, and two specimens (PEFO 36875 and PEFO 36876) have separate exoccipitals and opisthotics. Individuals from this site also display open neurocentral sutures on the vertebrae (sensu Brochu, 1992, 1996). In phytosaurs and crocodylians, complete closure of the neurocentral sutures proceeds in a posterior to anterior sequence (Brochu, 1992, 1996; Irmis, 2007) that also occurs in these specimens of *R. callenderi*. Together with available taphonomic information (see Geologic Setting), these data suggest the possibility that PFV 297 preserves individuals that grouped together in life, at least perimortem. Ongoing study of the osteohistology of the majority of the individuals from the quarry will be published separately (Tulga, 2014).

Another Late Triassic monodominant assemblage of immature aetosauriforms is the Kaltental block (SMNS 5770) from the Stubensandstein of the German Keuper, which contains over 20 individuals of the small aetosaur *A. ferratus* that are almost completely articulated and piled on top of each other (Schoch, 2007: fig. 2). As noted by Schoch (2007), these specimens display numerous

indicators of skeletal immaturity (e.g., open neurocentral and scapulocoracoid sutures, and osteoderm ornamentation, but see Griffin et al., 2020), and also appear to comprise some sort of grouping in life. Other similar early pseudosuchian aggregations are rare, but include the monodominant bonebeds of the poposauroid *Lotosaurus adentus* (Hagen et al., 2018; Zhang, 1975), and the loricatan *Decuriasuchus quartacolonina* (França et al., 2011), as well as other more taxonomically diverse bonebeds containing an abundance of individuals from particular pseudosuchian species (e.g., Fiorillo et al., 2000; Martz et al., 2013; Nesbitt et al., 2020; Nesbitt & Stocker, 2008). These data suggest that social grouping of early pseudosuchians is underappreciated given its prevalence in extant relatives (e.g., summary in Grigg & Kirshner, 2015), but the nature and extent of this sociality is unknown.

7 | CONCLUDING REMARKS

R. callenderi is a key taxon for clarifying the phylogeny of pseudosuchian archosaurs. Although currently recovered as the sister taxon to Aetosauria (or member of a clade that is the sister taxon to Aetosauria), *R. callenderi* also presents numerous character states found only in other suchian clades such as rausuchids and early-diverging crocodylomorphs. We have lightheartedly referred to *R. callenderi* as the “duckbilled platypus” of the Triassic because of its shared characteristics with aetosaurs such as the laterally oriented squamosal and dorsal and ventral carapace of rectangular osteoderms, its plesiomorphic ilium with a highly reduced preacetabular process, the bulbous fourth trochanter of the femur and unique articulation of the nasal and premaxilla that are only otherwise known in *T. dabanensis*, the maxillary ridge ventral to the antorbital fossa and interdental plates as in *P. kirpatricki*, and of course a tooth morphology and buccal emargination that is convergent with early-diverging ornithischian dinosaurs.

As a non-aetosaur aetosauriform, *R. callenderi* is of major phylogenetic significance in determining the early diversification of major clades within Pseudosuchia as aetosauriforms represent a previously unrecognized group of suchian archosaurs that potentially have a wider geographic and temporal distribution (Marsh et al., 2020; Nesbitt et al., 2012; Nesbitt & Butler, 2013). The presence of at least 12 individuals from a single quarry at PEFO represents an important sample size allowing greater understanding of this taxon and its close relatives. Future studies need to focus on the functional morphology and osteohistological variability of *R. callenderi* as well as character state variability owing to intraspecific and ontogenetic sources of variation.

ACKNOWLEDGEMENTS


The authors thank Petrified Forest National Park Superintendents Lee Baiza, Cliff Spencer, and Brad Traver, Chiefs of Resource Management Karen Dorn and Pat Thompson, and the rest of the park staff for logistical support. Excavation work was assisted by Yasemin Tulu, Katie Brakora, Bruce Bailey, Franceska Sena, Meredith Fontana, Susan Drymala, Jake Tapaha, Ben Kligman, Emily Lessner, Pete Reser, and the late Vin Morgan. Additional preparation of specimens was done by Pete Reser, Bruce Bailey, Emily Lessner, Cathy Lash, Matt Smith, and Kenny Bader. Thank you to Christian Sidor and Kelsey Abrams (UWBM) for preparation, photographs, and access to specimens at their institution. Additional assistance in the field was provided by the NPS Youth Conservation Corps and the Navajo Conservation Corps. Additional photography and drawings were done by Tyra Olstad. Dr. Pat Holroyd (UCMP) kindly provided access to collections in her care. K. Ritterbush (University of Utah) generously provided access to her petrographic microscope imaging system, and the osteoderm histological slides were imaged by J. Hambleton. Reviews by Hans-Dieter Sues, Julia B. Desojo, and Martin Ezcurra improved the manuscript. This is Petrified Forest National Park Paleontological Contribution No. 74. The views expressed herein are those of the authors and do not represent the official views of the U. S. Government.


AUTHOR CONTRIBUTIONS

William Parker: Conceptualization (equal); formal analysis (lead); funding acquisition (lead); investigation (lead); methodology (lead); project administration (lead); writing – original draft (equal); writing – review and editing (equal). **Sterling Nesbitt:** Conceptualization (supporting); formal analysis (equal); investigation (equal); methodology (equal); writing – original draft (equal); writing – review and editing (equal). **Randall Irmis:** Conceptualization (equal); formal analysis (equal); investigation (equal); methodology (equal); writing – original draft (equal); writing – review and editing (equal). **Jeffrey Martz:** Formal analysis (supporting); investigation (supporting); methodology (supporting); visualization (equal); writing – original draft (supporting); writing – review and editing (supporting). **Adam Marsh:** Data curation (supporting); formal analysis (supporting); investigation (supporting); methodology (equal); writing – review and editing (lead). **Matthew Brown:** Investigation (equal); methodology (equal); writing – original draft (equal); writing – review and editing (equal). **Michelle Stocker:** Formal analysis (supporting); investigation (supporting); methodology (supporting); resources (supporting); writing – review and editing (supporting). **Sarah Werning:** Formal analysis (supporting); investigation (supporting); methodology (supporting); visualization (supporting); writing – original


draft (supporting); writing – review and editing (supporting).


ORCID

William G. Parker  <https://orcid.org/0000-0002-6005-7098>

Sterling J. Nesbitt  <https://orcid.org/0000-0002-7017-1652>

Adam D. Marsh  <https://orcid.org/0000-0002-3223-8940>

Matthew A. Brown  <https://orcid.org/0000-0002-2713-1161>

Michelle R. Stocker  <https://orcid.org/0000-0002-6473-8691>

Sarah Werning  <https://orcid.org/0000-0002-2405-595X>

REFERENCES

- Arcucci, A., Previtiera, E., & Mancuso, A. C. (2019). Ecomorphology and bone microstructure of Proterochampsia from the Chafiares Formation. *Acta Palaeontologica Polonica*, *64*, 157–170.
- Ash, S. R. (2005). Synopsis of the Upper Triassic flora of Petrified Forest National Park and vicinity. *Mesa Southwest Museum Bulletin*, *9*, 53–61.
- Atchley, S. C., Nordt, L. C., Dworkin, S. I., Ramezani, J., Parker, W. G., Ash, S. R., & Bowring, S. A. (2013). A linkage among Pangean tectonism, cyclic alluviation, climate change, and biologic turnover in the Late Triassic: The record from the Chinle Formation, southwestern United States. *Journal of Sedimentary Research*, *83*, 1147–1161.
- Baird, I. L. (1970). The anatomy of the reptilian ear. In C. Gans & T. Parsons (Eds.), *Biology of the Reptilia 2, morphology B* (pp. 193–275). Academic Press.
- Baranyi, V., Reichgelt, T., Olsen, P. E., Parker, W. G., & Kürschner, S. (2018). Norian vegetation history and related environmental changes: New data from the Chinle Formation, Petrified Forest National Park (Arizona SW USA). *Geological Society of America Bulletin*, *130*, 775–795.
- Beuhler, H., Hunt, A. P., & Wright, J. (2001). The biochronological and paleoecological significance of the ornithischian dinosaur *Revueltosaurus callenderi* in the Upper Triassic of the American Southwest. *New Mexico Geology*, *23*, 64.
- Bever, G. S., Bell, C. J., & Maisano, J. A. (2005). The ossified braincase and cephalic osteoderms of *Shinisaurus crocodilurus* (Squamata, Shinisauridae). *Palaeontologia Electronica*, *8*, 1–36.
- Billingsley, G. (1985). General stratigraphy of the Petrified Forest National Park, Arizona. *Museum of Northern Arizona Bulletin*, *54*, 3–8.
- Botha, J., & Chinsamy, A. (2004). Growth and lifestyle adaptations of the Triassic non-mammalian cynodont *Trirachodon*. *Acta Palaeontologica Polonica*, *49*, 619–627.
- Botha-Brink, J., & Smith, R. M. H. (2011). Osteohistology of the Triassic archosauromorphs *Prolacerta*, *Proterosuchus*, *Euparkeria*, and *Erythrosuchus* from the Karoo Basin of South Africa. *Journal of Vertebrate Paleontology*, *31*, 1238–1254.
- Brinkman, D. B., Eberth, D. A., & Currie, P. J. (2007). From bonebeds to paleobiology: Applications of bonebed data. In R. R. Rogers, D. A. Eberth, & A. R. Fiorillo (Eds.), *Bonebeds:*

- Genesis, analysis, and paleobiological significance* (pp. 221–264). University of Chicago Press.
- Brochu, C. A. (1992). *Ontogeny of the postcranium in crocodylomorph archosaurs [M.A.]* (p. 340). University of Texas.
- Brochu, C. A. (1996). Closure of neurocentral sutures during crocodylian ontogeny: Implications for maturity assessment in fossil archosaurs. *Journal of Vertebrate Paleontology*, *16*, 49–62.
- Brusatte, S. L., Benton, M. J., Desojo, J. B., & Langer, M. C. (2010). The higher-level phylogeny of Archosauria (Tetrapoda: Diapsida). *Journal of Systematic Palaeontology*, *8*, 3–47.
- Butler, R. J., Nesbitt, S. J., Charig, A. J., Gower, D. J., & Barrett, P. M. (2018). *Mandasuchus tanyauchen*, gen. et sp. nov., a pseudosuchian archosaur from the Manda Beds (?Middle Triassic) of Tanzania. *Society of Vertebrate Paleontology Memoir*, *17*, 96–121.
- Butler, R. J., Porro, L. B., & Heckert, A. B. (2006). A supposed heterodontosaurid tooth from the Rhaetian of Switzerland and a reassessment of the European Late Triassic record of Ornithischia (Dinosauria). *Neues Jahrbuch für Geologie und Paläontologie Monatshefte*, *2006*, 613–633.
- Butler, R. J., Sullivan, C., Ezcurra, M. D., Liu, J., Lecuona, A., & Sookias, R. B. (2014). New clade of enigmatic early archosaurs yields insights into early pseudosuchian phylogeny and the biogeography of the archosaur radiation. *BMC Evolutionary Biology*, *14*, 128.
- Butler, R. J., Upchurch, P., & Norman, D. B. (2008). The phylogeny of the ornithischian dinosaurs. *Journal of Systematic Palaeontology*, *6*, 1–40.
- Camp, C. L. (1930). A study of the phytosaurs with description of new material from western North America. *Memoirs of the University of California*, *10*, 1–160.
- Case, E. C. (1922). New reptiles and stegocephalians from the Upper Triassic of western Texas. *Carnegie Institute of Washington Publication*, *321*, 1–84.
- Case, T. J. (1978). On the evolution and adaptive significance of postnatal growth rates in the terrestrial vertebrates. *Quarterly Review of Biology*, *53*, 243–282.
- Castanet, J. (2006). Time recording in bone microstructures of endothermic animals; functional relationships. *Comptes Rendus Palevol*, *5*, 629–636.
- Cerda, I. A., & Desojo, J. B. (2011). Dermal armour histology of aetosaurs (Archosauria: Pseudosuchia), from the Upper Triassic of Argentina and Brazil. *Lethaia*, *44*, 417–428.
- Cerda, I. A., Desojo, J. B., & Scheyer, T. M. (2018). Novel data on aetosaur (Archosauria, Pseudosuchia) osteoderm microanatomy and histology: Palaeobiological implications. *Palaeontology*, *61*, 721–745.
- Chatterjee, S. (1978). A primitive parasuchid (phytosaur) reptile from the Upper Triassic Maleri Formation of India. *Palaeontology*, *21*, 83–127.
- Chatterjee, S. (1985). *Postosuchus*, a new thecodontian reptile from the Triassic of Texas and the origin of tyrannosaurs. *Philosophical Transactions of the Royal Society of London, Series B*, *309*, 395–460.
- Chinsamy, A., & Elzanowski, A. (2001). Bone histology: Evolution of growth pattern in birds. *Nature*, *412*, 402–403.
- Chinsamy, A., Martin, L. D., & Dodson, P. (1998). Bone microstructure of the diving *Hesperornis* and the volant *Ichthyornis* from the Niobrara Chalk of western Kansas. *Cretaceous Research*, *19*, 225–235.
- Chinsamy, A., & Raath, M. A. (1992). Preparation of fossil bone for histological examination. *Palaeontologia Africana*, *29*, 39–44.
- Cope, E. D. (1869). Synopsis of the extinct Batrachia, Reptilia, and Aves of North America. *Transactions of the American Philosophical Society, Ns*, *14*, 1–252.
- Cubo, J., Le Roy, N., Martinez-Maza, C., & Montes, L. (2012). Paleohistological estimation of bone growth rate in extinct archosaurs. *Paleobiology*, *38*, 335–349.
- Cubo, J., Legendre, P., de Ricqlès, A., Montes, L., de Margerie, E., Castanet, J., & Desdevises, Y. (2008). Phylogenetic, functional, and structural components of variation in bone growth rate of amniotes. *Evolution and Development*, *10*, 217–227.
- de Buffrénil, V. (1982). Morphogenesis of bone ornamentation in extant and extinct crocodylians. *Zoomorphology*, *99*, 155–166.
- de Buffrénil, V., Clarac, F., Fau, M., Martin, S., Martin, B., Pellé, E., & Laurin, M. (2015). Differentiation and growth of bone ornamentation in vertebrates: A comparative histological study among the Crocodylomorpha. *Journal of Morphology*, *276*, 425–445.
- de França, M. A. G., Ferigolo, J., & Langer, M. C. (2011). Associated skeletons of a new middle Triassic “Rauisuchia” from Brazil. *Naturwissenschaften*, *98*, 389–395.
- de Margerie, E., Cubo, J., & Castanet, J. (2002). Bone typology and growth rate: Testing and quantifying ‘Amprino’s rule’ in the mallard (*Anas platyrhynchos*). *Comptes Rendus Biologies*, *325*, 221–230.
- de Margerie, E., Robin, J.-P., Verrier, D., Cubo, J., Groscolas, R., & Castanet, J. (2004). Assessing a relationship between bone microstructure and growth rate: A fluorescent labelling study in the king penguin chick (*Aptenodytes patagonicus*). *Journal of Experimental Biology*, *207*, 869–879.
- de Ricqlès, A., Padian, K., Knoll, F., & Horner, J. R. (2008). On the origin of high growth rates in archosaurs and their ancient relatives: Complementary histological studies on Triassic archosauriforms and the problem of a “phylogenetic signal” in bone histology. *Annales de Paléontologie*, *94*, 57–76.
- de Ricqlès, A. J., Padian, K., & Horner, J. R. (2003). On the bone histology of some Triassic pseudosuchian archosaurs and related taxa. *Annales de Paléontologie*, *89*, 67–101.
- Desojo, J. B., Arcucci, A. B., & Marsicano, C. A. (2002). Reassessment of *Cuyosuchus huenei*, a Middle-Late Triassic archosauriform from the Cuyo Basin, west-central Argentina. *New Mexico Museum of Natural History and Science Bulletin*, *21*, 143–148.
- Desojo, J. B., & Báez, A. M. (2007). Cranial morphology of the Late Triassic South American archosaur *Neoaetosauroides engaeus*: Evidence for aetosaurian diversity. *Palaeontology*, *50*, 267–276.
- Desojo, J. B., & Ezcurra, M. D. (2011). A reappraisal of the taxonomic status of *Aetosauroides* (Archosauria, Aetosauria) specimens from the Late Triassic of South America and their proposed synonymy with *Stagonolepis*. *Journal of Vertebrate Paleontology*, *31*, 596–609.
- Desojo, J. B., Ezcurra, M. D., & Kischlat, E. E. (2012). A new aetosaur genus (Archosauria: Pseudosuchia) from the early late Triassic of southern Brazil. *Zootaxa*, *3166*, 1–33.
- Desojo, J. B., Heckert, A. B., Martz, J. W., Parker, W. G., Schoch, R. R., Small, B. J., & Sulej, T. (2013). Aetosauria: A clade of

- armoured pseudosuchians from the Upper Triassic continental beds. In S. J. Nesbitt, J. B. Desojo, & R. B. Irmis (Eds.), *The Geological Society of London Anatomy, phylogeny and Palaeobiology of early archosaurs and their kin* (Vol. 379, pp. 203–239). Geological Society, Special Publications.
- Desojo, J. B., Von Baczko, M. B., & Rauhut, O. W. M. (2020). Anatomy, taxonomy and phylogenetic relationships of *Prestosuchus chiniquensis* (Archosauria: Pseudosuchia) from the original collection of von Huene, Middle-Late Triassic of southern Brazil. *Palaeontologia Electronica*, 23, a04. <https://doi.org/10.26879/21026palaeo-electronica.org/content/22020/22917-type-materials-of-prestosuchus>
- Drózdź, D. (2018). Osteology of a forelimb of an aetosaur *Stagonolepis olenkae* (Archosauria: Pseudosuchia: Aetosauria) from the Krasiejów locality in Poland and its probable adaptations for a scratch-digging behavior. *PeerJ*, 6, e5595.
- Dzik, J. (2003). A beaked herbivorous archosaur with dinosaur affinities from the early Late Triassic of Poland. *Journal of Vertebrate Paleontology*, 23, 556–574.
- Eberth, D. A., & Brinkman, D. B. (1997). Paleocology of an estuarine, incised-valley fill in the Dinosaur Park Formation (Judith River Group, Upper Cretaceous) of southern Alberta, Canada. *PALAIOS*, 12, 43–58.
- Eberth, D. A., Shannon, M., & Noland, B. G. (2007). A bonebeds database: Classification, biases, and patterns of occurrence. In R. R. Rogers, D. A. Eberth, & A. R. Fiorillo (Eds.), *Bonebeds: Genesis, analysis, and paleobiological significance* (pp. 103–219). University of Chicago Press.
- Emmons, E. (1856). *Geological report of the midland counties of North Carolina*. G. P. Putnam and Co.
- Ewer, R. F. (1965). The anatomy of the thecodont reptile *Euparkeria capensis* Broom. *Philosophical Transactions of the Royal Society of London, Series B*, 248, 379–435.
- Ezcurra, M. D. (2016). The phylogenetic relationships of basal archosauromorphs, with an emphasis on the systematics of proterosuchian archosauriforms. *PeerJ*, 4, e1778.
- Ezcurra, M. D., Fiorelli, L. E., Martinelli, A. G., Rocher, S., von Baczko, M. B., Ezpeleta, M., Taborda, J. R. A., Hechenleitner, E. M., Trotteyn, M. J., & Desojo, J. B. (2017). Deep faunistic turnovers preceded the rise of dinosaurs in southwestern Pangaea. *Nature Ecology and Evolution*, 1, 1477–1483.
- Ezcurra, M. D., Nesbitt, S. J., Bronzati, M., Dalla Vecchia, F. M., Agnolin, F. L., Benson, R. B. J., Brissón Egli, F., Cabreira, S. F., Evers, S. W., Gentil, A. R., Irmis, R. B., Martinelli, A. G., Novas, F. E., Roberto da Silva, L., Smith, N. D., Stocker, M. R., Turner, A. H., & Langer, M. C. (2020). Enigmatic dinosaur precursors bridge the gap to the origin of Pterosauria. *Nature*, 588, 445–449.
- Ferigolo, J., & Langer, M. C. (2007). A Late Triassic dinosauriform from south Brazil and the origin of the ornithischian predeceps bone. *Historical Biology*, 19, 23–33.
- Fiorillo, A. R., Padian, K., & Musikasinthorn, C. (2000). Taphonomy and depositional setting of the *Placerias* Quarry (Chinle Formation: Late Triassic, Arizona). *PALAIOS*, 15, 373–386.
- Flynn, J. J., Nesbitt, S. J., Parrish, J. M., Ranivoharimanana, L., & Wyss, A. R. (2010). A new species of *Azendohsaurus* (Diapsida: Archosauromorpha) from the Triassic Isalo Group of southwestern Madagascar: Cranium and mandible. *Palaeontology*, 53, 669–688.
- Foth, C., Ezcurra, M. D., Sookias, R. B., Brusatte, S. L., & Butler, R. J. (2016). Unappreciated diversification of stem archosaurs during the Middle Triassic predated the dominance of dinosaurs. *BMC Evolutionary Biology*, 16, 1–10.
- Fraas, O. (1877). *Aetosaurus ferratus*, die gepanzerte Vogelechse aus dem Stubensandstein bei Stuttgart. *Jahreshefte des Vereins für Vaterländische Naturkunde in Württemberg*, 33, 1–21.
- Francillon-Vieillot, H., de Buffrénil, V., Castanet, J., Géraudie, J., Meunier, F. J., Sire, J. Y., Zylberberg, L., & de Ricqlès, A. (1990). Microstructure and mineralization of vertebrate skeletal tissues. In J. G. Carter (Ed.), *Skeletal biomineralization: Patterns, processes and evolutionary trends* (Vol. 1, pp. 471–530). Van Nostrand Reinhold.
- Galton, P. M. (1983). The oldest ornithischian dinosaurs in North America from the Late Triassic of Nova Scotia, N.C., and PA. *Geological Society of America, Abstracts with programs*, 15, 122.
- Games, I. (1990). Growth curves for the Nile crocodile as estimated by skeletochronology. In: *Crocodyles: Proceedings of the 10th Working Meeting of the Crocodile Specialist Group, Volume 1*. Gland, Switzerland: IUCN - The World Conservation Union. p 111–121.
- García Marsà, J. A., Agnolin, F. L., & Novas, F. E. (2020). Comparative bone microstructure of three archosauromorphs from the Carnian, late Triassic Chañares formation of Argentina. *Acta Palaeontologica Polonica*, 65, 387–398.
- Gauthier, J., & Padian, K. (1985). Phylogenetic, functional, and aerodynamic analyses of the origin of birds and their flight. In M. K. Hecht, J. H. Ostrom, G. Viohl, & P. Wellnhofer (Eds.), *The beginning of birds: Proceedings of the international archaeopteryx conference* (pp. 185–197). Freunde des Jura Museums.
- Good, S. C. (1998). Freshwater bivalve fauna of the Late Triassic (Carnian-Norian) Chinle, Dockum, and Dolores formations of the southwest United States. In P. A. Johnson & J. W. Haggart (Eds.), *Bivalves: An eon of evolution - Paleobiological studies honoring Norman D Newell* (pp. 223–249). University of Calgary Press.
- Gordon, C. M., Roach, B. T., Parker, W. G., & Briggs, D. E. G. (2020). Distinguishing regurgitalites and coprolites: A case study using a Triassic bromalite with soft tissue of the pseudosuchian archosaur *Revueltosaurus*. *PALAIOS*, 35, 111–121.
- Gower, D. J. (1999). The cranial and mandibular osteology of a new raiusuchian archosaur from the middle Triassic of southern Germany. *Stuttgarter Beiträge zur Naturkunde, Serie B*, 280, 1–49.
- Gower, D. J. (2002). Braincase evolution in suchian archosaurs (Reptilia: Diapsida): Evidence from the raiusuchian *Batrachotomus kupferzellensis*. *Zoological Journal of the Linnean Society*, 136, 49–76.
- Gower, D. J. (2003). Osteology of the early archosaurian reptile *Erythrosuchus africanus* Broom. *Annals of the South African Museum*, 110, 1–88.
- Gower, D. J., & Nesbitt, S. J. (2006). The braincase of *Arizonasaurus babbitti* - further evidence for the non-monophyly of 'raiusuchian' archosaurs. *Journal of Vertebrate Paleontology*, 26, 79–87.
- Gower, D. J., & Schoch, R. R. (2009). Postcranial anatomy of the raiusuchian archosaur *Batrachotomus kupferzellensis*. *Journal of Vertebrate Paleontology*, 29, 103–122.
- Gower, D. J., & Sennikov, A. G. (1996). Morphology and phylogenetic informativeness of early archosaur braincases. *Palaeontology*, 39, 883–906.

- Gower, D. J., & Walker, A. D. (2002). New data on the braincase of the aetosaurian archosaur (Reptilia: Diapsida) *Stagonolepis robertsoni* Agassiz. *Zoological Journal of the Linnean Society*, 136, 7–23.
- Gower, D. J., & Weber, E. (1998). The braincase of *Euparkeria*, and the evolutionary relationships of birds and crocodylians. *Biological Reviews*, 73, 367–411.
- Gower, D. J., & Wilkinson, M. (1996). Is there any consensus on basal archosaur phylogeny? *Philosophical Transactions of the Royal Society of London, Series B*, 263, 1399–1406.
- Griffin, C. T., Stocker, M. R., Colleary, C., Stefanic, C. M., Lessner, E. J., Riegler, M., Formoso, K., Koeller, K., & Nesbitt, S. J. (2020). Assessing ontogenetic maturity in extinct saurian reptiles. *Biological Reviews (Early View)*, 96, 470–525. <https://doi.org/10.1111/brv.12666>
- Grigg, G., & Kirshner, D. (2015). *Biology and evolution of Crocodylians*. CSIRO Publishing.
- Guarino, G. M., & Erismis, U. C. (2008). Age determination and growth by skeletochronology of *Rana holtzi*, an endemic frog from Turkey. *Italian Journal of Zoology*, 75, 237–242.
- Hagen, C. J., Roberts, E. M., Sullivan, C., Liu, J., Wang, Y., Owusu Agyemang, P. C., & Xu, X. (2018). Taphonomy, geological age, and paleobiogeography of *Lotosaurus adentus* (Archosauria: Posauroidea) from the Middle-Upper Triassic Badong Formation, Hunan, China. *PALAIOS*, 33, 106–124.
- Hay, O. P. (1930). *Second bibliography and catalogue of the fossil Vertebrata of North America*. Carnegie Institution.
- Heckert, A. B. (2002). A revision of the Upper Triassic ornithischian dinosaur *Reueltosaurus*, with a description of a new species. *New Mexico Museum of Natural History and Science Bulletin*, 21, 253–266.
- Heckert, A. B. (2005). *Krzyzanowskisaurus*, a new name for a probable ornithischian dinosaur from the Upper Triassic Chinle Group, Arizona and New Mexico, USA. *New Mexico Museum of Natural History and Science Bulletin*, 29, 76–82.
- Heckert, A. B., & Lucas, S. G. (1999). A new aetosaur (Reptilia: Archosauria) from the Upper Triassic of Texas and the phylogeny of aetosaurs. *Journal of Vertebrate Paleontology*, 19, 50–68.
- Heckert, A. B., & Lucas, S. G. (2002a). Revised Upper Triassic stratigraphy of the Petrified Forest National Park, Arizona, U.S.A. *New Mexico Museum of Natural History and Science Bulletin*, 21, 1–36.
- Heckert, A. B., & Lucas, S. G. (2002b). Osteoderms of juveniles of *Stagonolepis* (Archosauria: Aetosauria) from the lower Chinle Group, east-central Arizona. *New Mexico Museum of Natural History and Science Bulletin*, 21, 235–239.
- Heckert, A. B., & Lucas, S. G. (2003). Stratigraphy and paleontology of the lower Chinle group (Adamanian - latest Carnian) in the vicinity of St. Johns, Arizona. *New Mexico Geological Society Guidebook*, 54, 281–288.
- Heckert, A. B., & Lucas, S. G. (2006). Micro- and small vertebrate biostratigraphy and biochronology of the Upper Triassic Chinle Group, southwestern USA. *New Mexico Museum of Natural History and Science Bulletin*, 37, 94–104.
- Heckert, A. B., Lucas, S. G., Hunt, A. P., & Spielmann, J. (2007). Late aetosaur biochronology revisited. *New Mexico Museum of Natural History and Science Bulletin*, 41, 49–50.
- Heckert, A. B., Lucas, S. G., Rinehart, L. F., Celeskey, M. D., Spielmann, J. A., & Hunt, A. P. (2010). Articulated skeletons of the aetosaur *Typothorax coccinarum* Cope (Archosauria: Stagonolepididae) from the Upper Triassic Bull Canyon Formation (Revueltian: Early-mid Norian), eastern New Mexico, USA. *Journal of Vertebrate Paleontology*, 30, 619–642.
- Heckert, A. B., Mitchell, J. S., Schneider, V. P., & Olsen, P. E. (2012). Diverse new microvertebrate assemblage from the Upper Triassic Cummock Formation, Sanford Subbasin, North Carolina, USA. *Journal of Paleontology*, 86, 368–390.
- Hua, S., & de Buffrénil, V. (1996). Bone histology as a clue in the interpretation of functional adaptations in the *Thalattosuchia* (Reptilia, Crocodylia). *Journal of Vertebrate Paleontology*, 16, 703–717.
- Hunt, A. P. (1989). A new? Ornithischian dinosaur from the Bull Canyon Formation (Upper Triassic) of east-central New Mexico. In S. G. Lucas & A. P. Hunt (Eds.), *Dawn of the age of dinosaurs in the American southwest* (pp. 355–358). Albuquerque, NM.
- Hunt, A. P. (1994). *Vertebrate paleontology and biostratigraphy of the Bull Canyon Formation (Chinle Group, Upper Triassic), east-central New Mexico with revisions of the families Metoposauridae (Amphibia: Temnospondyli) and Parasuchidae (Reptilia: Archosauria)* [dissertation] (p. 404). University of New Mexico.
- Hunt, A. P. (2001). The vertebrate fauna, biostratigraphy and biochronology of the type Revueltian land-vertebrate faunachron, Bull Canyon Formation (Upper Triassic), east-central New Mexico. *New Mexico Geological Society Guidebook*, 52, 123–151.
- Hunt, A. P., & Lucas, S. G. (1994). Ornithischian dinosaurs from the Upper Triassic of the United States. In N. C. Fraser & H.-D. Sues (Eds.), *In the shadow of the dinosaurs: Early Mesozoic Tetrapods* (pp. 227–241). Cambridge University Press.
- Hunt, A. P., Lucas, S. G., & Spielmann, J. A. (2005). The postcranial skeleton of *Reueltosaurus callenderi* (Archosauria: Crurotarsi) from the Upper Triassic of Arizona and New Mexico, USA. *New Mexico Museum of Natural History and Science Bulletin*, 29, 66–75.
- Hutton, J. M. (1986). Age determination of living Nile crocodiles from the cortical stratification of bone. *Copeia*, 1986, 332–341.
- Irmis, R. B. (2005). The vertebrate fauna of the upper Triassic Chinle Formation in northern Arizona. *Mesa Southwest Museum Bulletin*, 9, 63–88.
- Irmis, R. B. (2007). Axial skeleton ontogeny in the *Parasuchia* (Archosauria: Pseudosuchia) and its implications for ontogenetic determination in archosaurs. *Journal of Vertebrate Paleontology*, 27, 350–361.
- Irmis, R. B. (2008). *Perspectives on the origin and early diversification of dinosaurs [PhD]* (p. 421). University of California.
- Irmis, R. B., Martz, J. W., Parker, W. G., & Nesbitt, S. J. (2010). Re-evaluating the correlation between late Triassic terrestrial vertebrate biostratigraphy and the GSSP-defined marine stages. *Albertiana*, 38, 40–52.
- Irmis, R. B., Mundil, R., Martz, J. W., & Parker, W. G. (2011). High-resolution U-Pb ages from the Upper Triassic Chinle formation (New Mexico, USA) support a diachronous rise of dinosaurs. *Earth and Planetary Science Letters*, 309, 258–267.
- Irmis, R. B., Nesbitt, S. J., Padian, K., Smith, N. D., Turner, A. H., Woody, D. T., & Downs, A. (2007). A Late Triassic dinosauriform assemblage from New Mexico and the rise of dinosaurs. *Science*, 317, 358–361.
- Irmis, R. B., Nesbitt, S. J., & Sues, H.-D. (2013). Early Crocodylomorpha. In S. J. Nesbitt, J. B. Desojo, & R. B. Irmis (Eds.), *The Geological Society of London Anatomy, phylogeny*

- and *Palaeobiology of Early Archosaurs and Their Ki* (Vol. 379, pp. 275–302). Geological Society, Special Publications.
- Irmis, R. B., Parker, W. G., Nesbitt, S. J., & Liu, J. (2007). Early ornithischian dinosaurs: The Triassic record. *Historical Biology*, 19, 3–22.
- Jepsen, G. L. (1948). A Triassic armored reptile from New Jersey. State of New Jersey Miscellaneous Geologic Paper:1–20.
- Johns, M. E. (1988). *Architectural element analysis and depositional history of the Upper Petrified Forest Member of the Chinle Formation, Petrified Forest National Park, Arizona [M.S.]* (p. 163). Northern Arizona University.
- Kent, D. V., Olsen, P. E., Lepre, C., Rasmussen, C., Mundil, R., Gehrels, G. E., Giesler, D., Irmis, R. B., Geissman, J. W., & Parker, W. G. (2019). Magnetostratigraphy of the entire Chinle Formation (Norian age) in a scientific drill core from Petrified Forest National Park (Arizona, USA) and implications for regional and global correlations in the Late Triassic. *Geochemistry, Geophysics, Geosystems*, 20, 4654–4664.
- Kent, D. V., Olsen, P. E., Rasmussen, C., Lepre, C., Mundil, R., Irmis, R. B., Gehrels, G. E., Giesler, D., Geissman, J. W., & Parker, W. G. (2018). Empirical evidence for stability of the 405-kiloyear Jupiter-Venus eccentricity cycle over hundreds of millions of years. *Proceedings of the National Academy of Sciences*, 115, 6153–6158.
- Klein, N., Foth, C., & Schoch, R. R. (2017). Preliminary observations on the bone histology of the Middle Triassic pseudosuchian archosaur *Batrachotomus kupferzellensis* reveal fast growth with laminar fibrolamellar bone tissue. *Journal of Vertebrate Paleontology*, 37, e1333121.
- Kley, N. J., Sertich, J. J. W., Turner, A. H., Krause, D. W., O'Connor, P. M., & Georgi, J. A. (2010). Craniofacial morphology of *Simosuchus clarki* (Crocodyliformes: Notosuchia) from the Late Cretaceous of Madagascar. *Journal of Vertebrate Paleontology Memoir*, 10, 13–98.
- Krebs, B. (1974). Die Archosaurier. *Naturwissenschaften*, 61, 17–24.
- Lacerda, M. B., De França, M. A. G., & Schultz, C. L. (2018). A new erpetosuchid (Pseudosuchia, Archosauria) from the Middle-Late Triassic of southern Brazil. *Zoological Journal of the Linnean Society*, 184, 804–824.
- Langer, M., Ezcurra, M., Rauhut, O. W. M., Benton, M. J., Knoll, F., McPhee, B. W., Novas, F. E., Pol, D., & Brusatte, S. L. (2017). Untangling the dinosaur family tree. *Nature*, 551, E1–E3.
- Langer, M. C., & Benton, M. J. (2006). Early dinosaurs: A phylogenetic study. *Journal of Systematic Palaeontology*, 4, 309–358.
- Laurenti, J. N. (1768). *Specimen Medicum, Exhibens Synopsin Reptilium Emendatam Cum Experimentis Circa Venena*. Joan Thomae.
- Legendre, L. J., Segalen, L., & Cubo, J. (2013). Evidence for high bone growth rate in *Euparkeria* obtained using a new paleohistological inference model for the humerus. *Journal of Vertebrate Paleontology*, 33, 1343–1350.
- Lehman, T., & Chatterjee, S. (2005). Depositional setting and vertebrate biostratigraphy of the Triassic Dockum Group of Texas. *Journal of Earth System Science*, 114, 325–351.
- Linnaeus, C. (1758). *Systema Naturae per regna Tria Naturae, Secundum classis, ordines, genera, species cum Characteribus, Differentiis, Synonymis, Locis*. Laurentii Salvii.
- Litwin, R. J., Traverse, A., & Ash, S. R. (1991). Preliminary palynological zonation of the Chinle formation, southwestern U.S.A., and its correlation to the Newark Supergroup (eastern U.S.A.). *Review of Palaeobotany and Palynology*, 68, 269–287.
- Long, R. A., & Ballew, K. L. (1985). Aetosaur dermal armor from the Late Triassic of southwestern North America, with special reference to material from the Chinle Formation of Petrified Forest National Park. *Museum of Northern Arizona Bulletin*, 54, 45–68.
- Long, R. A., & Murry, P. A. (1995). Late Triassic (Carnian and Norian) tetrapods from the southwestern United States. *New Mexico Museum of Natural History and Science Bulletin*, 4, 1–254.
- Loughney, K. M., Fastovsky, D. E., & Parker, W. G. (2011). Vertebrate fossil preservation in blue paleosols from the Petrified Forest National Park, Arizona, with implications for vertebrate biostratigraphy in the Chinle Formation. *PALAIOS*, 26, 700–719.
- Lucas, S. G., Heckert, A. B., & Hunt, A. P. (2002). A new species of the aetosaur *Tytophorax*. *Upper Triassic Stratigraphy and Paleontology: Bulletin*, 21, 221.
- Lucas, S. G., & Hunt, A. P. (1993). Tetrapod biochronology of the Chinle group (upper Triassic), western United States. *New Mexico Museum of Natural History and Science Bulletin*, 3, 327–329.
- Maddison, W. P., & Maddison, D. R. (2019). Mesquite: a modular system for evolutionary analysis. Version 3.61. <http://www.mesquiteproject.org>
- Marsh, A. D., & Parker, W. G. (2020). New dinosauriform specimens from the Petrified Forest National Park and a global biostratigraphic review of Triassic dinosauriform body fossils. *PaleoBios*, 37, 1–56.
- Marsh, A. D., Smith, M. E., Parker, W. G., Irmis, R. B., & Kligman, B. T. (2020). Skeletal anatomy of *Acaenasuchus geoffreyi* Long and Murry, 1995 (Archosauria: Pseudosuchia) and its implications for the origin of the aetosaurian carapace. *Journal of Vertebrate Paleontology*, 40, e1794885.
- Martz, J. W., Mueller, B., Nesbitt, S. J., Stocker, M. R., Parker, W. G., Atanassov, M., Fraser, N., Weinbaum, J., & Lehane, J. R. (2013). A taxonomic and biostratigraphic re-evaluation of the Post Quarry vertebrate assemblage from the Cooper Canyon Formation (Dockum Group, Upper Triassic) of southern Garza County, western Texas. *Earth and Environmental Science Transactions of the Royal Society of Edinburgh*, 103, 339–364.
- Martz, J. W., & Parker, W. G. (2010). Revised lithostratigraphy of the Sonsela Member (Chinle Formation, Upper Triassic) in the southern part of Petrified Forest National Park, Arizona. *PLoS One*, 5(e9329), 9321–9326.
- Martz, J. W., & Parker, W. G. (2017). Revised formulation of the Late Triassic land vertebrate "faunachrons" of western North America. In K. E. Zeigler & W. G. Parker (Eds.), *Deciphering complex depositional systems* (pp. 39–124). Elsevier.
- Martz, J. W., Parker, W. G., Skinner, L., Ruccia, J. J., Umhoefer, P., & Blakey, R. C. (2012). Geologic map of Petrified Forest National Park, Arizona. Arizona Geological Survey Contributed Map CR-12-A, 1 map sheet, 1:50,000 map scale, 18 pp.
- Martz, J. W., & Small, B. J. (2006). *Tecovasuchus chatterjeei*, a new aetosaur (Archosauria: Stagonolepididae) from the Tecovas Formation (Carnian, Upper Triassic) of Texas. *Journal of Vertebrate Paleontology*, 26, 308–320.
- Martz, J. W., & Small, B. J. (2019). Non-dinosaurian dinosauriforms from the Chinle Formation (Upper Triassic)

- of the Eagle Basin, northern Colorado: *Dromomeron romeri* (Lagerpetidae) and a new taxon, *Kwanasaurus williamparkeri* (Silesauridae). *PeerJ*, 7, 7e7551. <https://doi.org/10.7717/peerj.7551>
- Mehl, M. G. (1915). *Poposaurus gracilis*, a new reptile from the Triassic of Wyoming. *Journal of Geology*, 23, 516–522.
- Mukherjee, D., & Ray, S. (2012). Taphonomy of an Upper Triassic vertebrate bonebed: A new rhynchosaur (Reptilia; Archosauromorpha) accumulation from India. *Palaeogeography, Palaeoclimatology, Palaeoecology*, 333–334, 75–91.
- Müller, R. T., von Baczko, M. B., Desojo, J. B., & Nesbitt, S. J. (2020). The first ornithosuchid from Brazil and its macroevolutionary and phylogenetic implications for Late Triassic faunas in Gondwana. *Acta Palaeontologica Polonica*, 65, 2019.
- Nesbitt, S. J. (2003). *Arizonasaurus* and its implications for archosaur divergence. Proceedings of the Royal Society of London. *Biological Sciences*, 270 (Supplement 2), S234–S237.
- Nesbitt, S. J. (2005a). A new archosaur from the upper Moenkopi Formation (Middle Triassic) of Arizona and its implications for raiusuchian phylogeny and diversification. *Neues Jahrbuch für Geologie und Paläontologie, Monatshefte*, 2005, 332–346.
- Nesbitt, S. J. (2005b). Osteology of the middle Triassic pseudosuchian archosaur *Arizonasaurus babbitti*. *Historical Biology*, 17, 19–47.
- Nesbitt, S. J. (2007). The anatomy of *Effigia okeeffeae* (Archosauria, Suchia), theropod-like convergence, and the distribution of related taxa. *Bulletin of the American Museum of Natural History*, 302, 1–84.
- Nesbitt, S. J. (2011). The early evolution of archosaurs: Relationships and the origin of major clades. *Bulletin of the American Museum of Natural History*, 352, 1–292.
- Nesbitt, S. J., Brusatte, S. L., Desojo, J. B., Liparini, A., de Franca, M. A. G., Weinbaum, J. C., & Gower, D. J. (2013). Raiusuchia. In S. J. Nesbitt, J. B. Desojo, & R. B. Irmis (Eds.), *The Geological Society of London Anatomy, phylogeny and Palaeobiology of early archosaurs and their kin* (Vol. 379, pp. 241–274). Geological Society, Special Publications.
- Nesbitt, S. J., & Butler, R. J. (2013). Redescription of the archosaur *Parringtonia gracilis* from the Middle Triassic Manda beds of Tanzania, and the antiquity of Erpetosuchidae. *Geological Magazine*, 150, 225–238.
- Nesbitt, S. J., Butler, R. J., Ezcurra, M. D., Barrett, P. M., Stocker, M. R., Angielczyk, K. D., Smith, R. M. H., Sidor, C. A., Niedźwiedzki, G., Sennikov, A. G., & Charig, A. J. (2017). The earliest bird-line archosaurs and the assembly of the dinosaur body plan. *Nature*, 544, 484–487.
- Nesbitt, S. J., Butler, R. J., Ezcurra, M. D., Charig, A. J., & Barrett, P. M. (2018). The anatomy of *Teleocrater rhadinus*, an early avemetatarsalian from the lower portion of the Lifua Member of the Manda Beds (~Middle Triassic). In C. A. Sidor & S. J. Nesbitt (Eds.), *Vertebrate and climatic evolution in the Triassic rift basins of Tanzania and Zambia. Society of Vertebrate Paleontology Memoir 17. Journal of Vertebrate Paleontology* (Vol. 37 (supplement 6), pp. 142–177).
- Nesbitt, S. J., Desojo, J. B., & Irmis, R. B. (2013). Anatomy, phylogeny and palaeobiology of early archosaurs and their kin. In S. J. Nesbitt, J. B. Desojo, & R. B. Irmis (Eds.), *The Geological Society of London Anatomy, phylogeny and Palaeobiology of early archosaurs and their kin* (Vol. 379, pp. 1–7). Geological Society, Special Publications.
- Nesbitt, S. J., Flynn, J. J., Pritchard, A. C., Parrish, J. M., Ranivoharimanana, L., & Wyss, A. R. (2015). Postcranial osteology of *Azendohsaurus madagaskarensis* (?Middle to Upper Triassic, Isalo Group, Madagascar) and its systematic position among stem archosaur reptiles. *Bulletin of the American Museum of Natural History*, 398, 1–126.
- Nesbitt, S. J., Irmis, R. B., & Parker, W. G. (2007). A critical re-evaluation of the late Triassic dinosaur taxa of North America. *Journal of Systematic Palaeontology*, 5, 209–243.
- Nesbitt, S. J., Irmis, R. B., Parker, W. G., Smith, N. D., Turner, A. H., & Rowe, T. (2009). Hindlimb osteology and distribution of basal dinosauriforms from the Late Triassic of North America. *Journal of Vertebrate Paleontology*, 29, 498–516.
- Nesbitt, S. J., Liu, J., & Li, C. (2011). A sail-backed suchian from the Heshangou Formation (Early Triassic: Olenekian) of China. *Earth and Environmental Science Transactions of the Royal Society of Edinburgh*, 101, 271–284.
- Nesbitt, S. J., & Norell, M. A. (2006). Extreme convergence in the body plans of an early suchian (Archosauria) and ornithomimid dinosaurs (Theropoda). *Proceedings of the Royal Society of London, Biological Sciences*, 273, 1045–1048.
- Nesbitt, S. J., Sidor, C. A., Angielczyk, K. D., Smith, R. M., & Parker, W. G. (2012). Derivation of the aetosaur osteoderm carapace: Evidence from a new, exceptionally preserved “stem aetosaur” from the Middle Triassic (Anisian) Manda Beds of southwestern Tanzania. *Journal of Vertebrate Paleontology, Program and Abstracts*, 2013, 149.
- Nesbitt, S. J., Sidor, C. A., Angielczyk, K. D., Smith, R. M. H., & Tsuji, L. A. (2014). A new archosaur from the Manda Beds (Anisian, Middle Triassic) of southern Tanzania and its implications for character state optimizations at Archosauria and Pseudosuchia. *Journal of Vertebrate Paleontology*, 34, 1357–1382.
- Nesbitt, S. J., Sidor, C. A., Irmis, R. B., Angielczyk, K. D., Smith, R. M. H., & Tsuji, L. A. (2010). Ecologically distinct dinosaurian sister group shows early diversification of Ornithodira. *Nature*, 464, 95–98.
- Nesbitt, S. J., & Stocker, M. R. (2008). The vertebrate assemblage of the Late Triassic Canjilon Quarry (northern New Mexico, USA), and the importance of apomorphy-based assemblage comparisons. *Journal of Vertebrate Paleontology*, 28, 1063–1072.
- Nesbitt, S. J., Stocker, M. R., Parker, W. G., Wood, T. A., Sidor, C. A., & Angielczyk, K. D. (2018). The braincase and endocast of *Parringtonia gracilis*, a Middle Triassic suchian (Archosauria: Pseudosuchia). In C. A. Sidor & S. J. Nesbitt (Eds.), *Vertebrate and climatic evolution in the Triassic rift basins of Tanzania and Zambia* (Vol. 17, pp. 122–141). Society of Vertebrate Paleontology Memoir.
- Nesbitt, S. J., Zawiskie, J. M., & Dawley, R. M. (2020). The osteology and phylogenetic position of the loricatan (Archosauria: Pseudosuchia) *Heptasuchus clarki*, from the? Mid-Upper Triassic, southeastern Big Horn Mountains, central Wyoming (USA). *PeerJ*, 8, 1–57.
- Newton, E. T. (1894). Reptiles from the Elgin sandstone: Description of two new genera. *Philosophical Transactions of the Royal Society of London B, Biological Sciences*, 185, 573–607.
- Oelrich, T. M. (1956). The anatomy of the head of *Ctenosaura pectinata* (Iguanidae). *Miscellaneous Publications of the Museum of Geology*, 94, 1–122.

- O'Leary, M. A., & Kaufman, S. (2007). MorphoBank 2.5: Web application for morphological systematics and taxonomy.
- Olsen, P. E., Reid, J. C., Taylor, K. B., Whiteside, J. H., & Kent, D. V. (2015). Revised stratigraphy of Late Triassic age strata of the Dan River basin (Virginia and North Carolina, USA) based on drill core and outcrop data. *Southeastern Geology*, *51*, 1–31.
- Padian, K. (1990). The ornithischian form genus *Revueltosaurus* from the petrified Forest of Arizona (Late Triassic: Norian; Chinle formation). *Journal of Vertebrate Paleontology*, *10*, 268–269.
- Padian, K., de Ricqlès, A. J., & Horner, J. R. (2001). Dinosaurian growth rates and bird origins. *Nature*, *412*, 405–408.
- Parker, W. G. (2005a). A new species of the late Triassic aetosaur *Desmatosuchus* (Archosauria: Pseudosuchia). *Compte Rendus Paleovol*, *4*, 327–340.
- Parker, W. G. (2005b). Faunal review of the upper Triassic Chinle formation of Arizona. *Mesa Southwest Museum Bulletin*, *11*, 34–54.
- Parker, W. G. (2006). The stratigraphic distribution of major fossil localities in Petrified Forest National Park, Arizona. *Museum of Northern Arizona Bulletin*, *62*, 46–61.
- Parker, W. G. (2007). Reassessment of the aetosaur '*Desmatosuchus chamaensis*' with a reanalysis of the phylogeny of the Aetosauria (Archosauria: Pseudosuchia). *Journal of Systematic Palaeontology*, *5*, 41–68.
- Parker, W. G. (2008). Description of new material of the aetosaur *Desmatosuchus spurensis* (Archosauria: Suchia) from the Chinle formation of Arizona and a revision of the genus *Desmatosuchus*. *PaleoBios*, *28*, 1–40.
- Parker, W. G. (2013). Redescription and taxonomic status of specimens of *Episcoposaurus* and *Typhothorax*, the earliest known aetosaurs (Archosauria: Suchia) from the Upper Triassic of western North America, and the problem of proxy "holotypes". *Earth and Environmental Science Transactions of the Royal Society of Edinburgh*, *103*, 313–338.
- Parker, W. G. (2016a). Revised phylogenetic analysis of the Aetosauria (Archosauria: Pseudosuchia); assessing the effects of incongruent morphological character sets. *PeerJ*, *4*, e1583.
- Parker, W. G. (2016b). Osteology of the late Triassic archosaur *Scutarx deltatylus* (Archosauria: Pseudosuchia: Aetosauria). *PeerJ*, *4*, e2411.
- Parker, W. G., & Barton, B. J. (2008). New information on the Upper Triassic archosauriform *Vancleavea campi* based on new material from the Chinle Formation of Arizona. *Palaeontologia Electronica*, *11*(14A), 11–20.
- Parker, W. G., & Irmis, R. B. (2005). Advances in Late Triassic vertebrate paleontology based on new material from Petrified Forest National Park, Arizona. *New Mexico Museum of Natural History and Science Bulletin*, *29*, 45–58.
- Parker, W. G., Irmis, R. B., Nesbitt, S. J., Martz, J. W., & Browne, L. S. (2005). The Late Triassic pseudosuchian *Revueltosaurus calenderi* and its implications for the diversity of early ornithischian dinosaurs. *Proceedings of the Royal Society of London, Biological Sciences*, *272*, 963–969.
- Parker, W. G., & Martz, J. W. (2011). The Late Triassic (Norian) Adamanian-Revueltian tetrapod faunal transition in the Chinle Formation of Petrified Forest National Park, Arizona. *Earth and Environmental Science Transactions of the Royal Society of Edinburgh*, *101*, 231–260.
- Parker, W. G., & Nesbitt, S. J. (2013). Cranial remains of *Poposaurus gracilis* (Pseudosuchia: Poposauroida) from the Upper Triassic, the distribution of the taxon and its implications for poposauroid evolution. In S. J. Nesbitt, J. B. Desojo, & R. B. Irmis (Eds.), *Anatomy, phylogeny and Palaeobiology of early archosaurs and their kin* (pp. 503–523). Geological Society, Special Publications.
- Parker, W. G., Stocker, M. R., & Irmis, R. B. (2008). A new desmatosuchine archosaur (Archosauria: Pseudosuchia) from the Upper Triassic Tecovas Formation (Dockum Group) of Texas. *Journal of Vertebrate Paleontology*, *28*, 692–701.
- Parrish, J. M. (1986). Locomotor adaptations in the hindlimb and pelvis of the Thecodontia. *Hunteria*, *1*, 1–35.
- Parrish, J. M. (1993). Phylogeny of the Crocodylotarsi, with reference to archosaurian and crurotarsan monophyly. *Journal of Vertebrate Paleontology*, *13*, 287–308.
- Parrish, J. M. (1994). Cranial osteology of *Longosuchus meadei* and the phylogeny and distribution of the Aetosauria. *Journal of Vertebrate Paleontology*, *14*, 196–209.
- Ponce, D. A., Cerda, I. A., Desojo, J. B., & Nesbitt, S. J. (2017). The osteoderm microstructure in doswelliids and proterochampsids and its implications for palaeobiology in stem archosaurs. *Acta Palaeontologica Polonica*, *62*, 819–831.
- Ramezani, J., Fastovsky, D. E., & Bowring, S. A. (2014). Revised chronostratigraphy of the lower Chinle Formation strata in Arizona and New Mexico (USA): High-precision U-Pb geochronological constraints on the Late Triassic evolution of dinosaurs. *American Journal of Science*, *314*, 981–1008.
- Ramezani, J., Hoke, G. D., Fastovsky, D. E., Bowring, S. A., Therrien, F., Dworkin, S. I., Atchley, S. C., & Nordt, L. C. (2011). High-precision U-Pb zircon geochronology of the Late Triassic Chinle Formation, Petrified Forest National Park (Arizona, USA): Temporal constraints on the early evolution of dinosaurs. *Geological Society of America Bulletin*, *123*, 2142–2159.
- Rasmussen, C., Mundil, R., Irmis, R. B., Geisler, D., Gehrels, G. E., Olsen, P. E., Kent, D. V., Lepre, C., Kinney, S. T., Geissman, J. W., & Parker, W. G. (2020). U-Pb zircon geochronology and depositional age models for the Upper Triassic Chinle Formation (Petrified Forest National Park, Arizona, USA): Implications for Late Triassic paleoecological and paleoenvironmental change. *Geological Society of America Bulletin*, *133*, 539–558. <https://doi.org/10.1130/B35485.1>
- Reichgelt, T., Parker, W. G., Martz, J. W., Conran, J. G., van Konijnenburg-van Cittert, J. H. A., & Kürschner, W. M. (2013). The palynology of the Sonsela Member (Late Triassic, Norian) at Petrified Forest National Park, Arizona, USA. *Review of Palaeobotany and Palynology*, *189*, 18–28.
- Reyes, W. A., Parker, W. G., & Marsh, A. D. (2021). Cranial anatomy of *Typhothorax coccinarum* (Archosauria: Pseudosuchia) from the Upper Triassic Chinle Formation of Arizona. *Journal of Vertebrate Paleontology*, e1876080.
- Sanchez, S., Steyer, J. S., Schoch, R. R., & de Ricqlès, A. (2010). Palaeoecological and palaeoenvironmental influences revealed by long-bone palaeohistology: The example of the Permian branchiosaurid *Apateon*. Geological Society, London, Special Publications 339: 139–149.
- Säve-Söderbergh, G. (1947). Notes on the braincase in *Sphenodon* and certain Lacertilia. *Zoologiska Bidragen tot de Anatomie*, *25*, 489–516.

- Schachner, E. R., Irmis, R. B., Huttenlocker, A. K., Sanders, K., Cieri, R. L., & Nesbitt, S. J. (2020). Osteology of the Late Triassic bipedal archosaur *Poposaurus gracilis* (Archosauria: Pseudosuchia) from western North America. *Anatomical Record*, 303, 874–917.
- Scheyer, T. M., Desojo, J. B., & Cerda, I. A. (2014). Bone histology of phytosaur, aetosaur, and other archosauriform osteoderms (Eureptilia, Archosauromorpha). *Anatomical Record*, 297, 240–260.
- Schoch, R. R. (2007). Osteology of the small archosaur *Aetosaurus* from the Upper Triassic of Germany. *Neues Jahrbuch für Geologie und Paläontologie Abhandlungen*, 246, 1–35.
- Schoch, R. R., & Desojo, J. B. (2016). Cranial anatomy of the aetosaur *Paratypothorax andressorum* Long & Ballew, 1985, from the upper Triassic of Germany and its bearing on aetosaur phylogeny. *Neues Jahrbuch für Geologie und Paläontologie-Abhandlungen*, 279, 73–95.
- Schumacher, G.-H. (1973). The head muscles and hyolaryngeal skeleton of turtles and crocodylians. In C. Gans & T. J. Parsons (Eds.), *Biology of the Reptilia, volume 4, morphology D* (pp. 101–199). Academic Press.
- Sengupta, S., Ezcurra, M. D., & Bandyopadhyay, S. (2017). A new horned and long-necked herbivorous stem-archosaur from the Middle Triassic of India. *Scientific Reports*, 7(8366), 1–9.
- Sereno, P. C. (1991). Basal archosaurs: phylogenetic relationships and functional implications. *Society of Vertebrate Paleontology Memoir*, 2, 1–53.
- Small, B. J. (1985). *The Triassic thecodontian reptile Desmatosuchus: Osteology and relationships* (p. 83). Texas Tech University.
- Small, B. J. (2002). Cranial anatomy of *Desmatosuchus haplocerus* (Reptilia: Archosauria: Stagonolepididae). *Zoological Journal of the Linnean Society*, 136, 97–111.
- Sookias, R. B., Dilkes, D., Sobral, G., Smith, R. M., Wolvaardt, F. P., Arcucci, A. B., Bhullar, B.-A. S., & Werneburg, I. (2020). The craniomandibular anatomy of the early archosauriform *Euparkeria capensis* and the dawn of the archosaur skull. *Royal Society Open Science*, 7, 200116.
- Stein, K., & Prondvai, E. (2014). Rethinking the nature of fibrolamellar bone: An integrative biological revision of sauropod plexiform bone formation. *Biological Reviews*, 89, 24–47. <https://doi.org/10.1111/brv.12041>
- Stein, K., & Sander, P. M. (2009). Histological core drilling: A less destructive method for studying bone histology. In M. A. Brown, J. F. Kane, & W. G. Parker (Eds.), *Methods in Fossil Preparation: Proceedings of the First Annual Fossil Preparation and Collections Symposium*. Petrified Forest National Park (pp. 69–80).
- Stocker, M. R. (2010). A new taxon of phytosaur (Archosauria: Pseudosuchia) from the Late Triassic (Norian) Sonsela Member (Chinle Formation) in Arizona, and a critical reevaluation of *Leptosuchus* Case 1922. *Palaeontology*, 53, 997–1022.
- Stocker, M. R. (2012). A new phytosaur (Archosauriformes, Phytosauria) from the Lot's Wife beds (Sonsela Member) within the Chinle Formation (Upper Triassic) of Petrified Forest National Park, Arizona. *Journal of Vertebrate Paleontology*, 32(3), 573–586.
- Stocker, M. R., Nesbitt, S. J., Criswell, K. E., Parker, W. G., Witmer, L. M., Rowe, T. B., Ridgely, R., & Brown, M. A. (2016). A dome-headed stem archosaur exemplifies convergence among dinosaurs and their distant relatives. *Current Biology*, 26, 1–7.
- Stocker, M. R., Zhao, L.-J., Nesbitt, S. J., Wu, X.-C., & Li, C. (2017). A short-snouted, Middle Triassic phytosaur and its implications for the morphological evolution and biogeography of Phytosauria. *Scientific Reports*, 7(46028), 1–8.
- Sues, H.-D. (1992). A remarkable new armored archosaur from the Upper Triassic of Virginia. *Journal of Vertebrate Paleontology*, 12, 142–149.
- Sues, H.-D. (2003). An unusual new archosauromorph reptile from the Upper Triassic Wolfville Formation of Nova Scotia. *Canadian Journal of Earth Sciences*, 40, 635–649.
- Sues, H. D., & Olsen, P. E. (2015). Stratigraphic and temporal context and faunal diversity of Permian-Jurassic continental tetrapod assemblages from the Fundy rift basin, eastern Canada. *Atlantic Geology*, 51, 139–205.
- Sues, H. D., Olsen, P. E., Carter, J. G., & Scott, D. M. (2003). A new crocodylomorph archosaur from the Upper Triassic of North Carolina. *Journal of Vertebrate Paleontology*, 23, 329–343.
- Sulej, T. (2010). The skull of an early Late Triassic aetosaur and the evolution of the stagonolepidid archosaurian reptiles. *Zoological Journal of the Linnean Society*, 158, 860–881.
- Swofford, D. L. (2002). *PAUP* Phylogenetic analysis using parsimony (* and other methods)*. 4.0b10a ed. Sinauer Associates.
- Taborda, J. R. A., Desojo, J. B., & Cerda, I. A. (2013). *Growth curve of Aetosauroides scagliai Casimiquela 1960 (Pseudosuchia: Aetosauria) inferred from osteoderm histology* (Vol. 379, pp. 413–423). Geological Society of London, Special Publication.
- Therrien, F., & Fastovsky, D. E. (2000). Paleoenvironments of early theropods, Chinle Formation (Late Triassic), Petrified Forest National Park, Arizona. *PALAIOS*, 15, 194–211.
- Tulga, S. (2014). Insights on archosaurian growth: A case study of an assemblage of *Revoltoosaurus callenderi* from Petrified Forest National Park, Arizona. *Journal of Vertebrate Paleontology Online Supplement*, 242.
- von Baczko, M. B., Desojo, J. B., & Ponce, D. (2020). Postcranial anatomy and osteoderm histology of *Riojasuchus tenuisiceps* and a phylogenetic update on Ornithosuchidae (Archosauria, Pseudosuchia). *Journal of Vertebrate Paleontology*, 39, e1693396.
- von Baczko, M. B., & Ezcurra, M. D. (2013). Ornithosuchidae: A group of Triassic archosaurs with a unique ankle joint. In S. J. Nesbitt, J. B. Desojo, & R. B. Irmis (Eds.), *The Geological Society of London Anatomy, phylogeny and Palaeobiology of early archosaurs and their kin* (Vol. 379, pp. 187–202). Geological Society, Special Publications.
- Walker, A. D. (1961). Triassic reptiles from the Elgin area: *Stagonolepis*, *Dasygnathus* and their allies. *Philosophical Transactions of the Royal Society of London, Series B*, 244, 103–204.
- Walker, A. D. (1964). Triassic reptiles from the Elgin area: *Ornithosuchus* and the origin of carnosaurs. *Philosophical Transactions of the Royal Society of London, Series B*, 248, 53–134.
- Walker, A. D. (1972). New light on the origin of birds and crocodyles. *Nature*, 237, 257–263.
- Walker, A. D. (1990). A revision of *Sphenosuchus acutus* Houghton, a crocodylomorph reptile from the Elliott Formation (Late Triassic or Early Jurassic) of South Africa. *Philosophical Transactions: Biological Sciences*, 330, 1–120.
- Weinbaum, J. C. (2011). The skull of *Postosuchus kirkpatricki* (Archosauria: Paracrocodyliformes) from the Upper Triassic of the United States. *PaleoBios*, 30, 18–44.
- Weinbaum, J. C., & Hungerbühler, A. (2007). A revision of *Poposaurus gracilis* (Archosauria: Suchia) based on two new

- specimens from the Late Triassic of the southwestern U.S.A. *Paläontologische Zeitschrift*, 81, 131–145.
- Whatley, R. L., Behrensmeyer, A. K., & Parker, W. G. (2013). Revealing new Triassic microvertebrate faunas in the upper Chinle Formation, Petrified Forest National Park, Arizona. *IMR Crossroads in Science*, 1, 40–52.
- Whiteside, J. H., Grogan, D. S., Olsen, P. E., & Kent, D. V. (2011). Climatically driven biogeographic provinces of Late Triassic tropical Pangea. *Proceedings of the National Academy of Sciences*, 108, 8972–8977.
- Whiteside, J. H., Lindström, S., Irmis, R. B., Glasspool, I. J., Schaller, M. F., Dunlavy, M., Nesbitt, S. J., Smith, N. D., & Turner, A. H. (2015). Extreme ecosystem instability suppressed tropical dinosaur dominance for 30 million years. *Proceedings of the National Academy of Sciences*, 112, 7909–7913.
- Wilson, J. A. (1999). A nomenclature for vertebral laminae in sauro-pods and other saurischian dinosaurs. *Journal of Vertebrate Paleontology*, 19, 639–653.
- Wilson, J. W. (1994). Histological techniques. In P. Leiggi & P. May (Eds.), *Vertebrate paleontological techniques, Volume one* (pp. 205–234). Cambridge University Press.
- Witmer, L. M. (1997). Craniofacial air sinus systems. In P. J. Currie & K. Padian (Eds.), *Encyclopedia of dinosaurs* (pp. 151–159). Academic Press.
- Woody, D. T. (2006). Revised stratigraphy of the lower Chinle Formation (Upper Triassic) of Petrified Forest National Park, Arizona. *Museum of Northern Arizona Bulletin*, 62, 17–45.
- Wu, X.-C., & Russell, A. P. (2001). Redescription of *Turfanosuchus dabanensis* (Archosauriformes) and new information on its phylogenetic relationships. *Journal of Vertebrate Paleontology*, 21, 40–50.
- Wynd, B. M., Nesbitt, S. J., Stocker, M. R., & Heckert, A. B. (2020). A detailed description of *Rugarhynchos sixmilensis*, gen. et comb. Nov. (Archosauriformes, Proterochampsia), and cranial convergence in snout elongation across stem and crown archosaurs. *Journal of Vertebrate Paleontology*, 39, e1748042.
- Zhang, F.-K. (1975). A new thecodont *Lotosaurus*, from Middle Triassic of Hunan. *Vertebrata Palasiatica*, 13, 144–147.
- Zittel, K. A. (1887–1890). *Handbuch der Palaeontologie*. 1. Abteilung: Palaeozoologie, Band 3. München and Leipzig.

SUPPORTING INFORMATION

Additional supporting information may be found in the online version of the article at the publisher's website.

How to cite this article: Parker, W. G., Nesbitt, S. J., Irmis, R. B., Martz, J. W., Marsh, A. D., Brown, M. A., Stocker, M. R., & Werning, S. (2022). Osteology and relationships of *Revueltosaurus callenderi* (Archosauria: Suchia) from the Upper Triassic (Norian) Chinle Formation of Petrified Forest National Park, Arizona, United States. *The Anatomical Record*, 305(10), 2353–2414. <https://doi.org/10.1002/ar.24757>